İSTANBUL TECHNICAL UNIVERSITY ★ INSTITUTE OF SCIENCE AND TECHNOLOGY

**WIND TURBINE MODELLING AND CONTROLLER
DESIGN**

**M.Sc. Thesis by
Gürol ÇOKÜNLÜ, Mech.Eng.**

(518041011)

Date of submission :   10 May 2007

Date of defence examination: 13 June 2007

Supervisor (Chairman):   Prof. Dr. Süleyman TOLUN

Members of the Examining Committee   Prof.Dr. Mete ŞEN (İ.T.Ü.)

Prof.Dr. Mehmet Şerif KAVSAOĞLU (İ.T.Ü.)

JUNE 2007

İSTANBUL TEKNİK ÜNİVERSİTESİ ★ FEN BİLİMLERİ ENSTİTÜSÜ

**RÜZGAR TÜRBİNİ MODELLEME VE KONTROLCÜ
TASARIMI**

YÜKSEK LİSANS TEZİ

Mak. Müh. Gürol ÇOKÜNLÜ

(518041011)

Tezin Enstitüye Verildiği Tarih :   10 Mayıs 2007

Tezin Savunulduğu Tarih : 13 Haziran 2007

Tez Danışmanı :   Prof.Dr. Süleyman TOLUN

Diğer Jüri Üyeleri   Prof.Dr. Mete ŞEN (İ.T.Ü.)

Prof.Dr. Mehmet Şerif KAVSAOĞLU (İ.T.Ü.)

HAZİRAN 2007

FOREWORD

I want to thank my family for giving all support they can during my education period. Their existence with their smiling faces gave me courage and made everything easier. I also want to thank to RESTEK project group members (especially Utku Türkyılmaz) for helping to increase my knowledge about wind turbines. I have to mention here that I was always glad to work in laboratory of Prof Dr. Levent Güvenç and Assoc. Dr. Bilin Aksun Güvenç. I learned many things in the laboratory, started to feel as an engineer and increased my self confidence. And my friend Diyane Köseoğlu deserves to be thanked for her help in the most stressful part: formatting the thesis. Finally I want to thank my friends Çağatay Çakır, İlker Altay and my supervisor Prof. Dr. Süleyman Tolun for helping me during all thesis period. Çağatay Çakır helped me in controller design. İlker Altay helped me in modeling the whole system. At the beginning of the project I did not know anything about wind turbines. My supervisor with his knowledge and ideas helped me to model the wind turbine and the controller. He also made this design period enjoyable for me with his friendship. I am glad to work with a professor like him.

MAYIS 2007   Gürol ÇOKÜNLÜ

i

CONTENTS

ACRONYMS

DFIG	: Doubly-fed induction generator
FP	**:** Fixed pitch
FS	**:** Fixed speed
SCIG	**:** Squirrel-cage induction generator
VP	**:** Variable pitch
VS	**:** Variable speed
WECS	**:** Wind energy conversion systems

TABLE LIST

FIGURE LIST

SYMBOL LIST

α **:** Angle of attack
β **:** Plak eğilme rijitliği
β_d **:** Demanded pitch angle
β_o **:** Optimum pitch angle
λ **:** Tip speed ratio
λ_{min} **:** Minumum tip speed ratio
λ_o **:** Optimum tip speed ratio
λ_{Qmax} **:** Tip speed ratio for maximum torque coefficient
Ω_g **:** Generator speed
Ω_N **:** Rated rotational speed
Ω_r **:** Rotor speed
Ω_s **:** Synchronous speed
Ω_z **:** Zero torque speed
ρ **:** Air denstiy
θ_s **:** Torsion angle
A **:** Area swept by the blades
B_b **:** Blade damping
B_g **:** Intrinsic generator damping
B_r **:** Intrinsic rotor damping
B_s **:** Drive train damping
B_t **:** Tower damping
B_T **:** Intrinsic thrust damping
C_P **:** Power coefficient
C_{Pmax} **:** Maximum power coefficient
C_Q **:** Torque coefficient
C_{Qmax} **:** Maximum torque coefficient
C_T **:** Thrust coefficient
F_T **:** Thrust force
J_g **:** Generator inertia
J_r **:** Rotor inertia
K_b **:** Blade stiffness
K_s **:** Drive-train stiffness
K_t **:** Tower stiffness
$k_{r,b}$ **:** Rotor torque – pitch gain
$k_{r,V}$ **:** Rotor torque – wind speed gain
$k_{r,b}$ **:** Rotor torque – pitch gain
$k_{T,b}$ **:** Thrust – pitch gain
$k_{T,V}$ **:** Thrust – wind speed gain
m_b **:** Mass of each blade
m_t **:** Mass of tower and nacelle
N **:** Number of blades
P_N **:** Rated power
R **:** Rotor radius
T_g **:** Generator torque
T_N **:** Rated torque
T_r **:** Aerodynamic torque
T_s **:** Shaft torque

$\mathbf{V}$	**:** Wind speed
$\mathbf{V_{min}}$	**:** Cut-in wind speed
$\mathbf{V_{\Omega N}}$	**:** Wind speed for rated rotational speed
$\mathbf{V_N}$	**:** Rated wind speed
$\mathbf{V_{max}}$	**:** Cut-out wind speed
$\mathbf{V_e}$	**:** Effective wind speed
$\mathbf{V_{rel}}$	**:** Relative wind speed
$\mathbf{V_m}$	**:** Mean wind speed
$\mathbf{y_t}$	**:** Tower displacement

RÜZGAR TÜRBİNİ MODELLEME VE KONTROLCÜ TASARIMI

ÖZET

Bu çalışmada ilk olarak rüzgar ve rüzgarın türbin tasarımına etkileri anlatılmaktadır. Sonrasında rüzgar türbini bileşenleri tanıtılmıştır. Rüzgar türbiniyle iligili bilgi verildikten sonra sistem mekanik alt sistem, aerodinamik alt sistem, elektrik alt sistem ve hatve açısı alt sistemi olmak üzere parçalara ayrılmıştır. Mekanik sistem iki kütle ve burulma yayı ile ifade edilmiştir. Ardından bu gösterim için durum uzay modeli oluşturulmuştur. Diğer alt sistemlere göre hızlı cevap veren elektrik sistemi kararlı durum davranışıyla karakterize edilmiştir. Elektrik sistemin modellenmesinde lineer bir denklem kullanılmıştır. Bunun yanında hatve açısı sistemi ise birinci derece bir sistemle ifade edilmiştir.

Tezde sistemin aerodinamiği de anlatılmaktadır. Güç, aerodinamik tork, itki kuvveti, uç hız oranı, güç katsayısı ve tork katsayılarını veren denklemler çıkarılmıştır. Ayrıca bu katsayıların kontrolcü ve sistem performansı üzerindeki etkileri anlatılmıştır. Buna ek olarak, sabit hız sabit hatve açısı, sabit hız değişken hatve açısı, değişken hız sabit hatve açısı, değişken hız değişken hatve açısı sistemlerinin kontrol kriterleri ve stratejileri incelenmiştir.

Son bölümde 1,5 MW gücünde değişken hız sabit hatve açılı türbin modellenmiştir. Bu sistem için düşük dereceli bir durum uzay modeli tasarlanmıştır. Sonra sistemi iki kütle ve burulma yayı ile ifade etmek yerine şaft rijit kabul edilmiştir ve buna göre bir PI kontrolcü tasarlanmıştır. Basit sistem için tasarlanan PI kontrolcüsü değişken hız sabit hatve açılı karmaşık sistemi kontrol etmede kullanılmıştır.

SUMMARY

In this study, the wind and its effects on wind turbine design are explained at first. Then the components of the wind turbine are represented. Giving knowledge about wind turbines the system is divided into subsystems such as mechanical subsystem, aerodynamic subsystem, electrical subsystem and pitch subsystem. Mechanical system is described by a two mass and a torsional spring model. State space model for this representation is derived. The electrical system, which gives faster response than the other subsystems, is characterized by its steady state behavior. A linear equation is used to define the electrical system. Moreover, the pitch subsystem is represented by a first order system.

The aerodynamics of the system is also explained. The equations used to calculate the power, aerodynamic torque, thrust force, tip speed ratio, power coefficient and torque coefficient are derived. The effects of these coefficients on the controller effort and the system are explained. In addition to this, control objectives and strategies for fixed speed fixed pitch, fixed speed variable pitch, variable speed fixed pitch and variable speed variable pitch wind turbines are analyzed.

In the final section, a 1,5 MW variable speed fixed pitch turbine is modeled. A reduced order state space model is formed. Then instead of using two mass and torsional spring system, the shaft is assumed to be rigid to reduce the order of the system and a PI controller is designed for this system. This PI controller designed for simple system is used in the simulation to control the variable speed fixed pitch turbine   model.

1.   INTRODUCTION

Since ancient times, wind has been exploited in different ways, mainly for grain milling and water pumping. With the advent of the industrial era, wind energy was gradually replaced by fossil fuels, the windmills being practically relegated to pump water for agricultural use. In the 20th century, new designs enabled electricity generation at small-scale levels for battery charging uses. After the early 1970s oil crisis, wind technology experienced a revolution. Motivated by the oil price boost, many countries promoted ambitious wind energy R&D programs. As a result, new materials and modern turbine designs were developed, initiating the age of large-scale wind electricity generation. During the last decades, the increasing concern about the environment and the trends towards the diversification of the energy market has been reinforcing the interest in wind energy exploitation.

Nowadays, wind energy is by far the fastest-growing renewable energy resource. The progress of wind power around the world in recent years has exceeded all the expectations, with Europe leading the global market. In numbers, the wind turbine capacity installed in Europe increased during the last years at an average annual growth rate superior to 30%.

The wind energy industry so far has been supported by market incentives   backed by government policies fostering sustainable energy resources. Anyway, the cost of electricity provided by wind power facilities has been dropping drastically since the 1980s. These cost reductions are due to new technologies and higher production scales leading to larger, more efficient and more reliable wind turbines.

Control plays a very important role in modern wind energy conversion systems (WECS). In fact, wind turbine control enables a better use of the turbine capacity as well as the alleviation of aerodynamic and mechanical loads that reduce the useful life of the installation. Furthermore, with individual large-scale wind facilities

approaching the output rating of conventional power plants, control of the power quality is required to reduce the adverse effects on their integration into the network. Thus, active control has an immediate impact on the cost of wind energy. Moreover, high performance and reliable controllers are essential to enhance the competitiveness of wind technology.

WECS have to cope with the intermittent and seasonal variability of the wind. By this reason, they include some mechanism to limit the captured power in high wind speeds to prevent from overloading. One of the methods of power limitation basically reduces the blades lift as the captured power approximates its rated value. To this end, the turbines incorporate either electromechanical or hydraulic devices to rotate the blades – or part of them – with respect to their longitudinal axes. These methods are referred to as pitch control ones. Alternatively, there are passive control methods that remove the need for vulnerable active devices, thus gaining in hardware robustness. These methods are based on particular designs of the blades that induce stall at higher than rated wind speed. That is, a turbulent flow deliberately arises at high wind speeds such that aerodynamic torque decreases due to stronger drag forces and some loss of lift. Despite their hardware simplicity, passive stall controlled WECS undergo reduced energy capture and higher stresses that potentially increase the danger of fatigue damage.

WECS schemes with the electric generator directly connected to grid have predominated for a long time. In these WECS, the rotational speed is imposed by the grid frequency. Although reliable and low-cost, these fixed-speed configurations are too rigid to adapt to wind variations. In fact, since maximum power capture is achieved at the so-called optimum tip-speed-ratio, fixed-speed WECS operate with optimum conversion efficiency only at a single wind speed. In order to make a better use of the turbine, variable-speed WECS were subsequently developed. They incorporate electronic converters as an interface between the generator and AC grid, thereby decoupling the rotational speed from the grid frequency. These WECS also include speed control to track the optimum tip-speed-ratio up to rated speed. Additionally, the electronic converters can be controlled to perform as reactive power suppliers or consumers according to the power system requirements.

Fixed-speed pitch-controlled schemes prevailed in early medium to high power wind turbines. Later on, WECS comprising induction generators directly connected to grid and stall-regulated wind rotors dominated the market for many years. More recently, the increasing turbine size and the greater penetration of wind energy into the utility together with exigent standards of power quality were demanding the use of active-controlled configurations. On the one hand, variable-speed schemes finally succeeded, not only because of their increased energy capture but mainly due to their flexibility to improve power quality and to alleviate the loading on the drive-train and tower. On the other hand, the interest in pitch-controlled turbines has lately been reviving due to the tendency towards larger wind turbines, being mechanical stresses an increasing concern as turbines grow in size. By these reasons, variable-speed pitch-controlled wind turbines are currently the preferred option, particularly in medium to high power. In fact, the benefits of control flexibility (improved power quality, higher conversion efficiency, and longer useful life) largely outweigh the higher complexity and extra initial investments of variable-speed variable-pitch turbines.

2.   WIND AND WIND TURBINES

The wind is characterized by its speed and direction, which are affected by several factors, geographic location, climate characteristics, height above ground, and surface topography [1]. "The most critical factor influencing the power developed by a wind energy conversion system is the wind velocity. Due to the cubic relation ship between velocity and power, even a small variation in the wind speed by 10 per cent may enhance the productivity of the turbine by over 33 per cent. As the wind velocity and thus the power vary from place to place, the first step in planning a wind energy project is to identify a suitable site, having strong and impressive wind spectra [2]."

"Wind is stochastic in nature. Speed and direction of wind at a location vary randomly with time. Apart from the daily and seasonal variations, the wind pattern may change from year to year, even to the extent of 10 to 30 per cent. Hence, the behavior of the wind at a prospective site should be properly analyzed and understood. Realizing the nature of wind is important for a designer, as he can design his turbine and its components in tune with the wind characteristics expected at the site. Similarly a developer can assess the energy that could be generated from his project, if the wind regime characteristics are known [2]."

"Knowledge of the wind regime at a particular site is relevant to the following topics:

System Design: System design requires knowledge of representative average wind conditions, as well as information on the turbulent nature of the wind. This information is used in the design of a wind turbine intended for a particular site.

Performance Evaluation: Performance evaluation requires determining the expected energy productivity and cost effectiveness of a particular wind energy system based on the wind resource.

Siting: Citing requirements can include the assessment or prediction of the relative desirability of the candidate sites for one or more wind turbines.

Operations: Operation requirements include the need for wind resource information that can be used for load management, operational procedures (such as start-up and shut-down), and the prediction of maintenance or system life [3]."

2.1   Wind

"The world receives around $1.7*10^{14}$ kW of power from the sun in the form of solar radiation. This radiation heats up the atmospheric air. The intensity of this heating will be more at the equator (0° latitude) as the sun is directly overhead. Air around the poles gets less warm, as the angle at which the radiation reaches the surface is more acute. The density of air decreases with increase in temperature. Thus lighter air from the equator rises up into the atmosphere to a certain altitude and then spreads around. This causes a pressure drop around this region, which attracts the cooler air from the poles to the equator. This movement of air causes the wind [2]."

"Thus, the wind is generated due to the pressure gradient resulting from the uneven heating of earth's surface by the sun. As the very driving force causing this movement is derived from the sun, wind energy is basically an indirect form of solar energy. One or two per cent of the total solar radiation reaching the earth's surface is converted to wind energy in this way [2]."

"The wind described above, which is driven by the temperature difference, is called the geostrophic wind, or more commonly the global wind. Global winds, which are not affected by the earth surface, are found at higher altitudes. The rotation of earth leads to another phenomenon near its surface called the Coriolis effect, named after the famous mathematician Gustave Paspard Coriolis. Due to the Coriolis effect, the straight movement of air mass from the high pressure region to the low pressure region is diverted as shown in Figure 2.1. Under the influence of Coriolis forces, the air move almost parallel to the isobars. Thus, in the northern hemisphere, wind tends to rotate clockwise where as in the southern hemisphere the motion is in the anti-clockwise direction [2]."

High pressure region

Coriolis force

Force due to
pressure gradient

Resulting path

Low pressure region
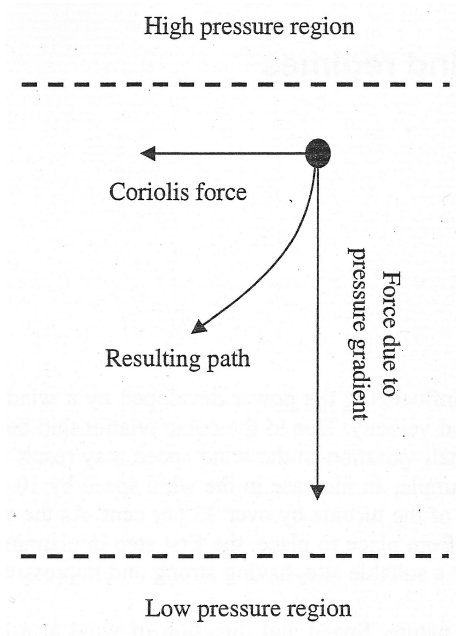
Figure 2.1 : Wind Direction affected by the Coriolis force

2.1.1 The local effects

The lower layer of the atmosphere is known as surface layer and extends to a height of 100 m [1]. In this region, the wind pattern is further influenced by several factors.

"Land and sea breezes are examples for the local wind effects. During the day time, land gets heated faster than the sea surface. As a result, the air near the land rises, forming a low pressure region. This attracts cool air to the land from the sea. This is called the sea breeze. During night time, the process gets reversed as cooling is faster on the land. Thus wind blows from the land to the sea, which is called the land breeze [2]."

"In mountain valleys, the air above the surface gets heated and rises up along the slopes during the day time. This is replaced by the cool air, resulting in the valley winds. During the night, the flow is from the mountain to the valley which is known as the mountain wind. Quite often, this phenomenon may create very strong air currents, developing powerful wind. Wind shear, turbulence and acceleration over the ridges are some other examples for local wind effects [2].

2.1.2 Wind shear

The flow of air above the ground is retarded by frictional resistance offered by the earth surface (boundary layer effect) [2]. This resistance may be caused by the roughness of the ground itself or due to vegetations, buildings and other structures present over the ground [2]. For example, a typical vertical wind profile at a site is shown in Figure 2.2. Theoretically, the velocity of wind right over the ground surface should be zero [2]. This phenomenon, called wind shear, is more appreciable as height decreases and has important effects on wind turbine operation [1]. Different mathematical models have been proposed to describe wind shear [1]. One of them is the Prandtl logarithmic law:

$$\frac{V_m(z)}{V_m(z_{ref})} = \frac{\ln(z/z_0)}{\ln(z_{ref}/z_0)} \tag{2.1}$$

where z is the height above ground level, z_{ref} is the reference height (usually 10 m) and z_0 is the roughness height [1]. Typical values of this parameter for different types of terrain are listed in Table 2.1. Another empirical formula often used to describe the effect of the terrain on the wind speed gradient is the following exponential law:

$$V_m(z) = V_m(z_{ref}) \left(\frac{z}{z_{ref}}\right)^a \tag{2.2}$$

where the surface roughness exponent α is also a terrain-dependent parameter [1]. Values of α for different types of surface are presented in the last column of Table 2.1.

2.1.3 Turbulence

By definition, turbulence includes all wind speed fluctuations with frequencies above the spectral gap [1]. Therefore, it contains all components in the range from seconds to minutes [1]. The speed and direction of wind change rapidly while it passes through rough surfaces and obstructions like buildings, trees and rocks. This is due to the turbulence generated in the flow [2]. Extent of this turbulence at the upstream and downstream is shown in Figure 2.3. In general, turbulence has a minor incidence on

the annual energy capture. However, it has a major impact on aerodynamic loads and power quality [1].
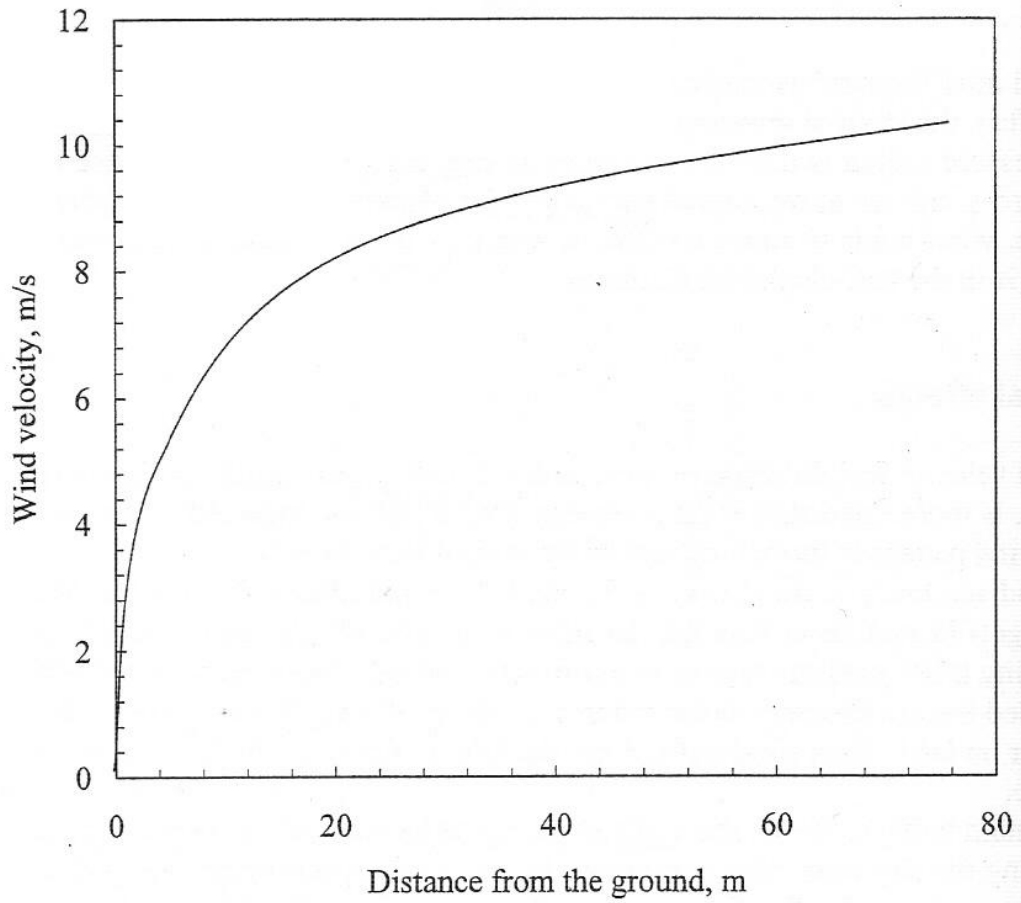
Figure 2.2 : Variation of wind velocity with height

Table 2.1 : Typical values of roughness length z_o and roughness exponent α for different types of surfaces

Type of Surface	z_0(mm)	A
Sand	0.2 to 0.3	0.10
mown grass	1 to 10	0.13
high grass	40 to 100	0.19
Suburb	1000 to 2000	0.32
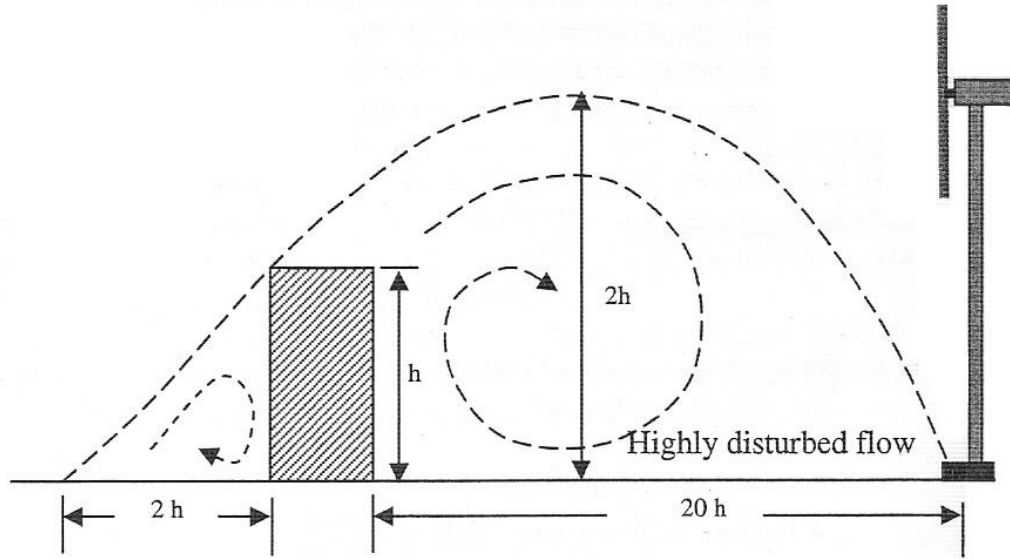
Figure 2.3 : Turbulence created by obstruction

Wind turbulence at a given point in space is stochastically described by means of its power spectrum. Two widely accepted models are the Von Karman spectrum:

$$\Phi(w) = \frac{K_v}{(1 + (wT_v)^2)^{5/6}} \tag{2.3}$$

and the Kaimal spectrum:

$$\Phi(w) = \frac{K_v}{(1 + wT_v)^{5/3}} \tag{2.4}$$

Both models are parameterized by constants T_v and K_v. Constant T_v determines the frequency bandwidth of the turbulence whereas K_v is associated to the turbulence power. In the time domain T_v is also a measure of the correlation time of the turbulence. Both parameters depend on the mean wind speed as well as on the topography of the terrain. For instance, in the case of the Von Karman spectrum, these coefficients are approximated by:

$$K_v = 0.475 s_v^2 \frac{L_v}{V_m(z)} \tag{2.5}$$

$$T_v = \frac{L_v}{V_m(z)} \qquad\qquad (2.6)$$

where L_v is the correlation length of the turbulence and σ_v is the turbulence intensity defined as the ratio of turbulence power:

$$P_v = \sqrt{\int_{-\infty}^{+\infty} \Phi(w)dw} \qquad\qquad (2.7)$$

to mean wind speed:

$$\sigma_v \cong \frac{P_v}{V_m(z)} \cong \frac{1}{\ln(z/z_0)} \qquad\qquad (2.8)$$

Both L_v and σ_v are specific to the terrain and are experimentally obtained from wind measures. The correlation length generally takes values ranging from 100 m to 300 whereas the turbulence intensity takes values between 0.1 and 0.2 [1].

Equation (2.8) shows that turbulence intensity decreases with height. It also turns out that turbulence intensity is higher when there are obstacles in the surroundings [1]. Intensity of the turbulence depends on the size and shape of the obstruction. Based on its nature, the turbulent zone can extend up to 2 times the height of the obstacle in the upwind side and 10 to 20 times in the downwind side. Its influence in he vertical direction may be prominent to 2 to 3 times the obstacle height. Hence before citing the turbine, the obstacles present in the nearby area should be taken into account. The tower should be tall enough to overcome the influence of the turbulence [2].

2.1.4 Acceleration Effect

A smooth ridge, as shown in Figure 2.4, accelerates the wind stream passing over it. The acceleration is caused by the squeezing of wind layers over the mount as shown in figure. The degree of acceleration depends on the shape of the ridge. This effect can be fully exploited for energy generation, if the slope of the ridge is between 6° and 16°. Angles greater than 27° and less than 3° are not favorable [2].
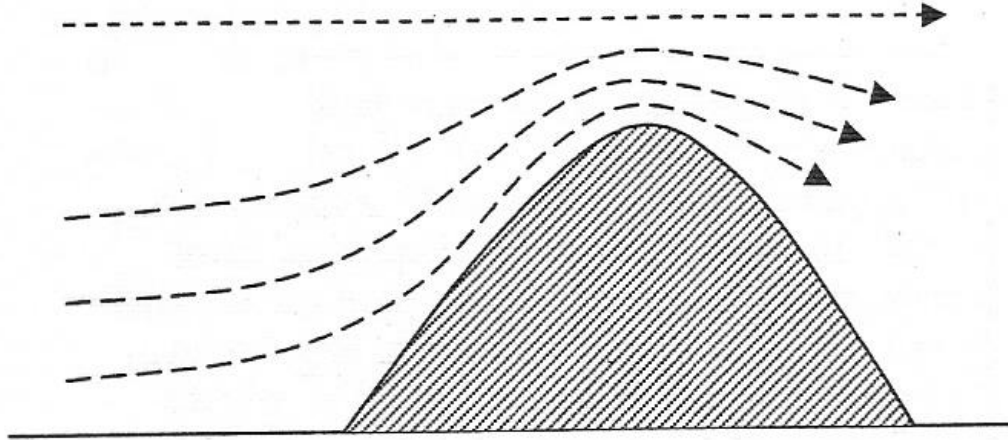
Figure 2.4 : The acceleration effect over ridges

Another important factor is the orientation of the ridge. The acceleration effect is high when the prevailing wind is perpendicular and low when it is parallel to the ridge line. Similarly, if the ridge concave side facing the wind, the effect is more desirable. Triangular shaped ridges offer better acceleration followed by the smooth and round geometry. Flat topped ridges may pose the problem of turbulence, especially in the lower region [2].

Mountain passes are another geographical feature causing acceleration of wind. While the flow passes through the notches in the mountain barriers, due the ventury effect, the wind velocity is enhanced. Geometrical configuration (Width, length, slope etc.) of the pass itself is the major factor determining the degree of this acceleration. A pass between two high hills, oriented parallel to the wind direction, would be a cleverly chosen site for wind turbines. The smoother the surface, the higher will be the acceleration [2].

2.1.5   Time variation

Velocity and direction of wind change rapidly with time. In tune with these changes, the power and energy available from the wind also vary. The variations may be short time fluctuation, day-night variation or the seasonal variation.

An example for the short time variation of wind speed is shown in Figure 2.5 (A), where the velocity is recorded for 30 s. Here the velocity fluctuates between 5.1 m/s

to 7.2 m/s within this time. This short-spanned change in wind speed is primarily due to the local geographic and weather effects. Stronger wind may be experienced during the day time rather than in night hours. This is termed as the diurnal variation. An example is illustrated in Figure 2.5 (B). The major reason for the velocity variation here is the difference in temperature between sea and land surface. It should be noted that the diurnal variation can be advantageous for wind energy generation as we may need more power during the day hours than at night.

Wind speed at a location may also change form season to season as shown in Figure 2.5 (C). In this case, the period between July to October is more or less lean for wind energy conversion. The root cause for seasonal variation is changes in daylight during the year due to the earth's tilt and elliptical orbit. This effect is more prominent near the poles. Knowledge of these time variations of velocity at a potential wind site is essential to ensure that the availability of power matches with the demand.

2.2   Wind Turbines

After describing the subsystems of the wind turbines, some relevant notions of aerodynamics will be presented and the expressions for the torque and forces developed on he wind turbines will be derived.

2.2.1   Wind turbine components

As it will be mentioned in the following subsection, the wind turbines are classified into vertical-axis and horizontal-axis ones depending on the position of the rotor axis. Only the horizontal-axis wind turbines are treated throughout this thesis.

The subsystems of a typical horizontal axis wind turbine are shown in Figure 2.6. These include:

The rotor, consisting of the blades and the supporting hub

The drive train, which includes the rotating parts of the wind turbine (exclusive of the rotor); it usually consists of shafts, gearbox, coupling a mechanical brake, and the generator
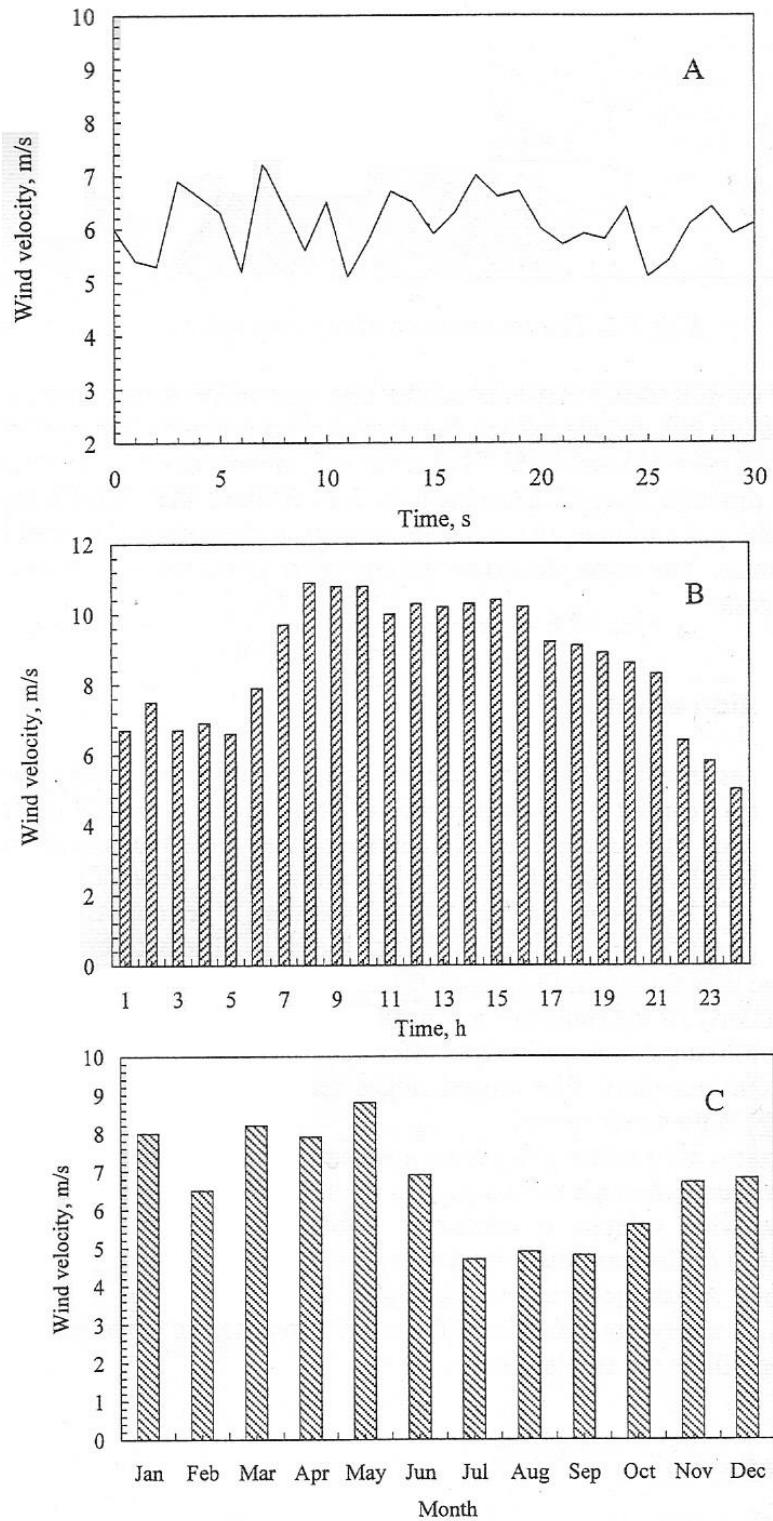
Figure 2.5 : Time variation of wind velocity

The nacelle and main frame, including wind turbine housing, bedplate, and the yaw system

The tower and the foundation

The machine controls

The balance of the electrical system, including cables, switchgear, transformers and possibly electronic power converters [3]
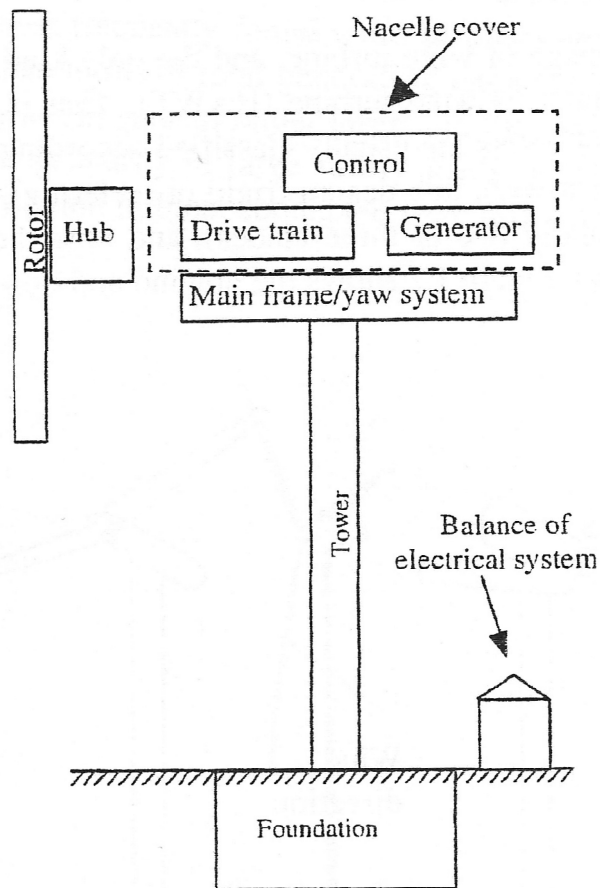
Figure 2.6 : Major components of a horizontal axis wind turbine

A detailed Figure showing the components of a horizontal axis wind turbine is given below.
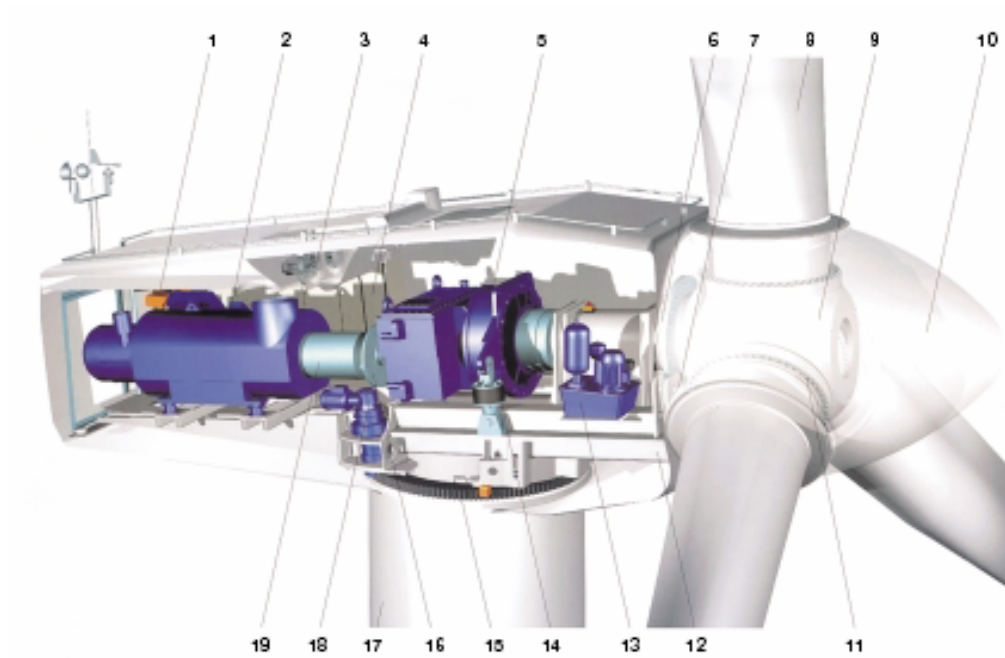
Figure 2.7 : System components of Gamesa-G52-850 kW

1- Service Crane   **11-** Blade Bearing

2- Generator   **12-** Bed Frame

3- Cooling System   **13-** Hydraulic Unit

4- Top Control Unit   **14-** Gear Reaction Arm

5- Gearbox   **15-** Yaw Ring

6- Main Shaft   **16-** Brake

7- Rotor Lock System   **17-** Tower

8- Blade   **18-** Yaw gears

9- Blade Hub   **19-** Transmission, high speed shaft

10- Nose cone

15

2.2.1.1 Rotor

Wind turbines are mechanical devices specially designed to convert part of the kinetic energy of the wind into useful mechanical energy. Several designs have been devised throughout the times. Most of them comprise a rotor that turns round propelled by lift or drag forces, which result from its interaction with the wind. Depending on the position of the rotor axis, wind turbines are classifed into vertical-axis and horizontal-axis ones [1].

Vertical Axis Turbines

Vertical axis wind turbines (VAWTs), such as the one shown in Figure 2.8 with C-shaped blades, are among the types of turbine that have seen the light of day in the past century [4]. The most successful vertical axis wind turbine is the one illustrated in Figure 2.8 named as the Darrieus rotor [1].

Figure 2.8 : Vertical Axis Wind Turbine

Classical water wheels allow the water to arrive tangentially to the water wheel at a right angle to the rotational axis of the wheel. Vertical axis wind turbines are designed to act correspondingly towards air. Though, such a design would, in principle, work with a horizontal axis as well, it would require a more complex design, which would hardly be able to beat the efficiency of a propeller-type turbine.

The major advantages of a vertical axis wind turbine, as the one illustrated in Figure 2.8, are that the generator and gearbox are placed on the ground and are thus easily accessible, and that no yaw mechanism is needed. Among the disadvantages is an overall much lower level of efficiency, the fact that the turbine needs total dismantling just to replace the main bearing, and that the rotor is placed relatively close to the ground where there is not much wind [4].

Horizontal Axis Turbines

*Horizontal axis wind turbines (HAWTs), such as the ones shown in Figure 2.9, constitute the most common type of wind turbine in use today. In fact all grid connected commercial wind turbines are today designed with propeller-type rotors mounted on a horizontal axis on top of a vertical tower. In contrast to the mode of operation of the vertical axis turbines, the horizontal axis turbines need to be aligned with the direction of the wind, thereby allowing the wind to flow parallel to the axis of rotation [4].

Figure 2.9 : Horizontal Axis, Upwind, Three Bladed Wind Turbine

Insofar as concerns horizontal axis wind turbines, a distinction is made between upwind and downwind rotors. Upwind rotors face the wind in front of the vertical tower and have the advantage of somewhat avoiding the wind shade effect from the presence of the tower. Upwind rotors need a yaw mechanism to keep the rotor axis aligned with the direction of the wind. Downwind rotors are placed on the lee side of the tower. A great disadvantage in this design is the fluctuations in the wind power due to the rotor passing through the wind shade of the tower which gives rise to more fatigue loads. Theoretically, downwind rotors can be built without a yaw mechanism, provided that the rotor and nacelle can be designed in such a way that the nacelle will follow the wind passively. This may, however, induce gyroscopic loads and hamper the possibility of unwinding the cables when the rotor has been yawing passively in the same direction for a long time, thereby causing the power cables to twist. As regards large wind turbines, it is rather difficult to use slip rings or mechanical collectors to circumvent this problem. Whereas, upwind rotors need to be rather inflexible to keep the rotor blades clear of the tower, downwind rotors can be made more flexible. The latter implies possible savings with respect to weight and may contribute to reducing the loads on the tower. The vast majority of wind turbines in operation today have upwind rotors [4].

The rotor consists of the hub and blades of the wind turbine. These are often considered to be its most important components from both a performance and overall cost standpoint.

Blade

Rotor blades are usually made of a matrix of fiber-glass mats, which are impregnated with a material such as polyester, hence the term glass fiber reinforced polyester, GRP. The polyester is hardened after it has impregnated the fiber-glass. Epoxy is sometimes used instead of polyester. Likewise, the basic matrix is sometimes made wholly or partly of carbon fibers, which form a lighter, but more expensive material with a high strength. Wood-epoxy laminates are sometimes used in large rotor blades [4].

The design of the outer contour of a wind turbine rotor blade is based on aerodynamic considerations. The cross-section of the blade has a streamlined asymmetrical shape, with the flattest side facing the wind. Once the aerodynamic outer contour is given, the blade is to be designed to be sufficiently strong and stiff. The blade profile is a hollow profile usually formed by two shell structures glued together, one upper shell on the suction side, and one lower shell on the pressure side. To make the blade sufficiently strong and stiff, so-called webs are glued onto the shells in the interior of the blade, thus forming a boxlike structure and cross-section as shown in Figure 2.10. From a structural point of view, this web will act like a beam, and simple beam theory can be applied to model the blade for structural analysis in order to determine the overall strength of the blade [4].
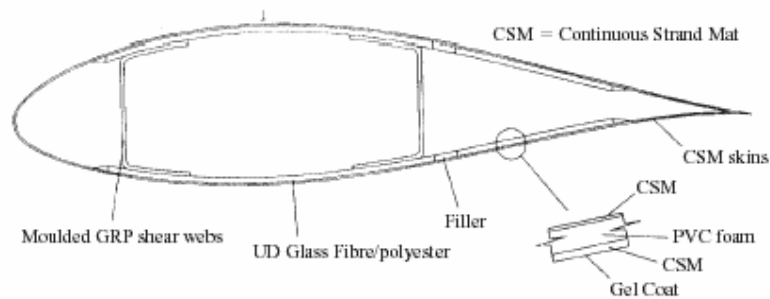
Figure 2.10 : Glass-fiber Blade Construction Using Blade Skins in Forward Portion of Blade Cross Section and Linking Shear Webs
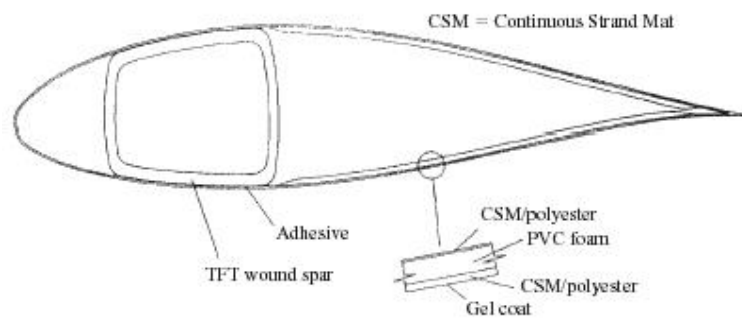
Figure 2.11 : Glass-fiber Blade Construction Using Compact Spar Wound with Transverse Filament Tape (TFT) on Mandrel.
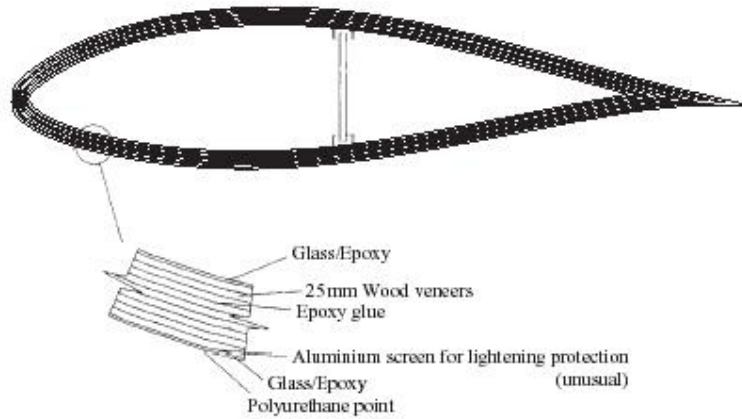
Figure 2.12 : Wood/Epoxy Blade Construction Utilizing Full Blade Shell
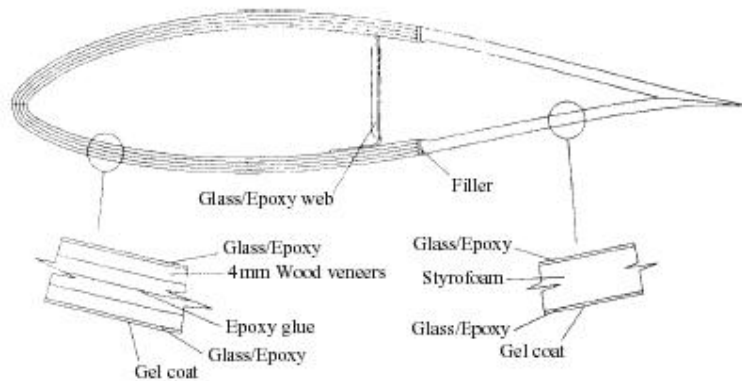
Figure 2.13 : Wood/Epoxy Blade Construction Utilizing Forward Half ofBlade Shell

It is important that the blade sections near the hub are able to resist forces and stresses from the rest of the blade. Therefore, the blade profile near the root is both thick and wide. Further, along the blade, the blade profile becomes thinner so as to obtain acceptable aerodynamic properties. As the blade speed increases towards the tip, also the lift force will increase towards the tip. Decreasing the chord width towards the tip will contribute to counteract this effect. In other words, the blade tapers from a point somewhere near the root towards the tip. In general, the blade profile constitutes a compromise between the desire for strength and the desire for good aerodynamic properties. At the root, the blade profile is usually narrower and tubular to fit the hub [4].

The blade is twisted along its axis so as to enable it to follow the change in the direction of the resulting wind along the blade, which the blade will experience when it rotates. Hence, the pitch will vary along the blade. The pitch is the angle between the chord of the blade profile and the rotor plane. Figure 2.14 illustrates the twist of a blade. Note in this context that the pitch angle, which is referred to throughout this document, usually refers to the collective rotation of the entire blade relative to the rotor plane [4].
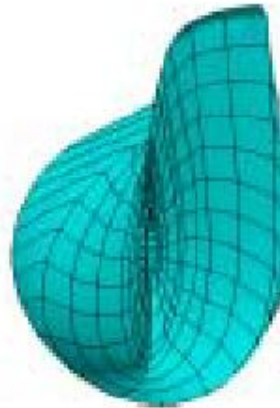
Figure 2.14 : View of a blade from the tip, illustrating the twist of the blade: the wind comes in from the left, and the pitch is 0° at the tip and about 25° at the hub.

For a blade, four non-coincident trajectories can be defined:

- mass axis, the span wise locus of section mass centers
- elastic axis, the span wise locus of points about which no section is exposed to bending deflection
- control axis, the axis of mechanical feathering, which is determined by the blade retention and pitching mechanism
- aerodynamic axis, the blade section quarter chord for a conventional airfoil shape within linear performance limits

These four trajectories are not axes in the true sense, since they – owing to the geometry of the blade – are not straight lines. However, for calculations for a particular section of the blade, four axes, perpendicular to the section, can be defined as the tangents to the trajectories at their respective intersections with the section [4].

Hub

The hub is the fixture for attaching the blades to the rotor shaft. It usually consists of nodular cast iron components for distribution of the blade loads to the wind support structure, i.e. ultimately to the tower. A major reason for using cast iron is the complex shape of the hub, which makes it hard to produce in any other way. In addition hereto, it must be highly resistant to metal fatigue. Thus, any welded hub structure is regarded as less feasible [4].
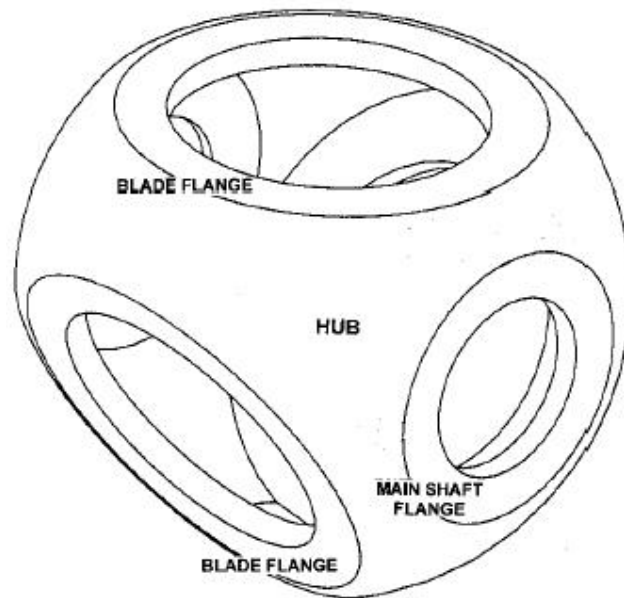
Figure 2.15 : View of wind turbine hub

The moments and forces transmitted to the hub and tower depend on the type of hub. Three types of hub are common:

- hingeless rigid hub, has cantilevered blades and transmits all moments to the tower
- teetering rotor, has two rigidly connected blades supported by a teeter pin joint, which can only transmit inplane moments to the hub. Flapwise moments are not transmitted
- articulated hub, has free hinges in flapping and lead-lag, so there is no mechanical restraint moment on the blades in either flapping or lead-lag

The hingeless hub is the most common configuration for wind turbine hubs [4].

Figure 2.15 shows an example of such a hub, and Figure 2.16 shows the hub in context of the transmission system, in which it forms part of the link between the rotor blades and the generator.
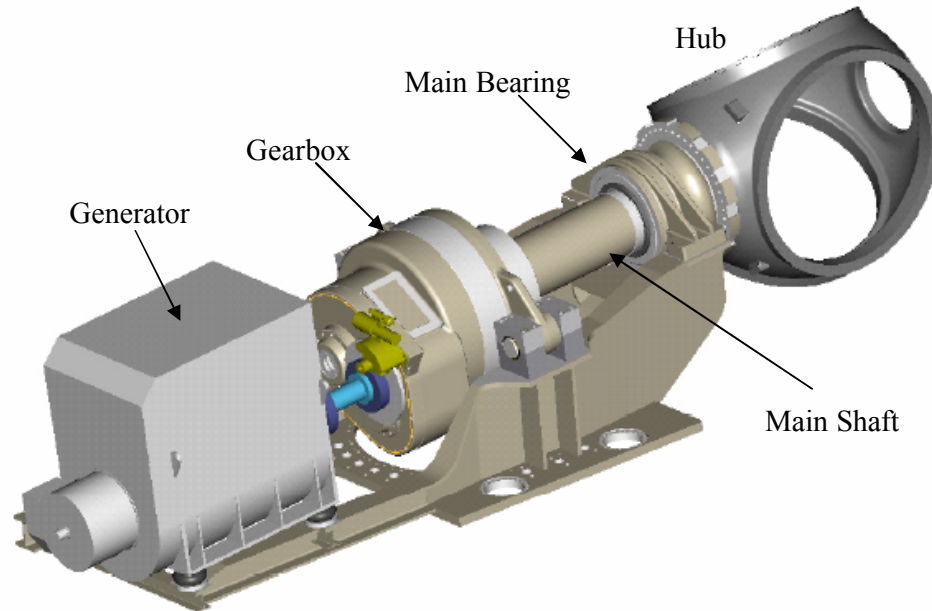
Figure 2.16 : Transmission system consisting of hub, one main bearing, main shaft, gearbox and generator

2.2.1.2 Drive train

The drive train consists of the rotating parts of the wind turbine. These typically include a low-speed shaft or main shaft (on the rotor side), a gearbox, and a high speed shaft (on the generator side). Other drive train components include the support bearings, one or more couplings, a brake and the rotating parts of the generator [3].

Main Shaft

The main shaft transmits the rotational energy from the rotor hub to the gearbox or directly to the generator. Moreover, the purpose of the main shaft is to transfer loads to the fixed system of the nacelle. In addition to the aerodynamic loads from the rotor, the main shaft is exposed to gravitational loads and reactions from bearings and gear [4].

The main shaft is also subjected to torsional vibrations in the drive train. Such vibrations will usually be of importance to possible frictional couplings like shrink fit couplings between shaft and gear [4].

A wind turbine can be exposed to large transient loads. Therefore, it has to be considered whether the chosen structural material possesses the necessary ductility. This is particularly important if the turbine is to be operated at low temperatures. Since corrosion may imply a considerable reduction of the assumed fatigue capacity, it should be ensured that the shaft is protected against corrosion. Suitable quality assurance should be implemented to make sure that the geometrical and mechanical assumptions for the design are fulfilled, e.g. surface roughness, that the specified values of material parameters are met, and that the imperfections of the material do not exceed any critical level [4].

Main Bearing

The main bearing of a wind turbine supports the main shaft and transmits the reactions from the rotor loads to the machine frame. On account of the relatively large deformations in the main shaft and its supports, the spherical roller bearing type shown in Figure 2.17 is often used [4].
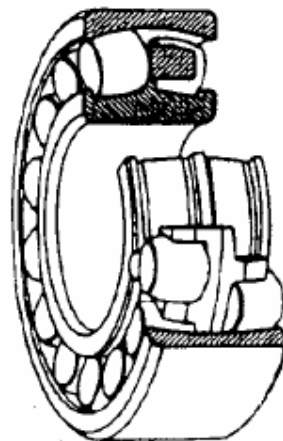
Figure 2.17 : Spherical roller bearing, from Bonus

Spherical roller bearings have two rows of rollers with a common sphered raceway in the outer ring. The two inner ring raceways are inclined at an angel to the bearing axis. The bearings are self-aligning and consequently insensitive to errors in respect

of alignment of the shaft relative to the housing and to shaft bending. In addition to high radial load capacity, the bearings can accommodate axial loads in both directions [4].

The allowable angular misalignment is normally 1-2.5 degrees depending on the bearing series. This is sufficient to compensate for deformations in shafts, housing and machine frame caused by the rotor loads and, subsequently, to prevent excessive edge loads, which would result in possible damage to the bearing [4].

The main bearings are mounted in bearing housings bolted to the main frame. The quantity of bearings varies among the different types of wind turbines. Many wind turbines have two bearings, each with its own flanged bearing housing. Some turbines with two bearings use the hub as a housing. Some turbines have only one main bearing, given that the gearbox functions as a second main bearing. Each bearing arrangement has its own advantages and disadvantages [4].

Gearbox

The most common gear types used in main gears for wind turbines can be identified and classified as follows, based on their geometrical design:

Spur and helical gears consist of a pair of gear wheels with parallel axes. Spur gears have cylindrical gear wheels with radial teeth parallel to the axes. In helical gears, the teeth are helical, i.e. they are aligned at an angle with the shaft axes. Double-helical gears have two sets of helical teeth on each wheel. Helical gears are sometimes referred to as spiral gears or oblique gears. See Figure 2.18.
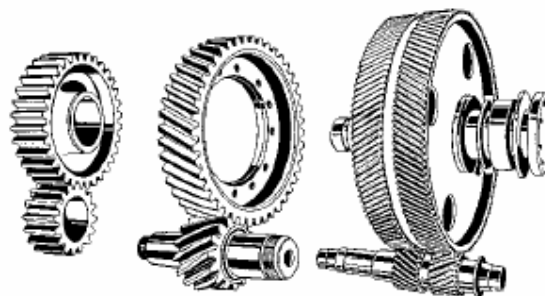
Figure 2.18 : Examples of spur and helical gears

Epicyclic or planetary gears consist of epicyclic trains of gear wheels, i.e. gears where one or more parts – so called planets – travel around the circumference of another fixed or revolving part. See Figure 2.19.
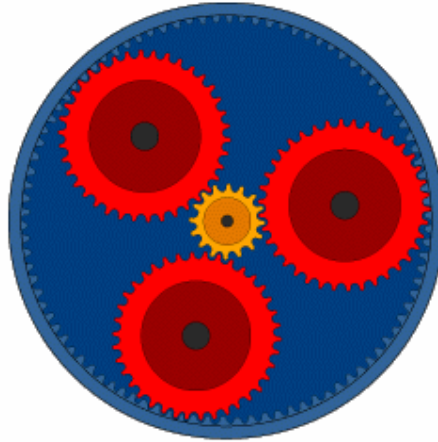
Figure 2.19 : Planetary gear principle, outer fixed annulus with three revolving planets and one rotating planet carrier in the middle

Planetary gears in combination with one or more parallel axis gears form the most commonly applied gear type for the main gear in wind turbines. Gears in which the power is transferred from one wheel to two or more meshing wheels are referred to as gears with a split power path.

Couplings

The major types of couplings are listed in the following along with issues of importance for their design.

Flange couplings

The flange thickness just outside the flange fillet is normally to be at least 20% of the required shaft diameter.

Coupling bolts are to be prestressed so that a suitable amount of prestress remains even under the most severe running conditions, in particular, with regard to bending moments. The level of safety is to be demonstrated in both the ultimate limit state

and the fatigue limit state. The same minimum safety factors as those for shaft design apply.

If the torque transmission is based only on friction between the mating surfaces of flange couplings, the friction torque (including the influence of axial forces and bending moments) is not to be less than 1.5 times the characteristic peak torque.

The torque transmission may also be based on a combination of shear bolts and friction between the mating flange surfaces. A basic principle is that both the friction alone (including the influence of axial forces and bending moments) and the shear bolts alone should be able to transmit the characteristic peak torque.

Shrink fit couplings

The friction connection is to be able to transmit at least 1.5 times the characteristic peak torque without slipping. Bending moment influence is to be considered.

For tapered mating surfaces where a slippage due to torque and/or axial force may cause a relative axial movement between the tapered members, the axial movement is to be prevented by a nut or similar. When a nut is required, the prestress is to be of the same magnitude as the axial force component from the tape.

The permissible material stress depends on the relative wall thickness, material type, and whether the coupling is demountable or not, and the usual range of permissible equivalent stress (von Mises) is 70% to 110% of the yield strength of the hub.

Key connections

The connection is to be able to transmit the characteristic peak torque.

The shear stress in the key is not to exceed 50% of the yield strength in shear. The pressure on the side of the keyway is not to exceed 85% of the yield strength of the key.

The yield strength to be applied in checks according to these two criteria is not to exceed 2/3 of the tensile strength of the key, and it is not to exceed twice the yield strength of the shaft or the hub, whichever is involved.

In principle, there is to be no clearance between the hub and the shaft, however, a certain amount of minimum interference fit is required, e.g. approximately 0.02% of the shaft diameter.

Torsionally elastic couplings

Rubber couplings are to be designed such that a failure of a rubber element does not cause loss of the connection between the rotor and the brake.

Tooth couplings

Tooth couplings are to have a reasonable degree of safety with respect to surface durability and tooth strength. This is subject to special consideration.

Mechanical Brake

Mechanical brakes are usually used as a backup system for the aerodynamic braking system of the wind turbine and/or as a parking brake, once the turbine is stopped, e.g. for service purposes. Mechanical brakes are sometimes also used as part of the yaw system. In a mechanical brake, brake callipers, brake discs and brake pads form crucial parts. A hydraulic system is usually used for the actuation and release of the brake.

Mechanical brakes can be active or passive, depending on how the hydraulic system of the brake is applied:

Active Brake: the pressure of the hydraulic system actively pushes the brake pads against the brake disc.

Passive Brake: the pressure of the hydraulic system keeps a spring tight. Once the pressure is released, the spring is also released and will push the brake pads against the brake disc.

In either case, the hydraulic pressure of the hydraulic system is crucial in order to be able to operate the brake as intended. The hydraulic pressure is usually provided by means of an accumulator. For active systems, it is particularly important to make sure that the pressure in the accumulator is always available, and it is important to have redundancy in this respect, i.e. an extra pressure source is necessary for backup.

The type of spring used in a mechanical brake to keep up a pressure is often a coil spring of the disc spring type. This type of spring is nonlinear and has the advantage that it is capable of maintaining an approximately constant spring pressure over a considerable range of deflection.

Generator

Generators will be discussed in the next section.

2.2.1.3 Nacelle and main frame

This category includes the nacelle enclosure, the machine bedplate or machine support frame and the yaw orientation system.

Nacelle Enclosure

The purpose of the nacelle enclosure is to protect the machinery and the control system of the wind turbine against rain and moisture and against salt and solid particles, such as sand grains in the air. The nacelle enclosure is also meant to protect against noise and is therefore often covered with some noise reducing material. The enclosure needs to be tight to fulfill its purpose. However, it also needs to have ventilation to allow for adequate cooling of the gear system. The nacelle enclosure is to be designed for wind load. In this context, it is important to choose correct lift and drag coefficients.

The nacelle enclosure is usually used also as a walkway and needs to be designed with sufficient dimensions for this purpose. In this context, it is particularly important to consider the design of the fixtures of the enclosure.

Moreover, it is important that the nacelle enclosure can be opened to allow for removal of damaged components for replacement, for example, by means of a helicopter.

Artificial light has to be installed to ensure safe access and working conditions.
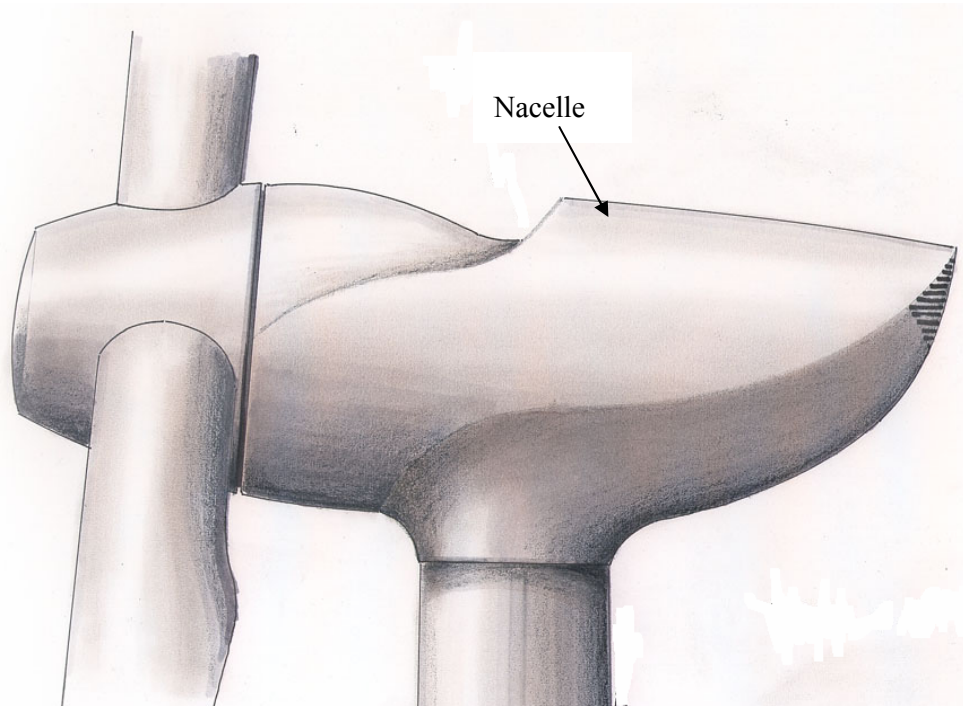
Figure 2.20 : Nacelle of Winwind 3MW wind turbine

Machine Support Frame

The machine support frame is located on top of the tower and supports the machinery, including the gear box. Usually, it also provides support for the nacelle cover. In contrast to the tower, the machine support frame is usually a very turbine-specific structure, which can be constructed in many different ways and according to many different layouts. It can be a welded, bolted or cast steel structure. Sometimes it is formed as an integral part of the gear box, i.e. the gear box itself acts as the machine frame. Sometimes it is integrated with the yaw system. Sometimes it is as simple as a big plate. It is, in general, a much less standardized product than a tower.

For design of the machine support frame, the following issues are important to consider:

- a sufficient stiffness of the frame must be ensured in order to meet the stiffness requirements for the machinery. The gear box should not be able to move relative to the bearings, and the yaw system will not get sufficient mesh with the gear rim if the frame is not sufficiently stiff.

- sufficiently fine tolerances must be met during the manufacturing of the frame in order to facilitate the proper positioning and assembly of the yaw system and the transmissions.
- the frame must be designed against fatigue owing to its exposure to the rotor forces.
- access to the nacelle is obtained through the tower and the machine support frame, which implies that the machine support frame must include a hole of convenient size for personnel to pass.

The machine support frame is exposed to rotor loads consisting of thrust, yaw moment and tilt moment. These load components are not necessarily in phase. In addition hereto comes weight. Also, local forces wherever forces are being transmitted should be considered, i.e. forces at bearing housings, gear shafts, and yaw system. It is recommended to use finite element methods for structural analysis of the machine support frame.
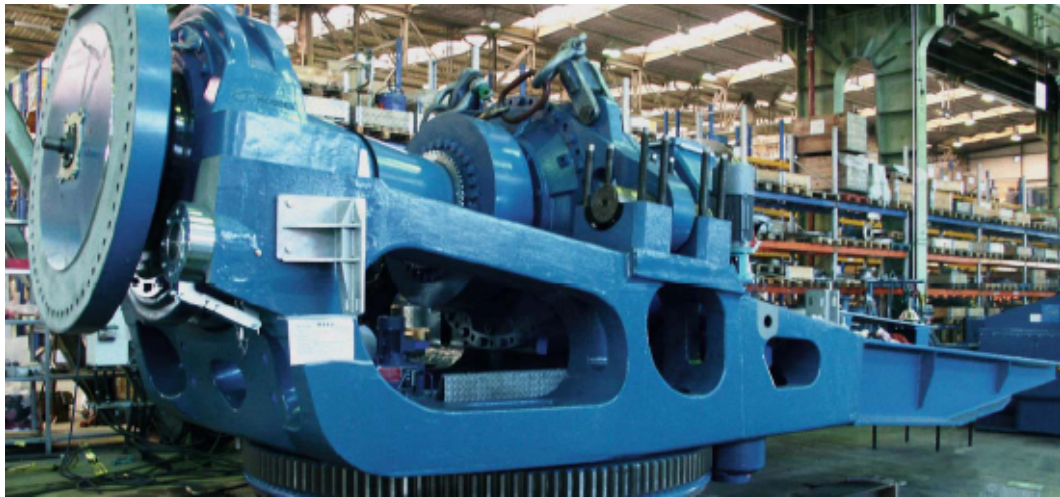
Figure 2.21 : Machine support frame of Nordex N90

Yaw System

Yaw denotes the rotation of the nacelle and the rotor about the vertical tower axis. By yawing the wind turbine, the rotor can be positioned such that the wind hits the rotor plane at a right angle. The yaw system provides a mechanism to yaw the turbine and to keep the rotor axis aligned with the direction of the wind. If situations occur where this alignment is not achieved, yaw errors are produced. The yaw error,

or the yaw angle, is defined as the angle between the horizontal projections of the wind direction and the rotor axis.

The yaw system can be either passive or active. A passive yaw system implies that the rotor plane is kept perpendicular to the direction of the wind by utilization of the surface pressure, which is set up by the wind and which produces a restoring moment about the yaw axis. For upwind turbines, this usually requires a tail vane in order to work properly. Also, coning of the rotor can help keeping the nacelle in place. Note that a passive yaw system may pose a problem in terms of cable twisting if the turbine keeps yawing in the same direction for a long time. An active yaw system employs a mechanism of hydraulic or electrically driven motors and gearboxes to yaw the turbine and keep it turned against the wind. Such active positioning of the turbine relative to the wind is also referred to as forced yaw. Most large horizontal axis wind turbines use forced yaw to align the rotor axis with thewind.

The mechanism used for an active yaw system usually consists of a number of electrically operated motors in conjunction with a gear that actuates a large toothed yaw ring in the tower circumference. Together with yaw brakes and yaw bearings, these components are most often delivered as standard components from a supplier, who also provides the pertaining design documentation. When used in a yaw system, it should be noted that these components may be exposed to conditions which have not been taken into account by the supplier. The following sections deal with the different components of an active yaw system, including the yaw ring, the yaw drive with the yaw motors, the yaw bearing, and the yaw brakes.

The yaw error is usually measured by means of direction sensors such as one or more wind vanes. The wind vanes are usually placed on top of the nacelle. Whenever the wind turbine is operating, an electronic controller checks the orientation of the wind vanes and activates the yaw mechanism accordingly. In addition to this automated yaw of the wind turbine, it should be possible to yaw the nacelle manually. Manual yaw is needed during start-up, service of the yaw system, and testing of the turbine.

2.2.1.4 Tower and the foundation

This category includes the tower structure and the supporting foundation.
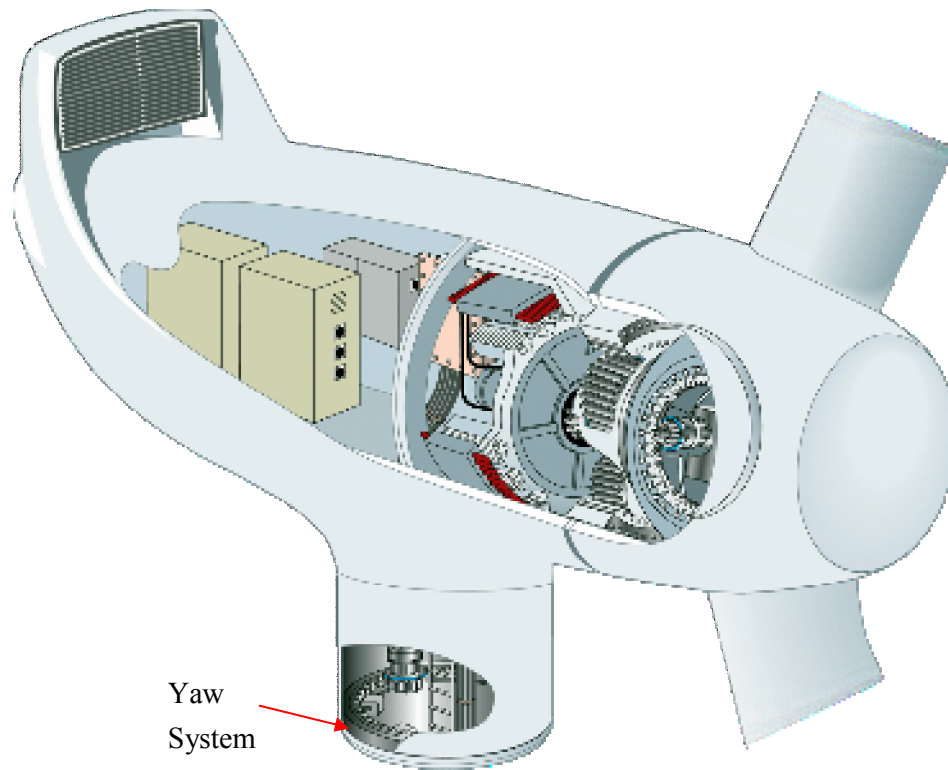
Figure 2.22 : Yaw System of Winwind 3 MW wind turbine

Tower

The tower of a wind turbine supports the nacelle and the rotor and provides the necessary elevation of the rotor to keep it clear off the ground and bring it up to the level where the wind resources are. The towers for large wind turbines are typically made of steel, but concrete towers are sometimes used. Nowadays, most towers are tubular towers; however, lattice towers are also in use. Guyed towers are used for relatively small wind turbines only. The tower is usually connected to its supporting foundation by means of a bolted flange connection or a weld.

In the context of wind turbines, the tower constitutes a low-technology component whose design is easy to optimize, and which therefore – during the design process – lends itself easily as an object for possible cost reduction. This may come in useful as the cost of a tower usually forms a significant part of the total cost of a wind turbine.

Figure 2.23 shows an array of the most common tower structures. The main features of the different tower types are briefly dealt with below.

Tubular steel tower   Tubular concrete tower   Lattice tower   Three-legged tower   Guy-wired pole tower

Figure 2.23 : Various tower structures

Tubular Towers

Most large wind turbines are delivered with tubular steel towers, which are manufactured in sections of 20-30 m length with flanges at either end. The sections are bolted together on the site. The towers are conical, their diameters increase towards the base, thereby increasing their strength towards the tower base, where it is needed the most, because this is where the load response owing to the wind loading is largest. Since the necessary shell thickness is reduced when the diameter increases, the conical shape allows for saving on the material consumption.

The maximum length of the tower sections is usually governed by requirements to allow for transportation. Also, the upper limit for the outer diameter of the tower is usually governed by such requirements, at least for land-based turbines – the maximum clearance under highway bridges in Denmark is 4.2 m. An advantage of tubular towers compared to other towers is that they are safer and more comfortable for service personnel and others that have to enter and climb the towers.

Lattice Towers

Lattice towers are manufactured by means of using welded steel profiles or L-section steel profiles. Since a lattice tower requires only about half as much material as a freely standing tubular tower with a similar stiffness, the basic advantage of lattice towers is reduced cost. It also gives less wind shade than a massive tower. The major

disadvantage of lattice towers is their visual appearance, although this is a debatable issue. Nevertheless, for aesthetic reasons lattice towers have almost disappeared from use for large, modern wind turbines.

Guyed Pole Towers

Many small wind turbines are built with narrow pole towers supported by guy wires. The advantage is weight savings and thereby reduced costs. The disadvantages include difficult access around the towers, which make them less suitable in farm areas. Finally, this type of tower is more prone to vandalism, thus compromising the overall safety.

Other Types

Some towers are designed as hybrids of the above types, for example the three-legged tower for a 95 kW turbine in Figure 2.23.

Foundation

Onshore wind turbines are usually supported by either a slab foundation or a pile foundation. Soil conditions at the specific site usually govern whether a slab foundation or a pile foundation is chosen. A slab foundation is normally preferred when the top soil is strong enough to support the loads from the wind turbine, while a pile supported foundation is attractive when the top soil is of a softer quality and the loads need to be transferred to larger depths where stronger soils are present to absorb the loads. When assessing whether the top soil is strong enough to carry the foundation loads, it is important to consider how far below the foundation base the water table is located. As regards offshore wind turbines, the foundation is a more comprehensive structure in that it includes a separate structure to transfer loads from the bottom of the wind turbine tower through the water to the supporting soils. In addition to the loads from the wind turbine, such a foundation structure will experience loads from current, waves and ice owing to its placement in a marine environment. Three basically different foundation structure concepts exist for offshore wind turbines:

- monopile
- gravity base

- tripod

The monopile is in principle a vertical pipe, driven or bored into the soil like any other pile, onto which the wind turbine tower is mounted. The gravity base foundation rests on the sea floor or on an excavated bottom by means of its own weight and is usually constructed from reinforced concrete. The wind turbine tower is mounted on top of this concrete structure. The gravity base foundation can also be constructed from steel in which case the necessary weight is achieved by placing a heavy ballast such as crushed olivine inside the cavities of the steel structure. The tripod foundation is a steel frame structure with three legs. The wind turbine tower is mounted on top of the tripod, while each leg is supported by either a driven pile or a suction bucket for transfer of loads to the supporting soils.

The choice of foundation type is much dependent on the soil conditions prevailing at the planned site of a wind turbine. Once a foundation concept has been selected and a foundation design is to be carried out, the following geotechnical issues need to be addressed:

- bearing capacity, i.e. geotechnical stability, e.g. against sliding and overturning
- degradation of soil strength in cyclic loading
- consolidation settlements
- differential settlements
- scour and erosion

.

3.   WIND TURBINE AERODYNAMICS

The turbine aerodynamics describes the forces developed on a wind turbine by an airflow. The two major approaches to derive aerodynamic models for wind turbines are the actuator disc theory and the blade element theory. The former explains in a simple manner the energy extraction process. Also, it provides a theoretical upper-bound to the energy conversion efficiency. The latter studies the forces produced by the airflow on a blade element. This theory is more suitable to explain some aerodynamic phenomena such as stall, as well as to study the aerodynamic loads [1].

3.1   Actuator Disc Model

This model is based on the momentum theory. The turbine is regarded as an actuator disc, which is a generic device that extracts energy from the wind. Consider the actuator disc is immersed in an airflow, which can be regarded as incompressible (Figure 3.1). Since the actuator disc extracts part of the kinetic energy of the wind, the upstream wind speed V is necessarily greater than the downstream speed $V_{-\infty}$. Consequently, for the stream tube just enclosing the disc, the upstream cross-sectional area A_∞ is smaller than the disc area AD, which in turn is smaller than the downstream cross-sectional area $A_{-\infty}$. This is because, by definition, the mass flow rate must be the same everywhere within the tube:

$$\mathsf{r}A_\infty V = \mathsf{r}A_D V_D = \mathsf{r}A_{-\infty} V_{-\infty} \qquad (3.1)$$

The air that passes through the disc undergoes a speed drop $V - V_{-\infty}$. Hence, the force F_D developed by the actuator disc on the incident airflow is the total speed drop times the mass flow rate:

$$F_D = (V - V_{-\infty})\mathsf{r}A_D V_D \qquad (3.2)$$

Usually, the speed at the disc is written as:

$$V_D = (1 - a)V \qquad (3.3)$$

37
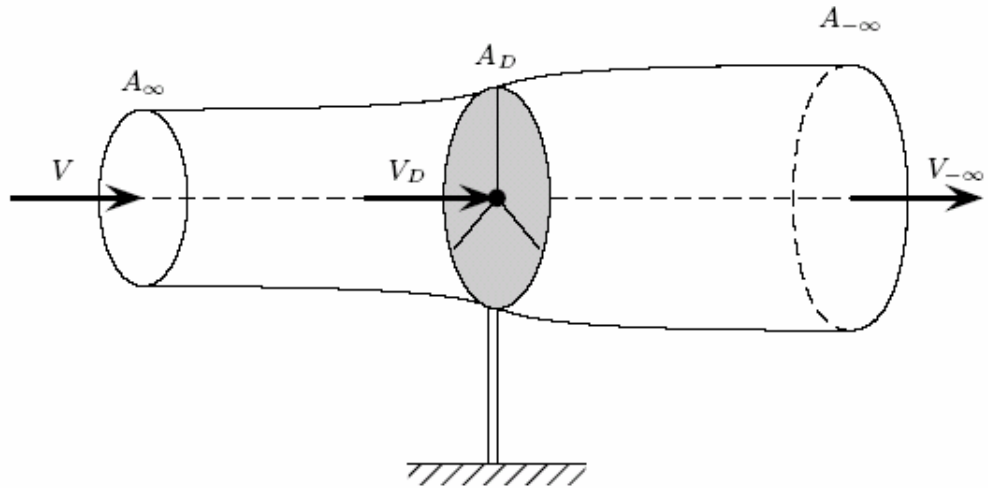
Figure 3.1 : Airflow through an actuator disc

where a is defined as the axial flow interference factor. The force F_D is originated by the pressure drop introduced by the actuator disc, that is:

$$F_D = (p_D^+ - p_D^-)A_D = (V - V_{-\infty})\Gamma A_D V(1-a) \tag{3.4}$$

where p_D^+ and p_D^- are the air pressure immediately before and after the disc. Figure 3.2 depicts how speed and pressure vary along the stream tube.
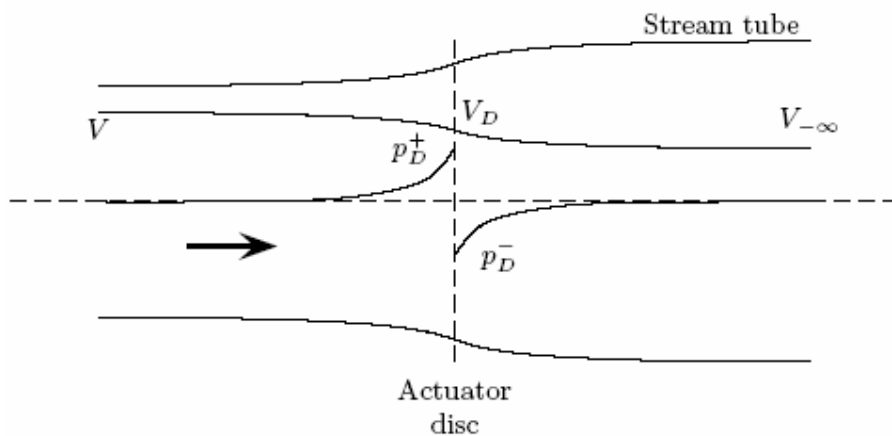
Figure 3.2 : Air speed and pressure throughout the stream tube

Bernoulli's equation is applied to obtain the pressure drop across the disc. This equation states that, under steady conditions, the total energy of the flow remains

constant provided no work is done on the fluid. This equation can be applied upstream and downstream because no work is done on the fluid but for the actuator disc:

$$\frac{1}{2}rV_D^2 + p_D^+ + rgz = \frac{1}{2}rV^2 + p_0 + rgz \tag{3.5}$$

$$\frac{1}{2}rV_D^2 + p_D^- + rgz = \frac{1}{2}rV_{-\infty}^2 + p_0 + rgz \tag{3.6}$$

where g is the gravity, p_0 is the atmospheric pressure and the flow is regarded as horizontal. Subtracting these equations, it is obtained:

$$p_D^+ - p_D^- = \frac{1}{2}r(V^2 - V_{-\infty}^2) \tag{3.7}$$

The replacement of (3.7) into (3.4) gives:

$$V_{-\infty} = (1 - 2a)V \tag{3.8}$$

It turns out that the momentum theory applies up to $a = 0.5$. This can be seen on noting in (3.8) that V$_{-\infty}$ becomes negative for larger values of a, what is obviously impossible.

By comparing (3.3) with (3.8), it follows that half of the speed drop occurs upstream of the disc and half downstream.

From (3.4), the force of the actuator disc on the airflow is:

$$F_D = 2rA_DV^2a(1-a) \tag{3.9}$$

Then, the power extracted from the wind by the actuator disc is given by:

$$P_D = F_DV_D = 2rA_DV^3a(1-a)^2 \tag{3.10}$$

3.2   Power Coefficient

A conventional way of characterizing the ability of a wind turbine to capture wind energy is the power coefficient, which is defined as the ratio of extracted power to wind power:

$$C_P = \frac{P_D}{P_V}$$

(3.11)

As the power in the wind passing through an area A_D with speed V is:

$$P_V = \frac{1}{2} r A_D V^3$$

(3.12)

using (3.10) and (3.12), the power coefficient results:

$$C_P = \frac{2 r A_D V^3 a (1-a)^2}{0.5 r A_D V^3} = 4a(1-a)^2$$

(3.13)

3.3   The Betz Limit

The maximum value of C_P occurs when:

$$\frac{dC_P}{da} = 4(1-a)(1-3a) = 0$$

(3.14)

which gives a value of $a = \frac{1}{3}$.

Hence,

$$C_{P\,max} = \frac{16}{27} = 0.593$$

(3.15)

This upper-bound applies for any type of wind turbine, even for vertical-axis ones though its derivation is different. The power coefficient of modern commercial wind turbines reaches values of about 0.5, well below the theoretical limit, though greater values have been reported for some particular designs. The power coefficient is usually provided by manufacturers. However, this data is not given as function of the

interference factor a, but as function of the tip-speed-ratio and pitch angle that will be explained later in this thesis.

3.4   Blade Element Model

The blade element theory is useful to derive expressions of developed torque, captured power and axial thrust force experienced by the turbine. This theory is based on the analysis of the aerodynamic forces applied to a radial blade element of infinitesimal length. To carry out the analysis, the stream tube just containing the turbine swept area is divided into concentric annular stream tubes of infinitesimal radial length, each of which can be treated independently.

Figure 3.3 illustrates a transversal cut of the blade element viewed from beyond the tip of the blade. In this figure, the aerodynamic forces acting on the blade element are also depicted. The blade element moves in the airflow at a relative speed V_{rel}, which as a first approach can be imagined as the composition of the upstream wind speed V and the tangential blade element speed $r\Omega_r$. In a later paragraph, some corrections will be introduced to account for the local flow variations caused by the turbine. Anyway, how V_{rel} is actually composed is immaterial for the moment. The airflow establishes a differential pressure around the blade element, which results in a force perpendicular to the local air movement direction, the so-called lift force f_L. Additionally, a drag force f_D is done in the flow direction.
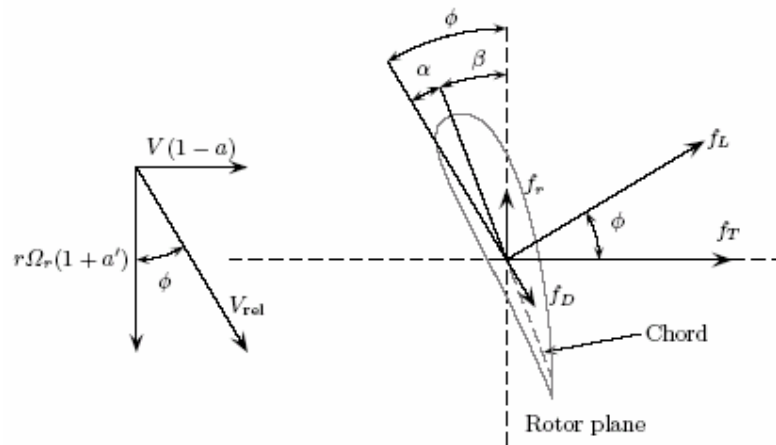
Figure 3.3 : Forces on a blade element

The lift and drag forces per unit length are generally expressed in terms of the lift and drag coefficients C_L and C_D:

$$f_L = \frac{rc}{2} V_{rel}^2 C_L(a) \tag{3.16}$$

$$f_D = \frac{rc}{2} V_{rel}^2 C_D(a) \tag{3.17}$$

where c is the chord length of the blade element. Both lift and drag coefficients are functions of the incidence angle α defined as the angle that the flow makes with the chord. As observed in Figure 3.3:

$$a = f - b \tag{3.18}$$

where f is the angle between the local flow direction and the rotor plane and the so-called pitch angle β is measured between the chord and the rotor plane. Note that the chord length and the pitch angle may vary along the blade, i.e., they may be functions of the radial distance r of the blade element to the axis of rotation.

Figure 3.4 plots typical shapes of coefficients $C_L(\alpha)$ and $C_D(\alpha)$ of an aerofoil. For low incidence angles, it is observed that C_L increases in proportion to α whereas $C_D(\alpha)$ remains almost constant and very low. However, an abrupt change occurs at $a \cong 13\,°$. When the incidence angle exceeds this critical value, the airflow is no more laminar and separates from the upper side of the aerofoil. This yields a differential pressure that reduces the lift and increases the drag. Under these conditions, it is said that the aerofoil stalls.

The lift and drag forces can be resolved into axial and tangential components. The former is called axial thrust force, and can be expressed per unit length as:

$$f_T = \frac{rc}{2} V_{rel}^2 (C_L(f - b)\cos(f) + C_D(f - b)\sin(f)) \tag{3.19}$$

This thrust force must be supported by the rotor, tower and foundations. On the other hand, the tangential force develops a rotational torque that produces useful work. This torque per unit length is given by:

$$t_r = \frac{rc}{2}V_{rel}^{2}(C_L(f-b)\sin(f) - C_D(f-b)\cos(f)) \qquad\qquad \textbf{(3.20)}$$
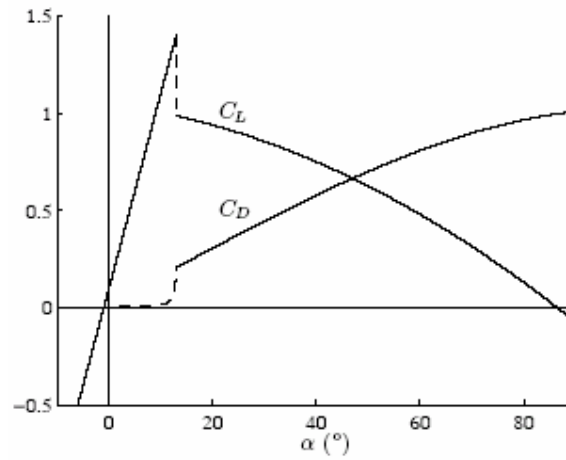
Figure 3.4 : Typical drift and drag coefficients of an aerofoil

Both lift and drag forces contribute to the axial thrust force. Further, the lift force develops useful torque whereas the drag opposes it. So, a high ratio C_L/C_D is desirable to achieve high conversion efficiency. In fact, the higher the ratio C_L/C_D, the higher will be the useful work. During stall, an abrupt drop of this ratio takes place. This is the basis for one of the most common methods to limit the captured power at winds exceeding the rated wind speed of the turbine.

To compute the contribution of each blade element to the global thrust force and rotational torque, the magnitude and direction of the relative air movement are needed. Therefore, let us redirect our attention to the relative speed V_{rel}. The analysis based on the actuator disc model showed that the airflow undergoes an overall speed drop $2aV$ (see Equation 3.8) and that half this speed drop occurs upstream so that the actual stream-wise speed at the disc is given by (3.3). Additionally, when the ideal actuator disc is replaced by a real turbine having a finite number of blades, the airflow suffers a change in its direction produced by the blade elements as reaction to the aerodynamic torque. This explains the helical wake that arises downstream of the turbines, which results from the superposition of the stream-wise speed and the rotational speed induced by the blades. The change in tangential speed is usually expressed as function of the tangential flow induction factor a'. Upstream of the disc the flow is axial, i.e., its rotational speed is zero. Immediately downstream of the

43

rotor area, the rotational speed is $2\Omega_r a'$. It is assumed that the rotational speed at the blade chord line is $\Omega_r a'$. Thus, the relative speed V_{rel} can be expressed as:

$$V_{rel} = V\sqrt{(1-a)^2 + \left(\frac{r\Omega_r}{V}(1+a')\right)^2} \tag{3.21}$$

$$\tan(\phi) = \frac{V}{r\Omega_r}\frac{1-a}{1+a'} \tag{3.22}$$

Note that the magnitude and direction of the relative wind speed vary along the blade span. Also, a and a' are generally not uniform over the blades.

3.5   Force, Torque and Power

The thrust force acting on the entire rotor and the total useful torque developed by the turbine are obtained by integrating (3.19) and (3.20) along the blades length. Commonly, thrust force, torque and power are expressed in terms of non-dimensional thrust (C_T), torque (C_Q) and power (C_P) coefficients as follows:

$$F_T = \frac{1}{2}\rho\pi R^2 C_T(\lambda,\beta)V^2 \tag{3.23}$$

$$T_r = \frac{1}{2}\rho\pi R^3 C_Q(\lambda,\beta)V^2 \tag{3.24}$$

$$P_r = C_P(\lambda,\beta)P_V = \frac{1}{2}\rho\pi R^2 C_P(\lambda,\beta)V^3 \tag{3.25}$$

where C_P and C_Q satisfy:

$$C_Q = \frac{C_P}{\lambda} \tag{3.26}$$

Note that the three coefficients are written in terms of the pitch angle and the so-called tip-speed-ratio λ defined as:

$$\lambda = \frac{\Omega_r R}{V} \tag{3.27}$$

This parameter is extremely important and, together with β in the case of variable-pitch rotors, determines the operating condition of a wind turbine. The parameter β will be used to denote pitch angle deviations introduced by pitch actuators in the case of variable-pitch wind turbines.

The torque and power coefficients are of special interest for control purposes. Figure 3.5 shows typical variations of C_Q and C_P with the tip-speed ratio and the pitch angle deviation. In the case of fixed-pitch wind turbines, C_Q and C_P vary only with λ, since $\beta = 0$ naturally. So, with some abuse of notation we will write $C_Q(\lambda)$ and $C_P(\lambda)$ to denote $C_Q(\lambda, 0)$ and $C_P(\lambda, 0)$, respectively. Figure 3.6 depicts typical coefficients $C_Q(\lambda)$ and $C_P(\lambda)$ of fixed pitch turbines in two-dimensional graphs.
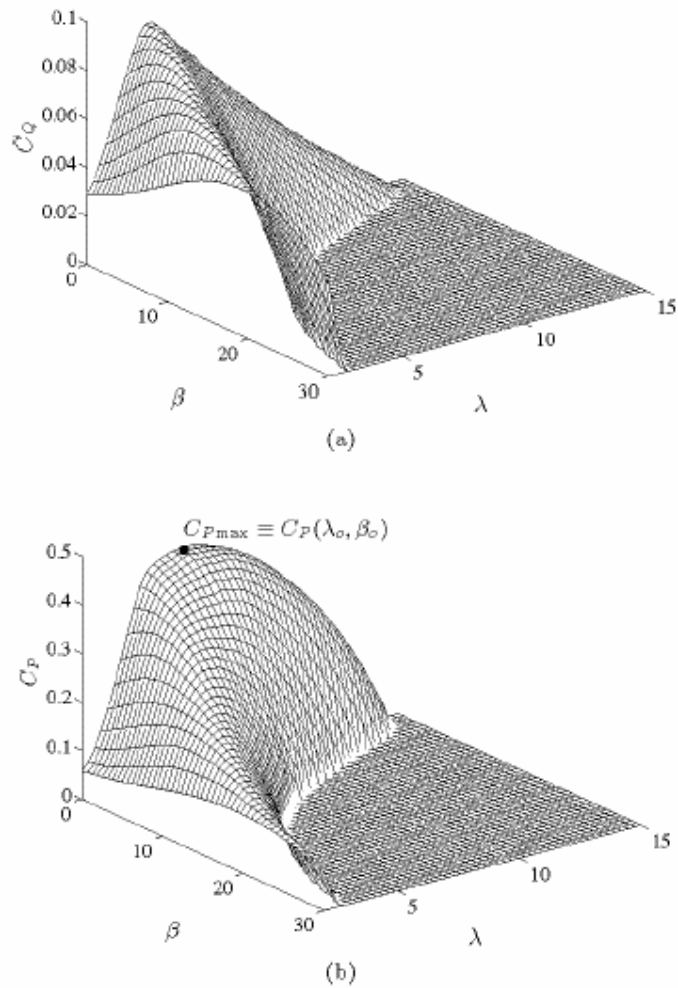
Figure 3.5 : Typical variations of (a)C_Q and (b)C_P for a variable pitch wind turbine
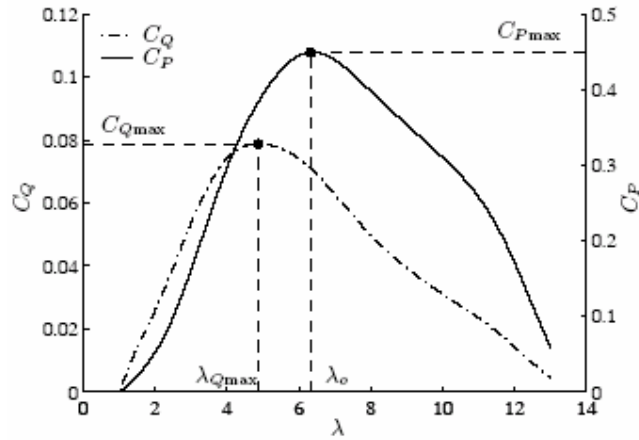
Figure 3.6 : Typical variations of C_Q and C_P for a fixed pitch turbine
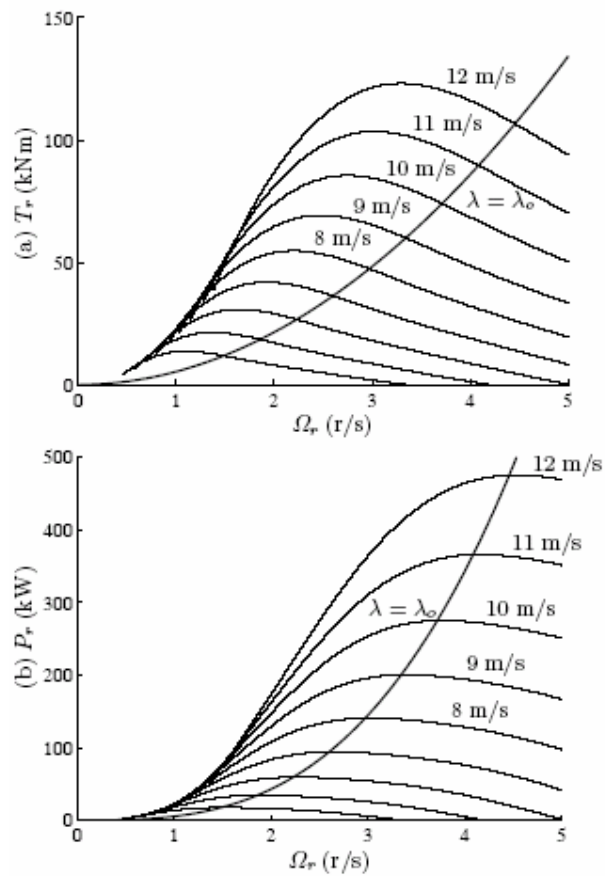
Figure 3.7 : (a) Torque and (b) power vs. rotor speed with wind speed as parameter and $\beta = 0$

The power coefficient C_P has its maximum at (λ_o, β_o), with β_o being a very small angle, ideally zero. This has a pair of important connotations. On the one hand, the

maximum at $\beta \cong 0$ means that any deviation of the pitch angle yields lower power capture. On the other hand, maximum conversion efficiency is accomplished at λo. So, fixed-speed turbines will operate with maximum efficiency just for a unique wind speed, whereas variable-speed turbines can potentially work with maximum efficiency over a wide wind speed range at least up to rated power. To realize the potential benefits of variable-speed operation, the rotational speed must be adjusted initially in proportion to the wind speed to maintain an optimum tip-speed-ratio. It can also be observed that the maximum of C_Q occurs at (λ_{Qmax}, βo), with $\lambda_{Qmax} < \lambda$o.

Figures 3.7 and 3.8 show aerodynamic torque and power vs. rotor speed with the wind speed and the pitch angle as parameters, respectively. The thick line plots the locus of maximum power efficiency ($\lambda = \lambda$o). It is observed that maximum torque and maximum power occur at different rotor speeds. More precisely, maximum torque occurs at lower speeds.
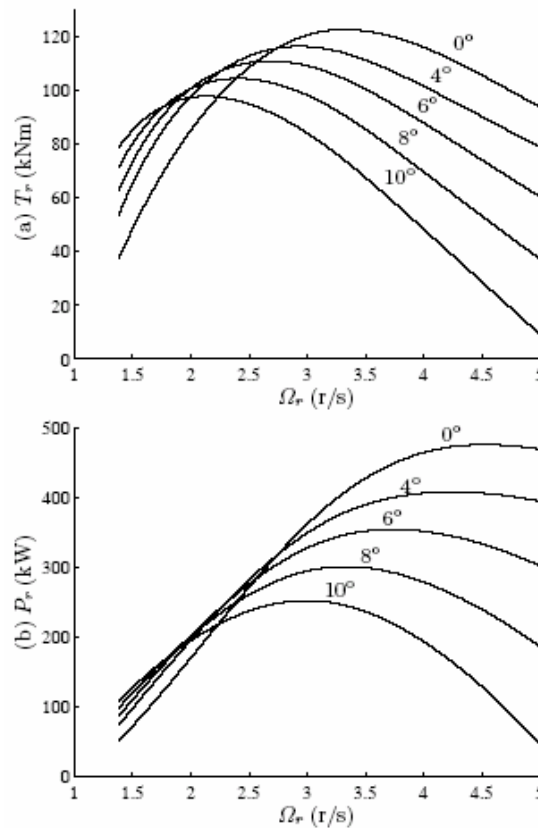
Figure 3.8 : (a) Torque and (b) power vs. rotor speed with pitch angle as parameter and V = 12 m/s

4.   MODELLING OF WIND TURBINES

The main components of a WECS are the rotor, the transmission system and the power generator unit.

Figure 4.1 outlines a horizontal-axis wind turbine. The rotor comprises the blades where the aerodynamic conversion takes place, the hub that links the blades to the transmission and the pitch servos, which are placed inside the hub, that rotate the blades around their longitudinal axes.
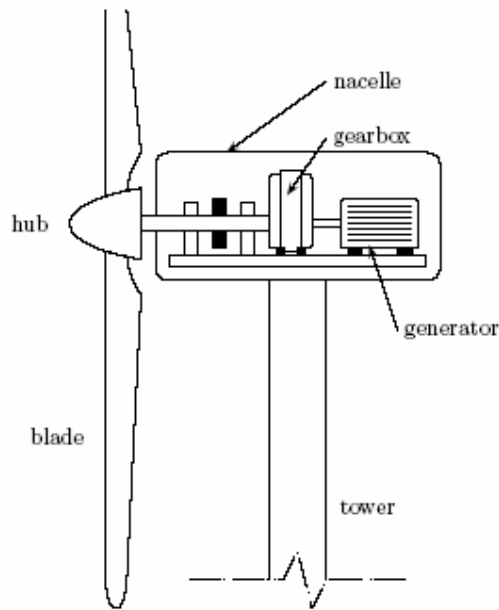
Figure 4.1 : WECS with horizontal axis wind turbine

The transmission system transmits the mechanical power captured by the rotor to the electric machine. It comprises the low- and high-speed shafts, the gearbox and the brakes. The gearbox increases the rotor speed to values more suitable for driving the generator, typically from 20-50 rpm to 1000-1500 rpm.

The electric generator is the device that converts mechanical power into electricity. Its electric terminals are connected to the utility network. In the case of variable-

speed WECS, an electronic converter is used as interface between the AC grid and the stator or rotor windings.

A model for the entire WECS can be structured as several interconnected subsystem models as it is shown in Figure 4.2. The aerodynamic subsystem describes the transformation of the three-dimensional wind speed field into forces on the blades that originate the rotational movement. The mechanical subsystem can be divided into two functional blocks, i.e., the drive-train and the support structure. The drive-train transfers the aerodynamic torque on the blades to the generator shaft. It encompasses the rotor, the transmission and the mechanical parts of the generator. The structure comprised by the tower and foundations supports the thrust force. The electrical subsystem describes the conversion of mechanical power at the generator shaft into electricity. Finally, there is the actuator subsystem that models the pitch servo behavior.

Since the dominant dynamics lie in the mechanical subsystem, the WECS will be regarded as a mechanical structure undergoing exogenous forces from the airflow and the electric machine.
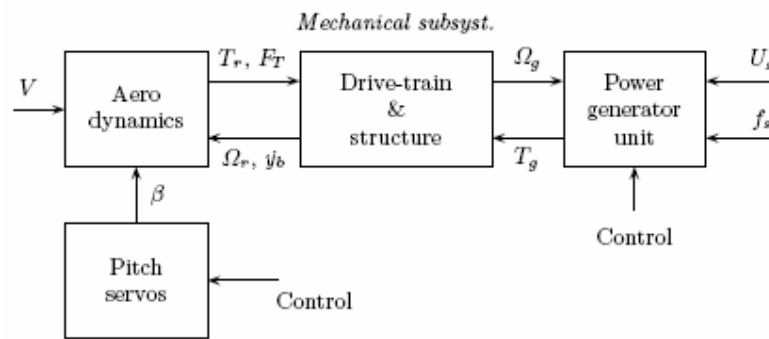
Figure 4.2 : Subsystem-level block diagram of a variable-speed variable-pitch WECS

4.1   Mechanical Subsystem

A horizontal-axis wind turbine is a complex mechanical system that consists of interacting devices with some degree of flexibility. Like any flexible structure, a wind turbine exhibits many vibration modes. Some oscillatory movements inherent to these modes are illustrated in Figure 4.3. The existence of these vibration modes

49

demands a careful design of the wind turbine and controller. Either the cyclic disturbances inherent to rotational sampling or an unsuitable control strategy may excite some of the vibration modes, hence resulting in lifetime reduction or even in fatigue breakdown.

For the modeling of the WECS, the most involved part is probably the mechanical subsystem. The complexity arises from the interaction of two flexible structures, the drive-train and the tower and foundations. Each of these structures is fixed to a reference frame that rotates with respect to the other. This leads to high-order nonlinear models. In addition, most of the forces applied to the structures come from a three-dimensional wind field.

There exists a wide range of computational tools specifically designed to derive models for WECS. The models obtained with these techniques are potentially very useful to validate turbine designs and to assess controller performance. However they are usually too complicated for control design purposes. Control-orientated models must be as simple as possible, capturing just the dynamic modes that may be excited by the controller.

(a) Torsion   (b) Flapwise

(c) Tower bending   (d) Edgewise
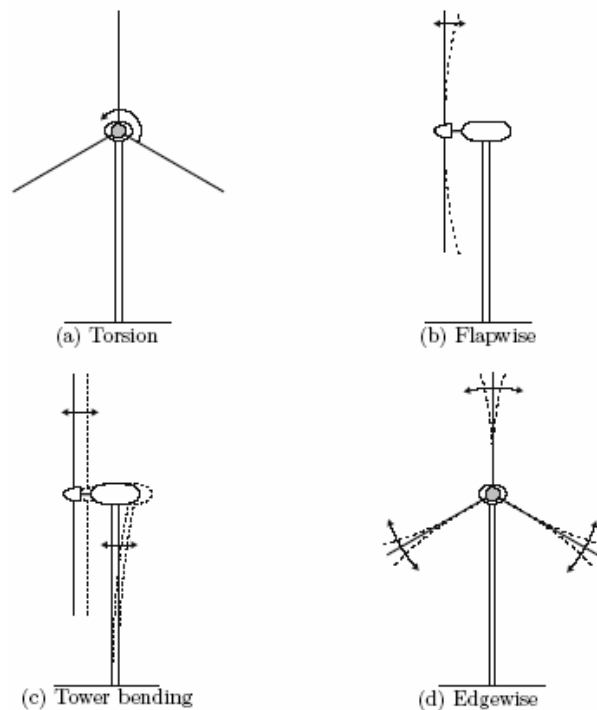
Figure 4.3 : Mode shapes for horizontal-axis wind turbines

Control-orientated models of WECS are generally derived using the so called Multibody System (MBS) approach. This technique provides reduced order models with deep physical insight. Conceptually, the mechanical structure is arranged into several rigid bodies linked by flexible joints. The amount of these joints or degrees of freedom determines the order of the model. Even a few degrees of freedom give rise to high order nonlinear models. Therefore, it is important to consider in the model just those degrees of freedom that are directly coupled to the control. On the one hand, speed control interacts with the modes in the plane of rotation, i.e., the torsion modes of the transmission and edgewise bending modes of the blades. Usually, it is sufficient to include in the model of variable-speed fixed-pitch wind turbines just one or two degrees of freedom in the plane of rotation, because most resonance frequencies fall beyond the controller bandwidth. This simplification leads to a linear model of reduced order. On the other hand, pitch control not only affects the aerodynamic torque but also the thrust force. Consequently, tower bending in the rotor axis direction and flapping should also be taken into account in the case of variable-pitch turbines.

Although simple models may not characterize thoroughly the dynamic behavior of the entire WECS, much can be learnt from them. Particularly, simple models are very helpful for a comparative analysis of different control strategies and for the controller design, whereas the unmodelled dynamics can be treated as uncertainties. By this reason, the model designed in this thesis will include just the first mode of the drive-train, the first mode of tower bending and the first mode of flapping.

Figure 4.4 shows a schematic diagram of the mechanical model. This model has three degrees of freedom, namely the torsion of the drive-train, the axial tower bending and the flapping. Figure 4.4a illustrates the drive-train, which is modeled as two rigid bodies linked by a flexible shaft. Figure 4.4b shows the model of the mechanical structure inspired in the work of Bindner [5]. It is assumed that the blades move in unison and support the same forces. Under this assumption, the model of the mechanical subsystem is linear.

With torsion of the drive-train, the fundamental resonance in the plane of rotation is actually denoted, which may lie either in the transmission or in the rotor. The drive-train model shown in Figure 4.4a is valid in any case. However, the flexible shaft

does not necessarily represents the transmission shafts but the most flexible part of the drive-train. The rigid bodies encompass all the mechanical devices and parts of them located at each side of the effective shaft. Accordingly, the terms 'rotor inertia' (Jr), 'generator inertia' (Jg), 'shaft stiffness' (Ks) and 'shaft damping' (Bs) denote model parameters, rather than physical ones.

A mechanical system of arbitrary complexity can be described by the equation of motion:

$$M\ddot{q} + C\dot{q} + Kq = Q\left(\dot{q}, q, t, u\right) \tag{4.1}$$

where **M**, **C** and **K** are the mass, damping and stiffness matrices and Q is the vector of forces acting on the system. For mechanical structures having few degrees of freedom, the Lagrange's equation:

$$\frac{d}{dt}\left(\frac{\partial E_k}{\partial \dot{q}_i}\right) - \frac{\partial E_k}{\partial q_i} + \frac{\partial E_d}{\partial \dot{q}_i} + \frac{\partial E_p}{\partial q_i} = Q_i \tag{4.2}$$

offers a systematic procedure to derive mathematical models. E_k, E_d and E_p denote the kinetic, dissipated and potential energy, respectively. Besides, q_i is the generalized coordinate and Qi stands for the generalized force.

For the model of Figure 4.4 the following generalized coordinates can be adopted:

$$q = \begin{bmatrix} y_t & z & q_r & q_g \end{bmatrix}^T \tag{4.3}$$

where y_t is the axial displacement of the nacelle, ζ is the angular displacement out of the plane of rotation and θ_r and θ_g are the angular positions of the rotor and generator, respectively. After these definitions, the energy terms E_k, E_d and E_p can be written as:
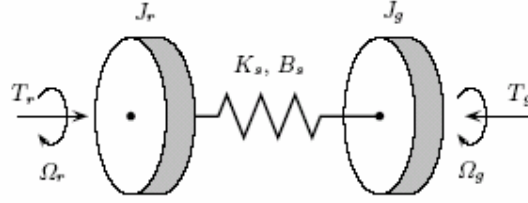
(a) Drive-train
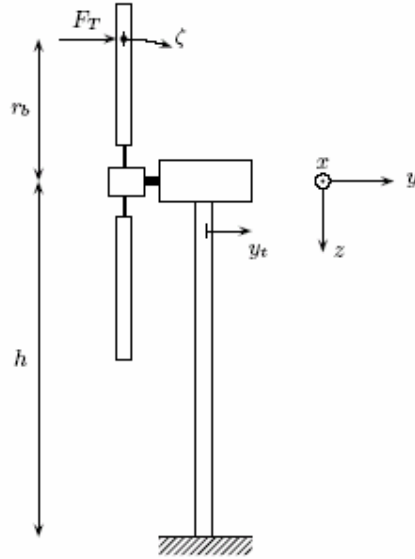
(b) Structure

Figure 4.4 : Schematic diagram of the mechanical subsystem

$$E_k = \frac{m_t}{2}\dot{y}_t^{\,2} + \frac{N}{2}m_b\left(\dot{y}_t + r_b\dot{z}\right)^2 + \frac{J_r}{2}\Omega_r^{\,2} + \frac{J_g}{2}\Omega_g^{\,2} \qquad (4.4)$$

$$E_d = \frac{B_t}{2}\dot{y}_t^{\,2} + \frac{N}{2}B_b\left(r_b\dot{z}\right)^2 + \frac{B_s}{2}\left(\Omega_r - \Omega_g\right)^2 \qquad (4.5)$$

$$E_p = \frac{K_t}{2}y_t^{\,2} + \frac{N}{2}K_b\left(r_b z\right)^2 + \frac{K_s}{2}\left(\Omega_r - \Omega_g\right)^2 \qquad (4.6)$$

where Ω_r and Ω_g are the rotational speeds of the rotor and generator, respectively, both of them referred to the low-speed side of the WECS. The remaining parameters are defined in Table 4.1. The vector of generalized loads is:

$$Q = \begin{bmatrix} NF_T & NF_T r_b & T_r & -T_g \end{bmatrix}^T \qquad (4.7)$$

In the previous equations the thrust forces distributed along each blade were replaced by a lumped force F_T applied at a distance r_b from the axis of rotation.

Table 4.1 : Parameters for the mechanical subsystem model referred to the low speed side of the WECS

Symbol	Description
m_t	Mass of the tower and nacelle
m_b	Mass of each blade
J_r	Inertia of the rotor
J_g	Inertia of the generator
K_t	Stiffness of the tower
K_b	Stiffness of each blade
K_g	Stiffness of the transmission
B_t	Damping of the tower
B_b	Damping of the blade
B_g	Damping of the transmission
N	Number of blades

Then, replacing (4.4) - (4.7) in the Lagrange's equation (4.2) yields the motion equation (4.1) with matrices:

$$M = \begin{bmatrix} m_t + Nm_b & Nm_b r_b & 0 & 0 \\ Nm_b r_b & Nm_b r_b^2 & 0 & 0 \\ 0 & 0 & J_r & 0 \\ 0 & 0 & 0 & J_g \end{bmatrix}$$

$$C = \begin{bmatrix} B_t & 0 & 0 & 0 \\ 0 & B_b r_b^2 & 0 & 0 \\ 0 & 0 & B_s & -B_s \\ 0 & 0 & -B_s & B_s \end{bmatrix}$$

$$K = \begin{bmatrix} K_t & 0 & 0 & 0 \\ 0 & K_b r_b^2 & 0 & 0 \\ 0 & 0 & K_s & -K_s \\ 0 & 0 & -K_s & K_s \end{bmatrix}$$

After some manipulation, the following state model arises:

$$\dot{x} = \begin{bmatrix} 0_4 & I_4 \\ -M^{-1}K & -M^{-1}C \end{bmatrix} x + \begin{bmatrix} 0_4 \\ M^{-1} \end{bmatrix} Q \qquad (4.8)$$

with the state x being defined as $x = \begin{bmatrix} q^T & \dot{q}^T \end{bmatrix}^T$.

Actually, the absolute angular positions of the drive-train components θ_r and θ_g are of no interest and moreover they may introduce numerical problems. So, it is convenient to remove them from the state and replace them with a single state variable $\theta_s = \theta_r - \theta_g$ denoting the torsion angle. After this substitution, the state model of the mechanical subsystem becomes:

$$\begin{aligned} \dot{x} &= Ax + Bu \\ y &= Cx \end{aligned} \qquad (4.9)$$

where the state input and output vectors are:

$$x = \begin{bmatrix} y_t & z & q_s & \dot{z} & \dot{y}_t & \Omega_r & \Omega_g \end{bmatrix} \qquad (4.10)$$

$$u = \begin{bmatrix} F_T & T_r & T_g \end{bmatrix}^T \qquad (4.11)$$

$$y = \begin{bmatrix} \dot{y}_t & \dot{z} & \Omega_r & \Omega_g \end{bmatrix}^T \qquad (4.12)$$

and the matrices A, B and C are:

$$A = \begin{bmatrix} 0_3 & L_{3x4} \\ -M^{-1}\tilde{K} & -M^{-1}C \end{bmatrix}, \quad B = \begin{bmatrix} 0_3 \\ M^{-1}Q \end{bmatrix}, \quad C = \begin{bmatrix} 0_{4x3} & I_4 \end{bmatrix}$$

with

$$
L_{3x4} = \begin{bmatrix} 1 & 0 & 0 & 0 \\ 0 & 1 & 0 & 0 \\ 0 & 0 & 1 & -1 \end{bmatrix}, \quad \tilde{K} = \begin{bmatrix} K_t & 0 & 0 \\ 0 & K_b r_b^{\,2} & 0 \\ 0 & 0 & K_s \\ 0 & 0 & -K_s \end{bmatrix}, \quad Q = \begin{bmatrix} N & 0 & 0 \\ N r_b & 0 & 0 \\ 0 & 1 & 0 \\ 0 & 0 & -1 \end{bmatrix}
$$

4.2   Aerodynamic Subsystem

The aerodynamic subsystem transforms the three-dimensional wind field into lumped forces acting on the rotor blades. As it is observed in the block diagram of Figure 4.2, the inputs to the aerodynamic subsystem are the wind speed V , the pitch angle β and the rotational and axial speeds of the rotor Ω_r and $\dot{y}_b = \dot{y}_t + r_b \dot{z}$, respectively. Its outputs are the aerodynamic torque T_r and the thrust force F_T. The input-output map of the aerodynamic subsystem is therefore described by the equations of torque and force derived in Section 3.5:

$$
\begin{bmatrix} F_T \\ T_r \end{bmatrix} = \begin{bmatrix} \dfrac{\mathsf{rp}R^2}{2} C_T\!\left(\dfrac{\Omega_r R}{V_e}, \mathsf{b} \right) V_e^{\,2} \\ \dfrac{\mathsf{rp}R^3}{2} C_Q\!\left(\dfrac{\Omega_r R}{V_e}, \mathsf{b} \right) V_e^{\,2} \end{bmatrix}
\tag{4.13}
$$

where the wind speed relative to the rotor is actually:

$$
V_e = V - \dot{y}_b
\tag{4.14}
$$

The additional term $\dot{y}_b$ accounts for the axial displacement of the blades caused by flapping and tower bending.

Note that (4.13) was derived in Section 3.5 assuming a stationary air-flow. In reality, the wind is not stationary and the aerodynamic torque and thrust force do not react instantaneously to a wind gust. Moreover, stall is a very complicated and rather unpredictable dynamic phenomenon that may exhibit some hysteresis. Nevertheless, more complicated dynamic models do not necessarily provide more reliable descriptions of the turbine behavior since these models are usually validated under unnatural conditions. By this reason, the stationary equations are conventionally accepted as dynamically valid ones for control analysis and design.

4.3 Electrical Subsystem

Induction generators are largely the most popular electric machines in WECS industry. Although synchronous generators can also be found, specially in autonomous systems, induction generators by far dominate the market for grid-connected wind turbines. Furthermore, modern wind turbines include sophisticated power electronics that modify the fundamental behavior of the induction machines. The dynamics of the electric machines, as well as of the power electronics associated to them, are much faster than the dominant mechanical modes. Therefore, a steady-state model of the power generator unit will be sufficient for our purposes.

Based on the electrical topology, wind-driven induction generators can be organized into three main categories sketched in Figure 4.5. Figure 4.5a illustrates the simplest configuration consisting of a standard squirrel-cage induction machine directly connected to the AC grid. In the arrangement shown in Figure 4.5b a fully-rated frequency converter is used as interface between the squirrel-cage induction generator and the grid. Finally, Figure 4.5c shows a doubly-fed induction generator with the stator windings connected directly to the grid and the rotor coupled to the grid through a static converter.

4.3.1 Directly coupled squirrel-cage induction generator

The squirrel-cage induction generator (SQIG) connected directly to the grid is a very reliable configuration because of the robust construction of the standard squirrel-cage machine and the simplicity of the power electronics. By this reason, this is the topology adopted in WECS based on the Danish concept.

In this scheme the voltage U_s and frequency f_s at the generator terminals are imposed by the grid. The steady-state torque - speed characteristic – or torque characteristic for short – is given by:

$$T_g = -\frac{3}{2}\frac{U_s^{\,2}}{w_s}\frac{R_r/s}{\left(R_r/s\right)^2+\left(w_s\,L_{lr}\right)^2} \tag{4.15}$$

(a) Directly coupled squirrel-cage induction generator

(b) Stator-controlled squirrel-cage induction generator

(c) Rotor-controlled doubly-fed induction generator
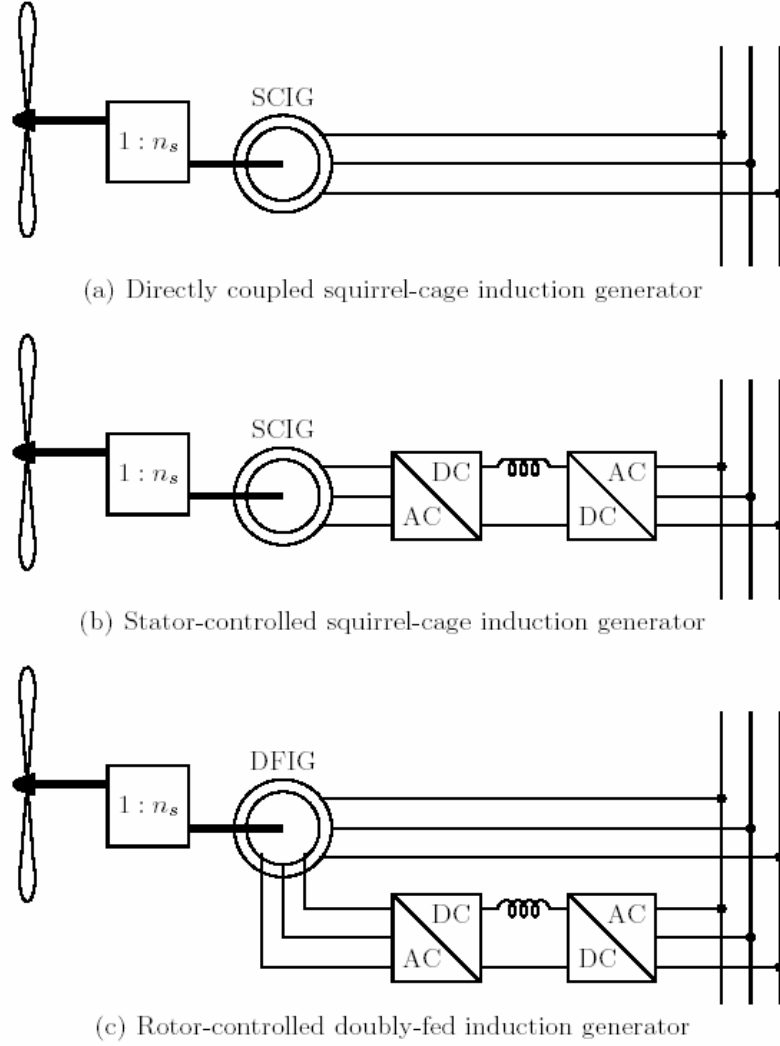
Figure 4.5 : Different connections of the induction generator to the grid

where $w_s = 2pf_s$ is the angular line frequency, R_r and L_{lr} are the resistance and leakage inductance of the rotor windings, respectively, and s is the generator slip defined as:

$$s = \frac{\Omega_s - \Omega_g}{\Omega_s} \tag{4.16}$$

The parameter Ω_s denotes the synchronous speed referred to the low-speed side of the drive-train. The synchronous speed is imposed by the line frequency. In fact, $\Omega_s = (p/2)w_s / n_s$ with p being the number of poles of the machine and n_s being

the gear ratio. Therefore, with U_s and f_s fixed, there is no active control on the generator.

The torque characteristic of the standard SCIG is depicted in Figure 4.6. It is observed that the machine operates as generator at super-synchronous speeds and as motor at sub-synchronous speeds. In both cases, the slip also represents the fraction of the mechanical power that is dissipated by the rotor resistance. Thus, large slip implies low efficiency. Consequently, SCIG work in normal operation with very low slip, typically around 2%. Therefore, the nonlinear torque characteristic can be linearly approximated by:

$$T_g = B_g (\Omega_g - \Omega_s) \tag{4.17}$$

where B_g is the slope of the real curve at Ω_s.

As can be observed, the generator speed Ω_g in normal operation is locked to the line frequency. By this reason, WECS having the electric machine directly connected to the AC grid are referred to as fixed-speed wind turbines. Although very simple and reliable, this configuration does not allow active control of the energy capture. In addition, the stiff connection to the AC grid provides negligible damping at the vibration modes of the drive-train.
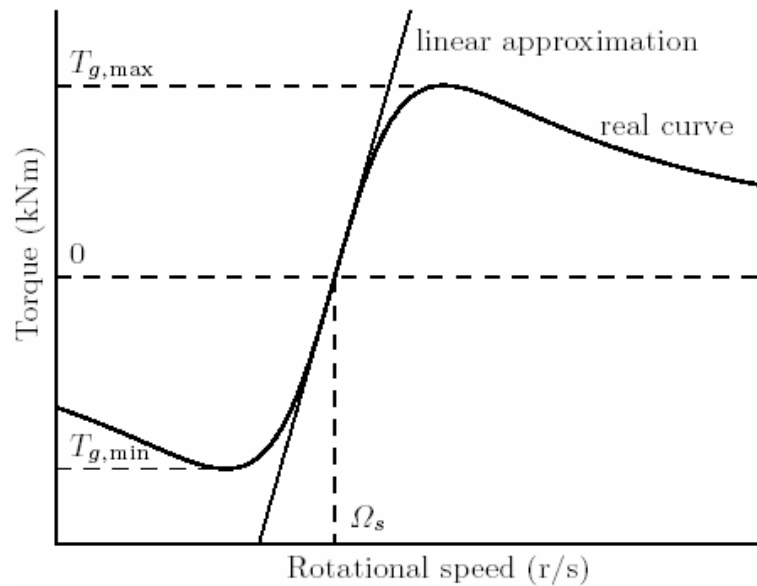

Figure 4.6 : Torque characteristic of the induction generator

59

4.3.2 Stator controlled squirrel-cage induction generator

Increasingly, advances in power electronics make it possible for static converters to handle large amounts of power at reasonable prices. Modern electronic converters are really useful to improve the quality of wind power. Additionally, they can be controlled to maximize the energy capture below rated power and to provide damping at the vibration modes of the drive-train. By these reasons, modern wind turbines are generally equipped with electronic converters that process all or part of the power supplied to the utility.

Conceptually, the arrangement shown in Figure 4.5b is the simplest variable-speed configuration, which retains the SCIG. A frequency converter is interposed between the generator and the AC grid. Thus, the WECS is completely uncoupled from the grid frequency. In this scheme, the frequency converter must handle all the energy supplied to the utility. In practice, the converter is rated up to 120% of nominal generator power. This is the main drawback of this scheme.

The frequency converter consists of two independent converters connected to a common DC-bus. The grid side converter transforms the three-phase AC grid voltage into a DC voltage. Additionally, the converter can potentially be controlled to produce or consume reactive power provided the apparent power does not exceed the converter rating. Therefore, the larger is the active power; the lower is the capability of the converter to handle reactive power. The stator side converter provides a three-phase voltage source of frequency f_s and voltage U_s uncoupled from the AC grid. Conventionally, this converter is controlled using the so-called U/f control technique. That is, the frequency f_s is controlled by keeping the ratio U_s/f_s constant. By this means the synchronous speed can be varied in a wide range whereas the magnetic flux of the machine is maintained more or less constant. Figure 4.7 depicts the torque characteristic of an induction generator parameterized by the stator frequency f_s under the assumption of constant stator flux. It is observed there that the torque characteristic of the SCIG is displaced in the x-axis direction as the stator frequency varies. Obviously, the mathematical law (4.15) describing the steady-state characteristic of the SCIG, as well as its linear approximation (4.17), is still valid keeping in mind that U_s/ω_s is constant. Actually, the synchronous speed Ω_s, which is

the shaft speed at no load condition (Tg = 0), can be regarded as control input to the electrical subsystem.
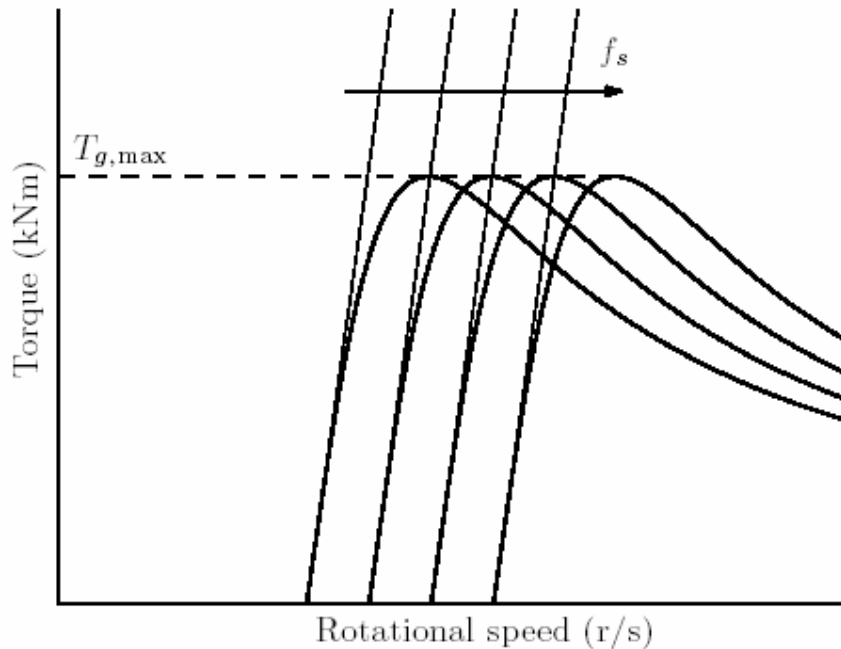
Figure 4.7 : Torque characteristic of the SCIG connected to grid through a U/f controlled frequency converter, with stator frequency as parameter

4.3.3   Rotor controlled doubly fed induction generator

The power generator unit sketched in Figure 4.5c is essentially a doubly-fed induction generator (DFIG) with variable frequency excitation of the rotor circuit. The stator windings are connected directly to the AC grid whereas the rotor windings are coupled through a partial scale back-to-back converter. Actually, this configuration accepts a wide range of power converters ranging from the early Kramer drive to four-quadrant pulse width modulated (PWM) frequency converters. Naturally, the control capabilities increase with the converter complexity. Independently of the converter used, the main advantage of this scheme is that the power electronics devices have to manage just a fraction of the captured power, typically around 30% of rated. The range of attainable rotational speeds is directly related to the converter rating relative to the machine rating. On the other hand, the

main drawback is the increased complexity of the DFIG, which is due to the presence of rotor windings, slip rings and brushes.

Modern large-scale wind turbines are mostly based on this configuration with a PWM frequency converter as an interface between the rotor windings and the AC grid. This scheme enables independent control of active and reactive power.

The fundamental behavior of the DFIG is inherently much more complicated than the SCIG one. Since the stator is connected directly to the grid, the synchronous speed remains constant and the magnetic flux is almost constant too. The differences with the standard SCIG arise in the rotor circuit. The frequency converter consists of a pair of power converters connected to a common DC bus. On the one hand, the grid side converter controls the DC bus voltage. In addition to handling the rotor branch power, it can be controlled to consume or produce reactive power. Obviously, the apparent power that the converter can manage is limited by its power rating. On the other hand, the rotor side converter controls the rotor currents in magnitude and phase. The field-orientation control technique suits very well to the control requirements. The electromagnetic variables of the machine can be referred to a reference frame fixed to the stator magnetic field, which rotates at the synchronous speed. In fact, the three-phase sinusoidal voltages and currents can be depicted as vectors in this rotating reference frame and can be resolved into orthogonal components in phase and in quadrature with the stator magnetic field, the so-called direct and quadrature components. The generator torque depends on the quadrature rotor current component whereas the stator reactive power is governed by the direct rotor current component. Therefore, active and stator reactive powers can be controlled independently by manipulating the quadrature and direct components of the rotor current, respectively. Obviously, the capability of the rotor side converter to control the stator reactive power is limited by the apparent power of the generator and the current limits of the power semiconductors.

As a result of the control strategy, the torque characteristic of the DFIG is very similar to that of the variable-speed SCIG where now the displacement in the *x*-axis direction is due to quadrature rotor voltage variations. Moreover, the zero-torque speed, also called no-load speed, is determined by this voltage component. For the

control purposes it is sufficient to choose this zero-torque speed as the manipulated control signal.

Because of the similarities in the steady-state torque characteristics, the analyses, control strategies and controller design carried out in this thesis are entirely valid for both schemes of variable-speed WECS depicted in Figures 4.5b and 4.5c. To unify the notation, Ω_z will be used to denote the zero-torque speed. This variable coincides with the synchronous speed for the configuration in Figure 4.5b and is determined by the quadrature rotor voltage for the configuration in Figure 4.5c. In any case, Ω_z will be regarded as control input to the electromechanical system and the torque characteristic will be approximated linearly by:

$$T_g = B_g (\Omega_g - \Omega_z) \tag{4.18}$$

4.4   Pitch Subsystem

Although passive stall regulation is a simpler alternative for power limitation, pitch control is usually preferred in medium to large wind turbines. Early wind turbine controllers relied on gradual changes of the pitch angle. The actuator consisted of counterweights that enable the rotation of the blades around their longitudinal axes. As turbine size increased, these rudimentary mechanisms were replaced by hydraulic or electromechanical devices. The higher flexibility of these devices permitted the implementation of efficient and reliable control strategies for power or speed limitation.

The pitch actuator is a nonlinear servo that generally rotates all the blades – or part of them – in unison. In closed loop the pitch actuator can be modeled as a first-order dynamic system with saturation in the amplitude and derivative of the output signal. Figure 4.8 shows a block diagram of the first-order actuator model. The dynamic behavior of the pitch actuator operating in its linear region is described by the differential equation:

$$\dot{b} = -\frac{1}{t} b + \frac{1}{t} b_d \tag{4.19}$$

where β and β_d are the actual and desired pitch angles, respectively. Typically, β ranges from -2° to 30° and varies at a maximum rate of ±10 deg/s. Power regulation may demand fast and large corrections of the pitch angle.
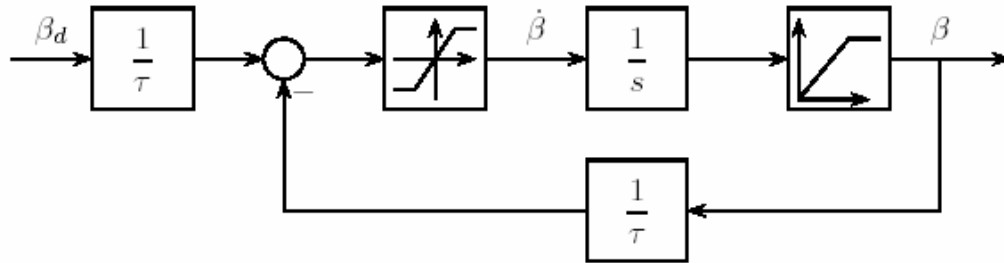

Figure 4.8 : Model of the pitch angle actuator

Consequently, the bounds on the rate of change and amplitude of the pitch angle have appreciable effects on the power regulation features. To reduce the risks of fatigue damage, these limits should not be reached during normal operation of the turbine.

5. CONTROL OBJECTIVES AND STRATEGIES

5.1 Control Objectives

A wind turbine is essentially a device that captures part of the wind energy and converts it into useful work. In particular, WECS connected to electric power networks must be designed to minimize the cost of supplied energy ensuring safe operation as well as acoustic emission and power quality standards.

The minimization of the energy cost involves a series of partial objectives. These objectives are actually closely related and sometimes conflicting. Therefore, they should not be pursued separately. Conversely, the question is to find a well balanced compromise among them. These partial goals can be arranged in the following topics:

Energy capture: Maximization of energy capture taking account of safe operation restrictions such as rated power, rated speed and cut-out wind speed, etc.

Mechanical loads: Preventing the WECS from excessive dynamic mechanical loads. This general goal encompasses transient loads alleviation, high frequency loads mitigation and resonance avoidance.

Power quality: Conditioning the generated power to comply with interconnection standards.

5.1.1 Energy capture

For a wind turbine, the generation capacity specifies how much power can be extracted from the wind taking into consideration both physical and economic constraints. It is usually represented as a curve on the generated power – wind speed plane, the so-called ideal power curve.

The ideal power curve for a typical wind turbine is sketched in Figure 5.1. It is observed that the range of operational wind speeds is delimited by the cut-in (V_{min}) and cut-out (V_{max}) wind speeds. The turbine remains stopped beyond these limits. Below cut-in wind speed, the available wind energy is too low to compensate for the operation costs and losses. Above cut-out wind speed, the turbine is shut down to prevent from structural overload. Constructing the turbine robust enough to support the underlying mechanical stresses under very high wind conditions would be completely uneconomical. In fact, even though wind speeds above V_{max} contain huge energy, their contribution to the annual average energy is negligible. This is corroborated by Figure 5.2 where a typical power density function at a given site is outlined. It is observed there that the energy left to be captured because of keeping the turbine stopped beyond the wind speed limits V_{min} and V_{max} is comparatively low.

It can also be noted in Figure 5.1 that the ideal power curve remains constant at rated power P_N above wind speed V_N named rated wind speed V_N. The rating of the turbine arises from a compromise between available energy and manufacturing costs. For instance, designing the turbine to extract all the available energy up to cut-out wind speed would lead to an increment in the cost per kW. In fact, wind speeds above V_N are not frequent enough to justify the extra sizing of the turbine required to capture power above rated.
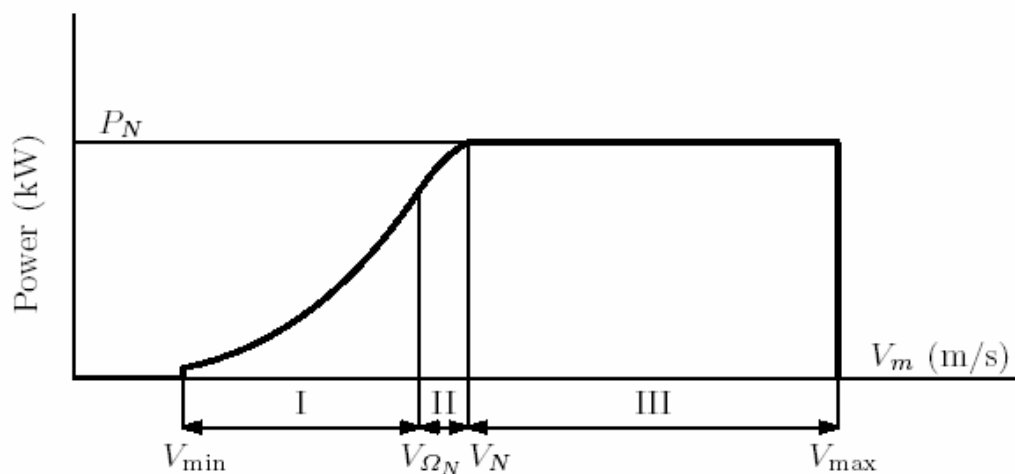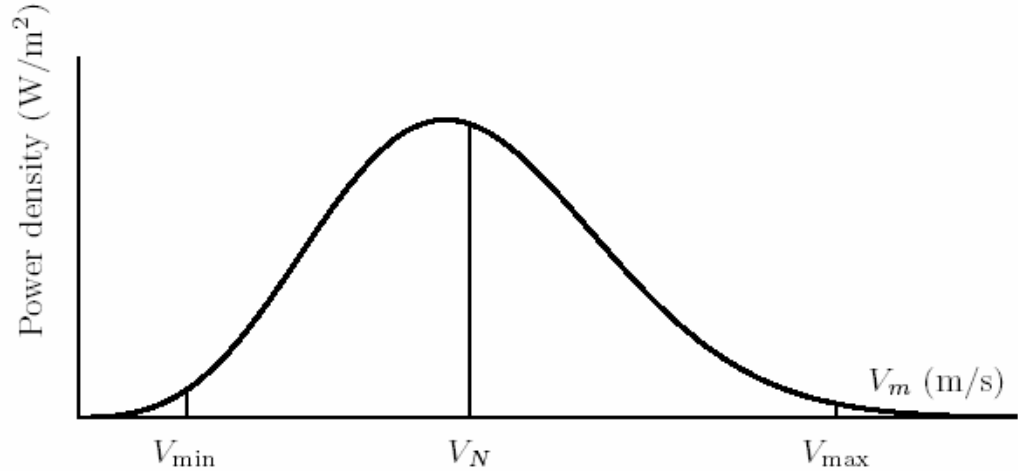

Figure 5.1 : Ideal Power Curve

Figure 5.2 : Power density vs. wind speed

The ideal power curve exhibits three different regions with distinctive generation objectives. At low wind speeds (region I), the available power is lower than rated power. The available power is defined as the power in the wind passing through the rotor area multiplied by the maximum power coefficient C_{Pmax}, that is:

$$P_{av} = C_{P\max} P_V = \frac{1}{2} \rho R^2 C_{P\max} V^3 \qquad (5.1)$$

So, the generation objective in region I is to extract all the available power. Therefore, the ideal power curve in this region follows a cubic parabola defined by (5.1).

On the other side, the generation goal in the high wind speed region (region III) is to limit the generated power below its rated value to avoid over-loading. In this region the available power exceeds rated power; therefore the turbine must be operated with efficiency lower than C_{Pmax}. Finally, there is region II, which is actually a transition between the optimum power curve of region I and the constant power line of region III. In this region, rotor speed is limited to maintain acoustic noise emission within admissible levels and to keep centrifugal forces below values tolerated by the rotor. Eventually, in the case that such a speed limit is not reached, region II may not exist and the optimum power curve may continue until getting to rated power.

67

5.1.2 Mechanical loads

Keeping in mind the minimization of the energy cost, the control system should not merely designed to track as tightly as possible the ideal power curve. In fact, the other control objectives must not be ignored. For instance, the mechanical loads wind turbines are exposed to must also be considered. Mechanical loads may cause fatigue damage on several devices, thereby reducing the useful life of the system. Since the overall cost of the WECS is therefore spread over a shorter period of time, the cost of energy will rise.

There are basically two types of mechanical loads, namely static and dynamic ones. Static loads result from the interaction of the turbine with the mean wind speed. Much more important from the control viewpoint are the dynamic loads, which are induced by the spatial and temporal distribution of the wind speed field over the area swept by the rotor. Dynamic loads comprise variations in the net aerodynamic torque that propagate down the drive-train and variations in the aerodynamic loads that impact on the mechanical structure. They are the so-called drive-train and structural loads, respectively.

There is also another common classification of dynamic loads. On the one hand there are the transient loads, which are induced by turbulence and gusts. They are predominantly of low frequency. Transient loads have very important implications in high wind speeds, particularly for the determination of the components rating. The transition between maximum power tracking (region I) and power regulation (region III) and the way power is limited in above rated wind speeds have a direct impact on transient loads. Unsuitable control strategies may inevitably lead to strong transient loads. Therefore, the planning of the control strategy must also take them into consideration. In addition, controller setup and design also influence the transient loads. In fact, the tighter the closed-loop system follows the steady-state control strategy curve after a wind gust, the heavier the transient loads will be.

On the other hand, rotational sampling induces high-frequency cyclic loads concentrated around spectral peaks at multiples of rotor speed. For an N-bladed wind turbine, the spectral peak at NP predominates in cyclic drive-train loads whereas the energy of cyclic structural loads is mainly concentrated around 1P and NP. When

propagated down the drive-train and structure, cyclic loads may excite some of the poorly damped vibration modes of the system. In this respect, control systems are increasingly important as the wind turbines are larger and their components more flexible. Cyclic loads are highly influenced by the control strategy as well as by the controller setup and design. For instance, the control of the electric generator affects the propagation of drive-train loads whereas the pitch control impacts directly on the structural loads. Therefore, inappropriate control designs might accentuate the vibration modes, potentially leading to the destruction of some mechanical devices such as gearbox or blades. The controller must provide damping at the vibration modes whenever possible in order to mitigate high frequency loads and reduce the risk of fatigue breakdown. On the other hand, the control strategy must avoid operation at points where those vibration modes that cannot be damped by the controller are likely to be excited.

5.1.3   Power quality

Power quality affects the cost of energy in several ways. For instance, poor power quality may demand additional investments in power lines, or may impose limits to the power supplied to the grid. Because of the long-term and short-term variability of the energy resource and the interaction with the power network, wind generation facilities are conventionally considered as poor quality suppliers. Therefore, the control system design must also take power conditioning into account. This control requirement is more and more relevant as the power scale of wind generation facilities approaches the output rating of conventional power plants. Power quality is mainly assessed by the stability of frequency and voltage at the point of connection to the grid and by the emission of flicker.

In general, frequency is a stable variable. Frequency variations in an electric power network are due to power unbalance. For instance, generators accelerate when the supplied power exceeds the consumption, hence increasing the frequency. Analogously, generators slow down when they cannot cover the power demand, thereby frequency decreases. Commonly, when connected to the bulk network, single wind turbines or small-scale wind farms do not affect the frequency. However, this is not the case when the wind turbine is part of an isolated power system or when we

are dealing with a large-scale wind farm. It may happen in these cases that the total power supplied by the wind generation facility needs to be regulated.

The interaction of wind turbines with the power network affects the voltages at the grid terminals. On the one hand, slow voltage excursions take place when the power extracted by the WECS changes with mean wind speed. The amplitude of these variations closely depends on the impedance of the grid at the connecting point and on the active and reactive power flow. A way of attenuating these voltage variations without affecting power extraction is by controlling the reactive power flow. This has been conventionally fulfilled, for instance, using capacitor banks or synchronous machines consuming or supplying reactive power. Nevertheless, with modern wind turbines being connected to grid through power converters, the current tendency is to take advantage of the control flexibility provided by the power electronics. How to control reactive power in the WECS configurations sketched in Figure 4.5 has been mentioned in Section 4.3. Reactive power, power factor or, directly, voltage regulation can be accomplished by an adequate control of the electronic converters. Any of these control schemes can be implemented independently of the control of the rest of the WECS. That is, reactive power control can be decoupled from pitch angle, and speed or torque control. Reactive power control is not treated in this book since it is more related with electronic power conversion than with wind energy conversion.

On the other hand, the cyclic loads originated by rotational sampling effects and propagated down the drive-train towards the grid produce fast fluctuations of grid voltage. Regretfully, the frequency of these cyclic loads may fall into the range of human eye sensitivity; thereby they induce flicker on the electric lines. Flicker is defined as an impression of unsteadiness sensation induced by a fluctuating light stimulus that causes consumer annoyance. These voltage fluctuations and flicker can be attenuated by including passive or active filters, or, in the case of variable-speed WECS, by controlling the reactive power handled by the electronic converters. Also, they can be smoothed indirectly by tackling the propagation of the cyclic loads. This is achieved incorporating dynamic damping to the drive-train by means of a suitable control of the generator torque characteristic.

5.2   Modes of Operation

It is said that a WECS reaches its steady-state operating point when the net torque applied to the system is zero, i.e., when the generator reaction torque equals the aerodynamic torque developed on the rotor (both torques referred to the same side of the gearbox). This steady-state condition is illustrated in Figure 5.3. There, the aerodynamic torque characteristic of the rotor is plotted for different values of wind speed and pitch angle. Also, the reaction torque characteristic of the generator is shown for two values of the zero-torque speed Ω_z. Clearly, the point where the reaction torque intersects the aerodynamic torque curve for a given wind speed is the operating point at that wind speed. For instance, given $\beta = \beta_0$ and $\Omega_z = \Omega_{zP}$, P_1 is the operating point at wind speed V_1; P_2 is the operating point at wind speed V_2, and so on. It turns out from Figure 5.3 that either the generator or the aerodynamic characteristic must be modified to operate the turbine at other operating points. This sort of flexibility is usually necessary to accomplish the control objectives.

Some WECS configurations, such as those sketched in Figures 4.5b and 4.5c, allow the control of their torque characteristic. Effectively, the generator characteristic can be displaced towards higher or lower speeds by means of a suitable control of the electronic converters. For instance, Figure 5.3 illustrates how the operating point shifts from P1 to Q1 when the zero-torque speed Ω_z controlled by the converters increases from Ω_{zP} to Ω_{zQ}. WECS enabled to change their reaction torque characteristic are said to operate at variable speed. This mode of operation is useful, for instance, to track the maximum power locus as wind speed varies below its rated value.

On the other hand, pitch control is the most popular way to change the aerodynamic torque response of the turbine. Figure 3.7 plots how the aerodynamic torque characteristic varies with pitch angle. Figure 5.3 shows also how the operating point is modified even though wind speed remains constant. In fact, the operating point changes from P_1 to R_1 when pitch angle increases from β_0 to β_R. Additionally, it can be observed that the operating point can be maintained constant despite wind changes by means of a suitable pitch angle adjustment. In the Figure, the operating point P_2 for $V = V_2$ and $\beta = \beta_0$ coincides with the operating point R_1 for $V = V_1$ and $\beta = \beta_R$. Variable-pitch operation is particularly useful to shape the aerodynamic
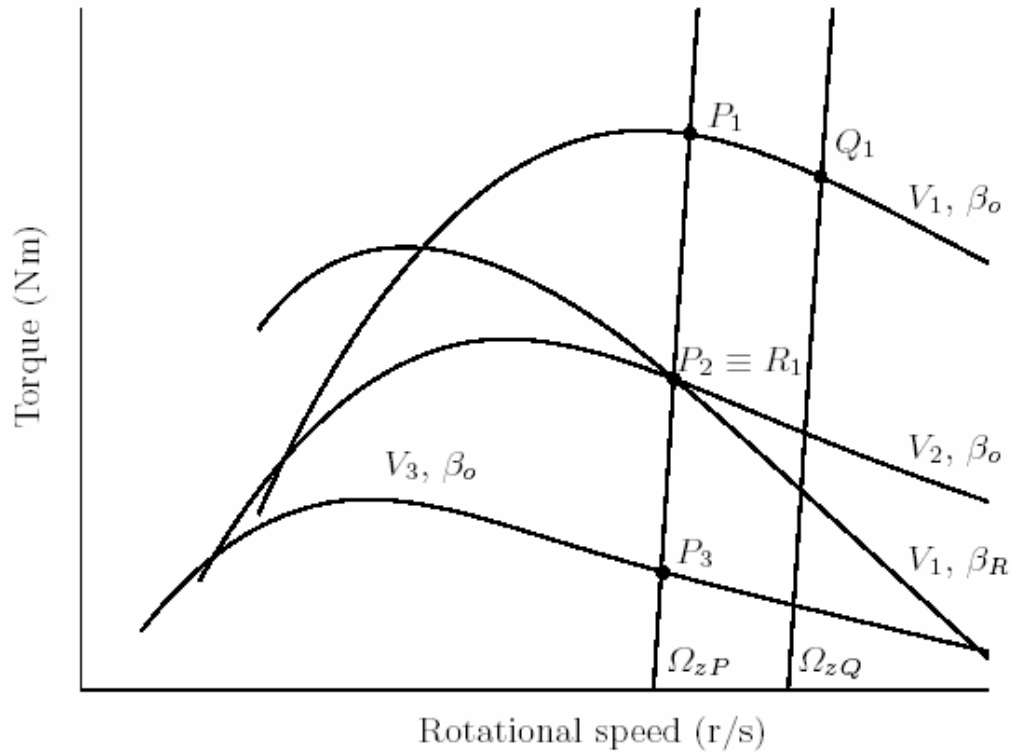
Figure 5.3 : Operating points for different operating conditions

response in above rated wind speeds. For instance, this allows the turbine to keep operating at a fixed point despite wind speed fluctuations.

The term 'modes of operation' denote the various ways wind turbines can be programmed to work. They are essentially determined by the feasible ways to actuate on the turbine. Fixed-speed, variable-speed, fixed-pitch and variable-pitch are the commonest ones. Since wind turbines work under different conditions, these modes of operation are usually combined to attain the control objectives over the full range of operational wind speeds. Accordingly, wind turbines can be classified into four categories, namely:

- Fixed-speed fixed-pitch (FS-FP)
- Fixed-speed variable-pitch (FS-VP)
- Variable-speed fixed-pitch (VS-FP)
- Variable-speed variable-pitch (VS-VP)

Obviously, the capability of a WECS to satisfy the control objectives closely depends on the flexibility of its operation modes.

Once the operation modes of the WECS are determined, it can be proceeded to shape the control strategy. Actually, the foregoing classification of wind turbines is extensive to control strategies.

5.3   Control Strategies

In some way, the control strategy describes how the turbine is programmed to approach in steady-state the ideal power curve in the power - wind speed plane (Figure 5.1). Thus, the control strategy settles the steady-state values of torque (or power) and rotor speed for each wind speed within the range of turbine operation. The control strategy affects the controller setup and design. In fact, the control schemes may differ from one region of operation to another. Further, the small-signal models used for the controller design are highly dependent on the modes and regions of operation.

Despite its stationary nature, the control strategy has a strong influence on the dynamic behavior of the WECS. Effectively, the closed-loop response of the system is closely related to the operating points because of the underlying nonlinearities in turbine aerodynamics. In particular, the planning of the transition between maximum power tracking and power regulation has a direct impact on the transient loads. Also, operation in some region may excite an undamped vibration mode. Consequently, the selection of the desired operating points must arise from a compromise between the control objectives. For instance, a transition region smoother than the ideal one depicted in Figure 5.1 alleviates significantly the transient loads at the cost of some loss in energy capture.

Probably the most suitable context to depict a control strategy is the torque - rotational speed - wind speed space. However, the curves are often projected onto the torque - rotational speed plane to assist interpretation. In both cases, the control strategy is represented by the operating locus of the turbine parameterized by wind speed.

5.3.1 Fixed-speed fixed-pitch

Fixed-speed fixed-pitch operation has been the dominant configuration during some decades. However, the number of commercial wind turbines based on this concept has declined lately.

In this scheme, the asynchronous electric machine is directly coupled to the power network. Thus, its torque characteristic cannot be modified. Consequently, the generator speed is locked to the power line frequency. By this reason, it is said that the WECS operates at fixed speed. In reality, the speed varies a few percent along the torque characteristic of the generator because of the slip.

Since no extra hardware is purposely added to implement the control strategy, FS-FP WECS are very simple and low-cost. As an adverse consequence, their performance is rather poor. In fact, no active control action can be done to alleviate mechanical loads and improve power quality. Further, conversion efficiency is far from optimal.

Figure 5.4 illustrates the basic control strategy for FS-FP wind turbines in the torque - rotational speed plane. The solid line depicts the reaction torque characteristic, whereas the grey lines represent the aerodynamic torque characteristics for different wind speeds between V_{min} and V_{max}. Recall that the points of intersection are the steady-state operating points of the WECS at the corresponding wind speeds.

Since neither the reaction torque nor the aerodynamic torque characteristics can be modified, all feasible operating points are constrained to the segment FD. Since rotational speed is almost constant along FD, power is more or less proportional to torque all along this operating locus. The operating point F corresponds to the cut-in wind speed V_{min} whereas D is the point where the reaction torque characteristic intersects the stall front, the upper boundary of all aerodynamic torque characteristics. This point determines the maximum power that can be extracted by the turbine. At wind speed V_D, for which the aerodynamic torque characteristic passes through point D, the turbine stalls. Therefore, higher wind speeds lead to lower aerodynamic power. That is why the operating point moves back along the generator torque characteristic until point G related to the cut-out wind speed V_{max} is reached. It is worthy to remark that there exists a superposition of operating points in

the segment GD. This means that the wind speed cannot be uniquely determined from the operating point.
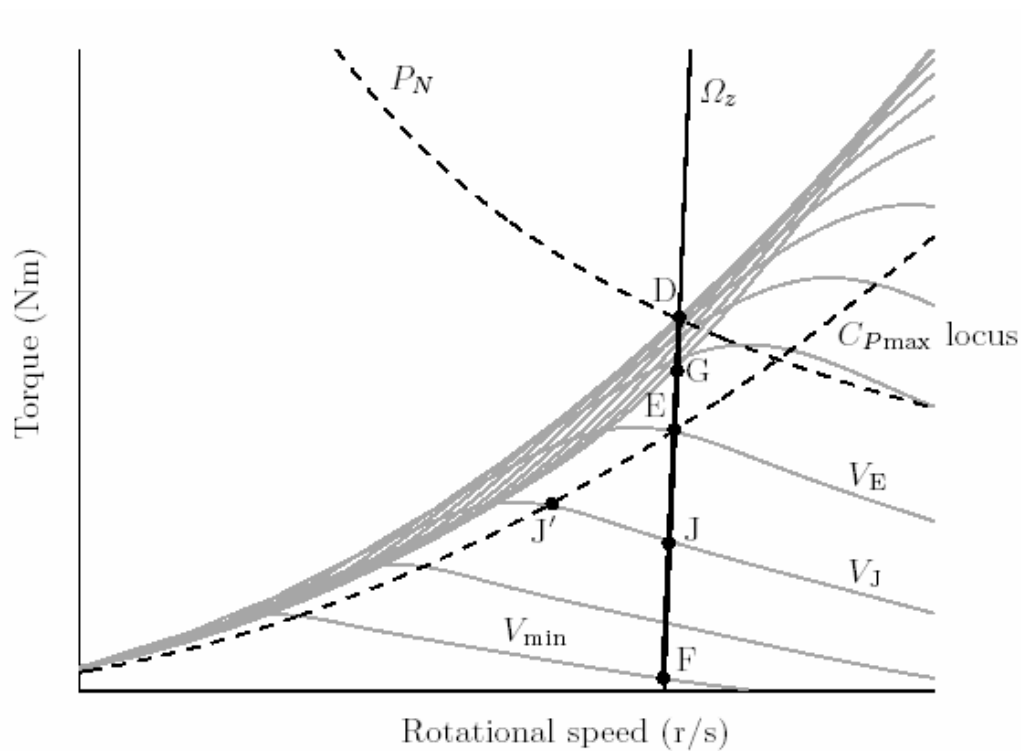

Figure 5.4 : Basic fixed-speed fixed-pitch control strategy

The parabola plotted in Figure 5.4 depicts the locus of maximum conversion efficiency, also called maximum power or C_{Pmax} locus. It shows up that the turbine operates with maximum efficiency at a unique wind speed V_E. This situation corresponds to point E where the maximum power locus, the reaction torque and the aerodynamic torque for $V = V_E$ intersect. At this point, wind and rotational speeds satisfy $\lambda_0 = R\Omega_E/V_E$. Suppose now that the WECS is operating at E when wind speed drops from V_E to V_J. Then, the new operating point is J, being $\Omega_J \cong \Omega_E$. At this point the tip-speed-ratio $\lambda_J \cong R\Omega_E/V_J$ is higher than λ_0, therefore the conversion efficiency decreases. In order to capture all the power available at wind speed V_J, the turbine should be operated at point J' where the rotational speed $\Omega_{J'} = \lambda_0 V_J / R$ is lower. This is impracticable with a fixed-speed control strategy.

FS-FP wind turbines are stall regulated at high wind speeds. That is, power limitation below rated power is accomplished by passive stall. Therefore, the selection of the

control strategy comes down to choose the transmission ratio of the gearbox for the generator characteristic to pass through point D. Note that this point is the intersection between the rated power hyperbola (which is the boundary of the safe operating region) and the stall front. So, rated power is exceeded at no wind speed.
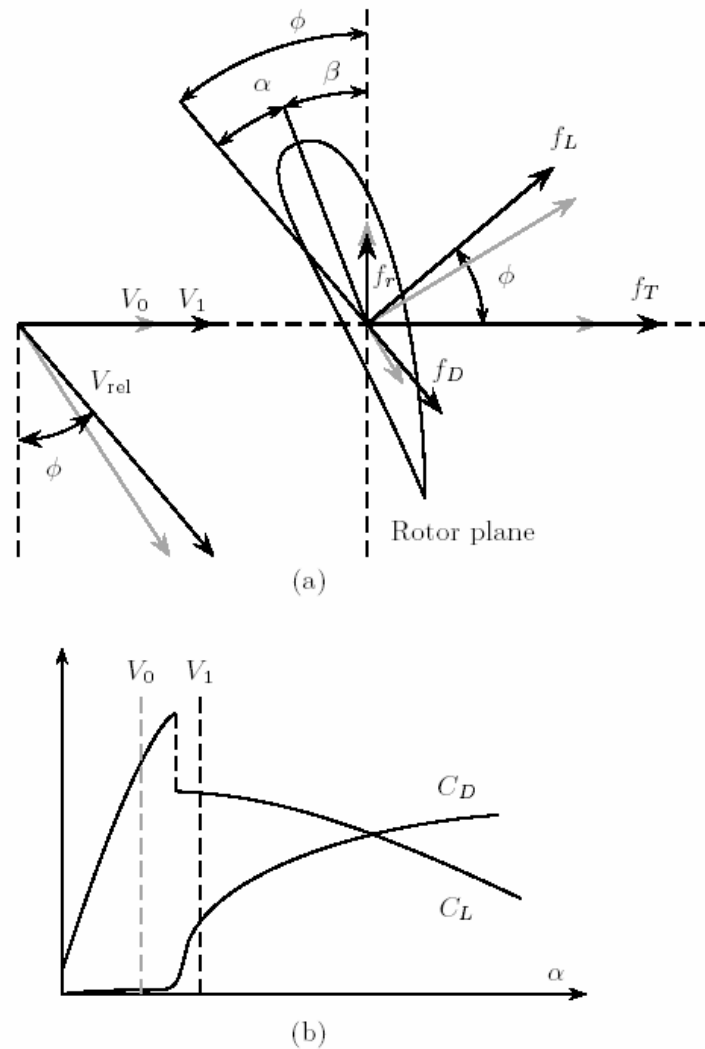

Figure 5.5 : Passive stall strategy for power limitation: (a) forces on a blade element and (b) drag and lift coefficients

Figure 5.5 helps to understand the passive stall method for power limitation. The figure qualitatively shows the forces acting on a blade element before (grey) and after (black) stall. Recall that rotational speed and pitch angle are fixed. Then, the incidence angle α increases as the wind speed experienced by the blade element rises from V_0 to V_1. When α exceeds a given value, the air flow ceases to be laminar and

separates from the upper side of the aerofoil. This induces a differential pressure that reduces the lift and increases abruptly the drag. Changes in lift f_L and drag f_D forces lead to a large increment in the axial thrust force f_T whereas the tangential force f_r decreases slightly. As a result, the aerodynamic torque and power decrease. It is said that the turbine stalls. An undesirable consequence of stall regulation is the increased thrust that causes heavier aerodynamic loads.

Figure 5.6 illustrates the power capture features of the basic FS-FP control strategy shown in Figure 5.4. The top part of the figure compares the actual and ideal power curves, whereas the bottom part shows the conversion efficiency vs. wind speed. The points marked in the figure are in correspondence with those of Figure 5.4. It can be observed that the extracted power does not match the ideal power curve. This means lower energy capture. In the low wind speed region, the turbine operates with maximum efficiency only at one point (point E). In above rated wind speeds, power regulation is rather poor. It is seen that rated power is attained only at one wind speed (point D) whereas power decreases at lower and higher wind speeds. This poor regulation is put down to the lack of flexibility of the operation mode.

In addition to the low conversion efficiency, fixed-speed operation suffers from other shortcomings more related with the dynamic behavior of the WECS. For instance, the poor regulation property translates into active and reactive power fluctuations on the power lines. Additionally, this mode of operation does not provide control actions to inject damping to the drive-train, which would attenuate high-frequency loads and flicker emission. Actually, the decline of FS-FP wind turbines is mainly due to their bad power quality, rather than to reduced energy capture.

5.3.2 Fixed-speed variable pitch

The FS-VP mode of operation has also often been employed in commercial wind turbines during past decades, particularly in medium to high power. Fixed-speed operation means that maximum power conversion is attainable only at a single wind speed. Therefore, conversion efficiency below rated wind speed cannot be optimized. This kind of turbine is usually programmed to operate at fixed pitch below rated wind speed. However, variable-pitch operation in low wind speeds could be potentially helpful to enhance somewhat the energy capture. In above rated wind

speeds, power is limited by continuously adjusting the pitch angle. There are basically two methods of power regulation by pitch control, namely pitch-to-feather and pitch-to-stall. The former method is conventionally referred to as pitch angle control, whereas the second method is also known as 'active stall' or 'combi stall'.
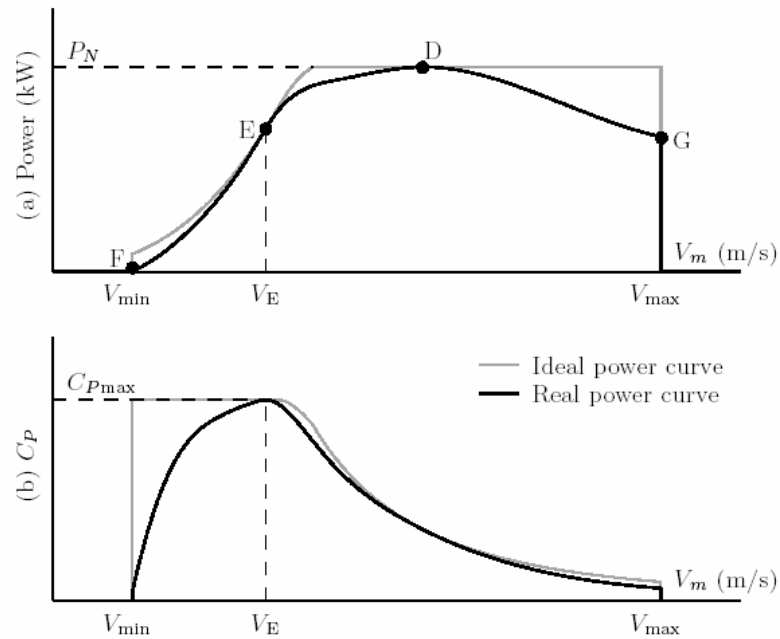

Figure 5.6 : Basic fixed-speed fixed-pitch control strategy: (a) output power and (b) conversion efficiency vs. wind speed

5.3.2.1 Power limitation by pitch-to-feather

This method essentially consists in feathering the blades as wind speed rises. Thus, it is based on an aerodynamic phenomenon completely different to stall. Figure 5.7 illustrates the method. In the top part of the figure, the forces acting on a blade element that experiences axial wind speeds V_0 and $V_1 > V_0$ are depicted by grey and black vectors, respectively. When wind speed rises from V_0 to V_1, the angle φ that the relative air flow makes with the rotor plane increases. As response, the controller raises the pitch angle β so that the incidence angle α decreases. As a result, the lift coefficient C_L drops whereas the drag coefficient C_D remains low. It can be thought that the controller adjusts the lift force f_L in order to keep the force f_r in the rotor plane constant. It can be observed in the figure that, contrary to what happens with passive stall, the thrust force f_T decreases as wind speed rises. Since thrust efforts

produce aerodynamic loading on the structure, this is a significant advantage of this method. As a disadvantage, pitch-to-feather regulation requires a considerable control effort since large pitch changes are necessary to compensate for wind power fluctuations.
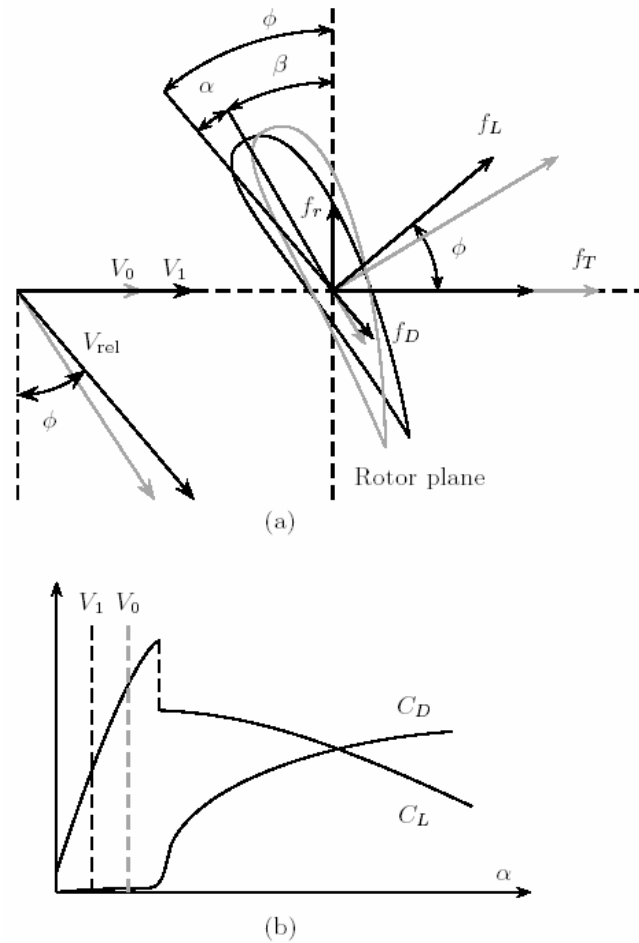

Figure 5.7 : Pitch-to-feather strategy for power limitation: (a) forces on a blade element and (b) drag and lift coefficients

5.3.2.2 Power limitation by pitch-to-stall

The alternative to pitch-to-feather is pitch-to-stall. In this case, the pitch angle is adjusted in the opposite direction. In fact, the pitch angle is reduced in order to increase the incidence angle, rather than to decrease it, as wind speed rises. That is, the pitch angle is controlled to actively induce stall above rated wind speed. Thanks to the control flexibility, this method holds better regulation features than passive stall. Figure 5.8 illustrates the method. The top part of the figure depicts the forces

acting on a blade element that experiences axial wind speeds V_0 (grey) and V_1 (black), with $V_1 > V_0$. The angle φ increases with wind speed. As a result, the incidence angle α tends to increase. In pitch-to-stall, the pitch angle β is reduced to increase further the incidence angle, hence reinforcing stall. Lift drops whereas drag rises abruptly. The composition of these forces results in a force in the rotor plane that remains constant, thus maintaining the aerodynamic power at its rated value. A disadvantage of this method, as well as of all methods based on stall, is that the thrust force increases drastically as the turbine goes into stall. This translates into heavy aerodynamic loads. As main attractive feature, this method requires a comparatively low control effort to regulate power. It is worthy to note that it is no more necessary for the control strategy to pass exactly through the point of intersection between the rated power hyperbola and the stall front. This gives in principle more freedom to design the transmission ratio.

5.3.2.3 Basic control strategy

Figure 5.9 depicts the basic pitch-to-feather control strategy for FS-VP wind turbines. The aerodynamic torque characteristic for different wind speeds within the operational envelope is also plotted with pitch angle as a parameter. Since there is no control on the reaction torque, rotational speed is almost constant all along the operating locus. Below rated wind speed, the control strategy is similar to the FS-FP one. That is, the turbine is operated at some point in the segment FD. Above rated wind speed, the controller adjusts the pitch angle to regulate aerodynamic power at rated; the turbine is programmed to operate at point D. It is observed how the aerodynamic torque characteristics are modified to pass through this point D.

In the case of pitch-to-stall, all trajectories pass through point D also, but the aerodynamic torque characteristics are shaped differently. This case can be interpreted as that the stall front moves rightwards as wind speed increases. Figure 5.10 shows the power regulation features of the basic control strategies for FS-VP wind turbines. The points marked in the figure are in correspondence with those of Figure 5.9. Since the operating points of the wind turbine on the torque - speed plane are the same no matter the control strategy is pitch-to-feather or pitch-to-stall, Figure 5.10 is valid for both cases. The top part of the figure compares the actual and ideal
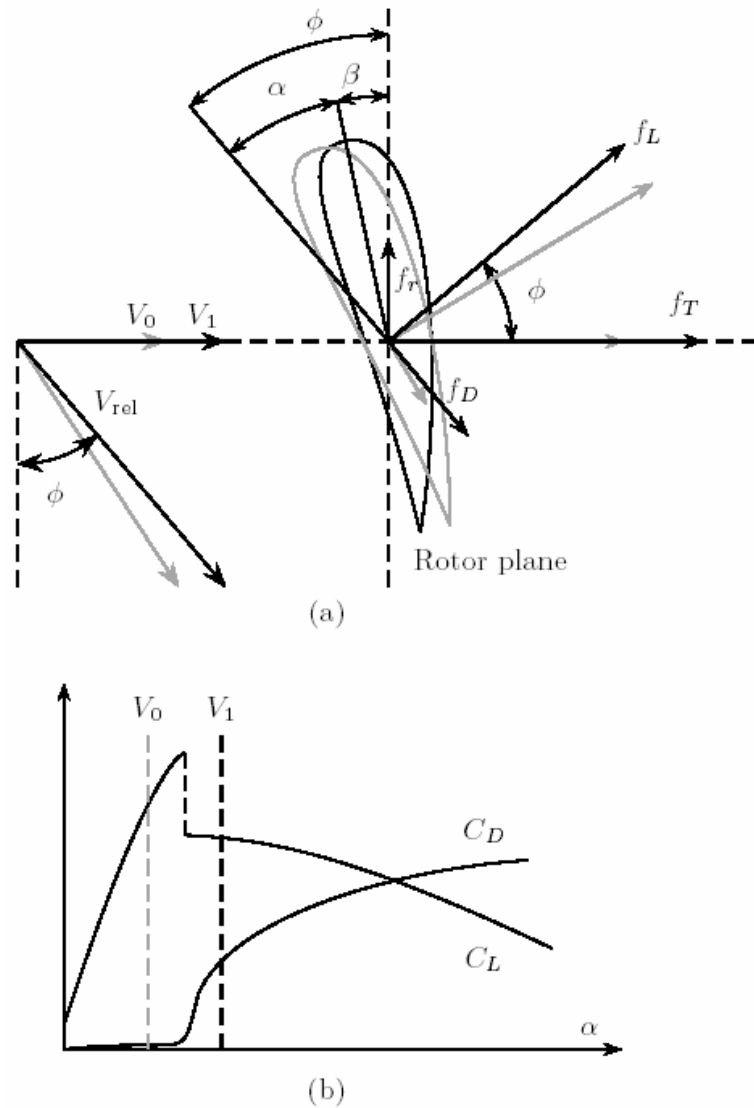
Figure 5.8 : Pitch-to-stall strategy for power limitation: (a) forces on a blade element and (b) drag and lift coefficients

power curves whereas the bottom part shows the conversion efficiency vs. wind speed. Below rated wind speed, the real power curve is similar to the one for the FS-FP control strategy plotted in Figure 5.6. Even though maximum conversion efficiency is attained only at wind speed V_E, variable-pitch wind turbines are designed to have near optimum conversion efficiency over a wide range of wind speeds below V_N. Above rated wind speed, ideal power regulation is achieved provided there are not pitch actuator constraints. That is, the theoretical power curve is attached to the ideal curve. The bottom part of the figure illustrates how the power coefficient is shaped above rated wind speed to match the ideal power curve.
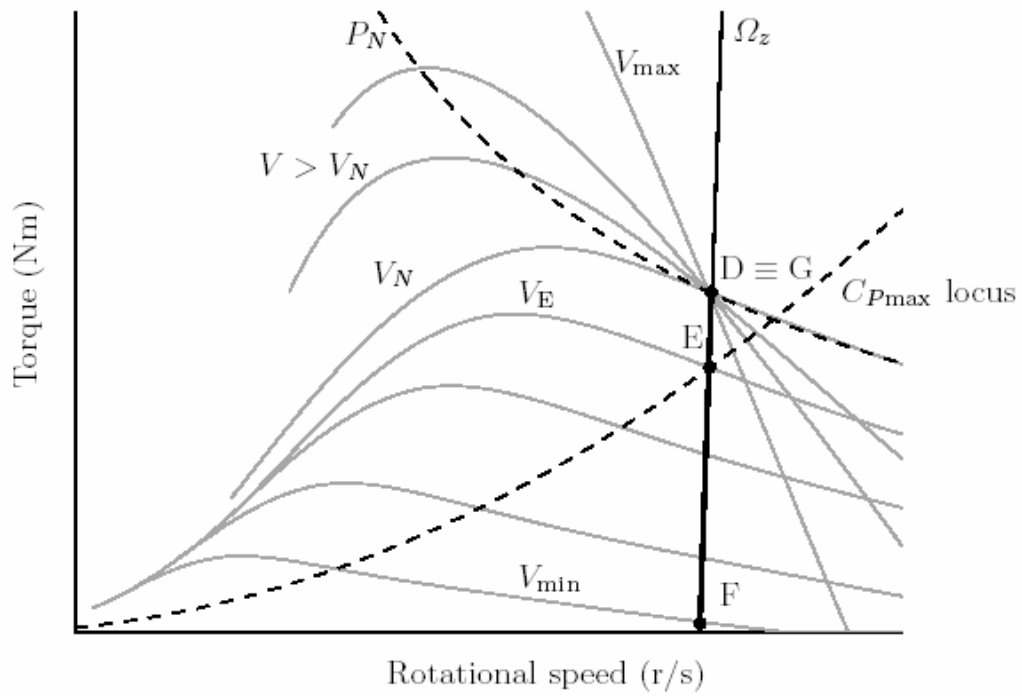
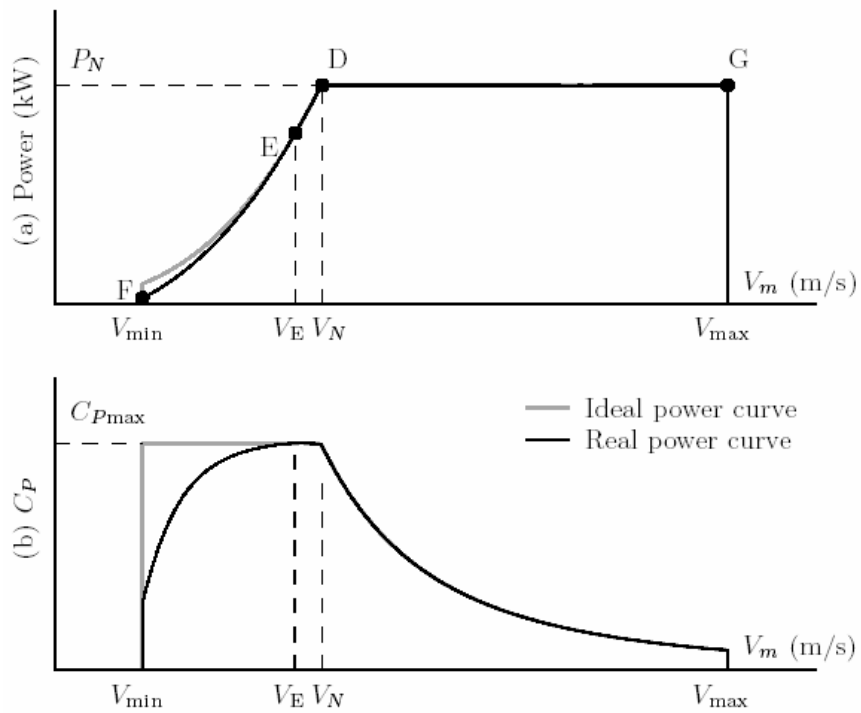**Figure 5.9 :** Basic fixed-speed variable-pitch (pitch-to-feather) control strategy

Figure 5.10 : Basic fixed-speed pitch-to-feather and pitch-to-stall control strategies: (a)output power and (b) power efficiency vs. wind speed

5.3.3 Variable-speed fixed-pitch

The variable-speed alternative to fixed-speed has become popular in commercial wind turbines, particularly for operation in low wind speeds. The benefits commonly ascribed to variable-speed operation are larger energy capture, dynamic loads alleviation and power quality enhancement. With wind energy currently reaching large penetration factors, the demands for power quality improvement gave a decisive impetus to the use of variable-speed schemes. Maximum efficiency conversion is achieved at $\beta = \beta_0$ and $\lambda = \lambda_0$. Therefore, to maximize energy capture below rated power, both the pitch angle and the tip-speed-ratio must be kept constant at these values. In particular, the condition $\lambda = \lambda_0$ means that the rotor speed must change proportionally to wind speed:

$$\Omega_{ro} = \frac{\lambda_o V}{R} \qquad\qquad (5.2)$$

As it is known, variable-speed operation requires decoupling the rotational speed from the line frequency. With this aim, one of the WECS configurations sketched in Figures 4.5b or 4.5c are typically adopted. A suitable control of the underlying electronic converters produces parallel displacements of the generator torque characteristic towards higher or lower speeds. Thus, the turbine can be controlled to operate at different points, for instance to track the optimum speed (5.2) as wind speed fluctuates. The maximum power locus on the torque vs. speed plane can be obtained by replacing λ, β and V in (3.24) with λ_o, β_o and $R\Omega_{ro}/\lambda_o$, respectively:

$$T_{ro} = \frac{1}{2\lambda_0^{\,3}} \rho R^5 C_{P\max} \Omega_{ro}^{\,2} = c\,\Omega_{ro}^{\,2} \qquad\qquad (5.3)$$

This is the equation of a parabola in the torque - rotational speed plane.

In low wind speeds, variable-speed wind turbines are controlled to track more or less tightly this $C_{P\max}$ locus. Thus, variable-speed control strategies essentially differ in the way power is limited above rated wind speed. For VSFP wind turbines, there are basically two approaches based on passive and speed-assisted stall, respectively.

5.3.3.1 Variable speed with passive stall regulation

This control strategy is identified by the points AEDG in Figure 5.11. Clearly, the turbine works at two different modes throughout its operating region. In the low wind speed region, more precisely between V_{min} and V_E, the turbine is programmed to operate along the quadratic curve AE. That is, the control strategy coincides with the C_{Pmax} locus. Clearly, the turbine is operated at variable speed in this region. For wind speeds above V_E the operating point of the turbine moves along the segment ED. That is, the turbine is operated at fixed speed in this wind speed region, hence performing like an FS-FP one. Therefore, power is limited by passive stall as described in Figure 5.5. Again, there exists a superposition of operating points before and after stall in the segment GD. Note that the generator torque characteristic containing the segment ED passes through the intersection point between the rated power hyperbola and the stall front. This is to capture as much energy as possible without overloading.
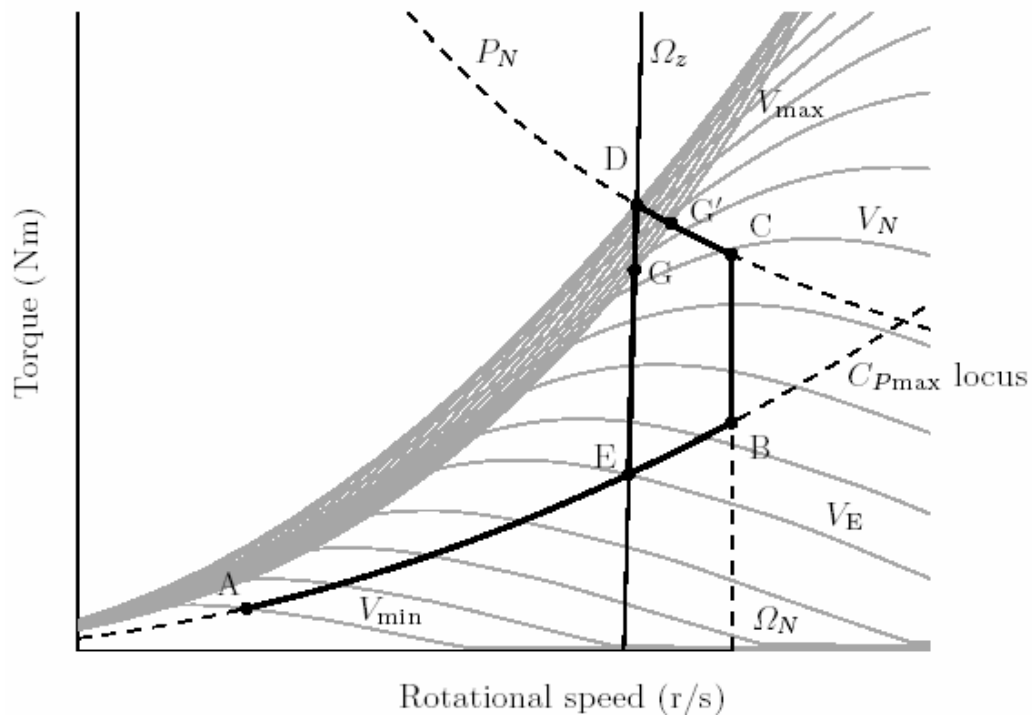

Figure 5.11 : Basic variable-speed fixed-pitch control strategies with passive (AEDG) and speed-assisted (ABCDG¦) stall regulation

Figure 5.12 shows the power capture properties of this control strategy. The top part of the figure compares the actual (black) and ideal (grey) power curves, whereas the bottom part displays the conversion efficiency (black) vs. the wind speed. The points A, E, D and G are in correspondence with those of Figure 5.11. It is observed that the real power curve is attached to the ideal one between V_{min} and V_E. Thus, power conversion is maximized in this speed range. At point E, the real power curve separates from the ideal one, leading to some loss in captured power.
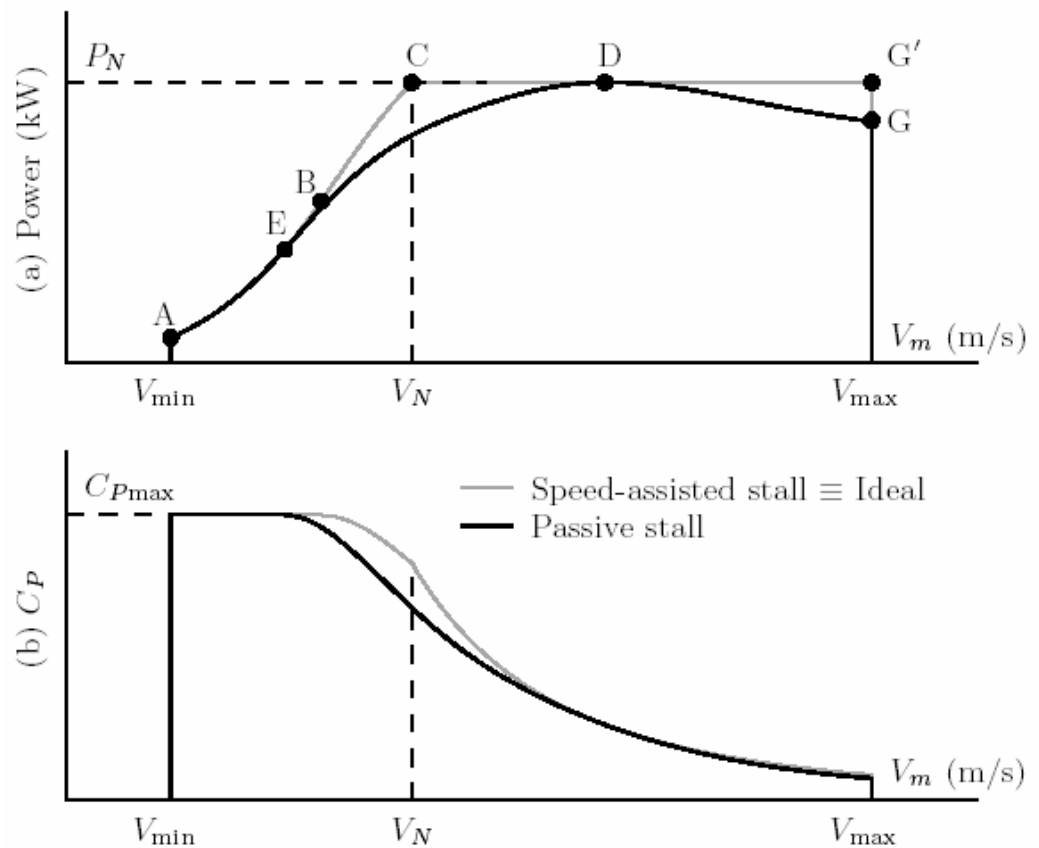
Figure 5.12 : Variable-speed fixed-pitch control strategies with passive stall regulation (AEDG) and speed-assisted stall regulation (ABCDG$^|$): (a) captured power and (b) power efficiency vs. wind speed

5.3.3.2 Variable speed with assisted stall regulation

This control strategy can be identified by the points ABCDG$^|$ in Figure 5.11. The wind turbine is operated at variable speed throughout its operational range. The control strategy coincides with the C_{Pmax} locus from A to B. All along this curve, rotational speed increases proportionally to wind speed until rated speed Ω_N is

reached at B. Since Ω_N cannot be exceeded, the operating point moves along the segment BC as wind speed increases from $V_{\Omega N}$ to V_N. That is, the operating speed of the WECS remains constant in this wind speed region. For wind speeds above rated, the operating point moves along the rated power hyperbola towards the stall front. At wind speed V_D, the control strategy reaches the stall front, the turbine stalls. For higher wind speeds the operating point moves back along the hyperbola until shut-down at G$^|$.

It turns out that this control strategy accomplishes the ideal power curve of Figure 5.1. This is corroborated in Figure 5.12 where the distinctive points of the control strategy are marked on the ideal power curve. The three regions are clearly distinguished in the torque - rotational speed graph.

Although this control strategy potentially enables maximum energy capture, it also brings with it some transient problems. Problems arise when the WECS operates under turbulent conditions around its rated operating point (point C). For instance, suppose the turbine is being operated at C and wind speed increases suddenly above V_N. Aerodynamic power tends to increase in consequence. To compensate for this increment, the operating point is moved leftwards along the rated-power hyperbola, thus leading to a reduction of rotational speed. Accordingly, part of the kinetic energy stored in the rotor is reduced. Necessarily, the energy in excess is transmitted through the drive-train and supplied to the AC grid. Thus, operation around the nominal point inevitably leads to undesirable transient loads and electric power fluctuations that degrade power quality. The amplitude of aerodynamic power fluctuations and, hence, of transient loads decreases as the operating point approaches the stall front.

5.3.4   Variable-speed variable-pitch

Variable-speed variable-pitch control strategies are being more and more common in commercial wind turbines. In this scheme, the turbine is programmed to operate at variable speed and fixed pitch below rated wind speed and at variable pitch above rated wind speed. Both pitch-to-feather and pitch-to-stall strategies can be followed. Figure 5.13 depicts the basic variable speed pitch-to-feather control strategy on the torque - rotational speed plane. In low wind speeds, the turbine is operated along the

C_{Pmax} locus between the points A and B. At point B, the rotational speed gets to its upper limit Ω_N. Therefore, rotational speed is regulated at this value on the segment BC as wind speed increases from $V_{\Omega N}$ to V_N. Above rated wind speed, the pitch angle is controlled in order to keep the turbine operating at point C. Note that the segment BC comes down to point $C^|$ when the intersection between the rated power hyperbola and the maximum efficiency parabola lies to the left of the rotational speed limit. In this case, the operating locus is reduced to the curve $AC^|$.

Variable-speed operation increases the energy capture at low wind speeds whereas variable-pitch operation enables an efficient power regulation at higher than rated wind speeds. It is important that this control strategy also achieves the ideal power curve of Figure 5.1. In addition, variable-pitch operation alleviates transient loads. This is an important advantage of this control strategy in comparison with VS-FP ones, particularly for large-scale wind turbines. Moreover, simultaneous control of pitch and speed above rated wind speed provides important benefits to the dynamic performance of the WECS under high wind conditions.
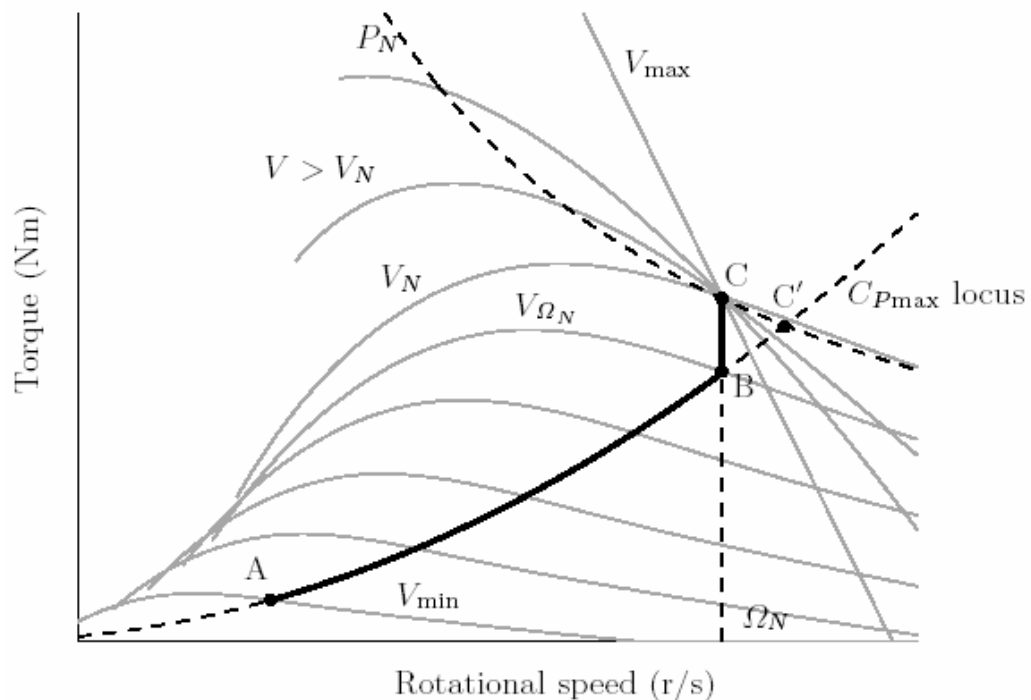

Figure 5.13 : Basic variable-speed variable-pitch (pitch-to-feather) control strategy

6. CONTROL OF 1.5 MW VARIABLE SPEED FIXED PITCH WIND TURBINE

In this section the state space model of variable speed fixed pitch wind turbine is derived. After making some assumptions a PI controller is designed for a simple wind turbine model to control the generator speed. At the end of this section 1.5 MW complicated wind turbine model designed in MATLAB is introduced. In addition to this the PI controller designed for the simple model is used to control this complicated model.

6.1 State Space Model of Variable Speed Fixed Pitch Wind Turbine

In the case of VS-FP wind turbines there is only one control action, which is applied to the electrical machine. So, the control does not interact directly with the tower dynamics. For this reason, it is common practice to use a reduced model of the WECS. This model basically takes into account the first resonance mode of the drive-train, whereas the neglected high-frequency dynamics can be treated as model uncertainty [1]. This model is suitable to describe the dominant system dynamics, to formulate the control strategy and to make a preliminary assessment of the controller performance [1]. After this order reduction, the dynamic model of the drive-train can be described by:

$$\begin{bmatrix} \dot{\Omega}_s \\ \dot{\Omega}_r \\ \dot{\Omega}_g \end{bmatrix} = \begin{bmatrix} 0 & 1 & -1 \\ -\dfrac{K_s}{J_r} & -\dfrac{B_s}{J_r} & \dfrac{B_s}{J_r} \\ \dfrac{K_s}{J_g} & \dfrac{B_s}{J_g} & -\dfrac{B_s}{J_g} \end{bmatrix} \begin{bmatrix} \Omega_s \\ \Omega_r \\ \Omega_g \end{bmatrix} + \begin{bmatrix} 0 \\ \dfrac{T_r}{J_r} \\ -\dfrac{T_g}{J_g} \end{bmatrix} \qquad (6.1)$$

where the aerodynamic torque T_r is given by:

$$T_r = \frac{1}{2} \rho R^3 C_Q(\lambda) V^2 \qquad (6.2)$$

and the generator torque T_g is a nonlinear function of the rotational speed. The generator usually operates in the linear region of its torque characteristic, which can therefore be approximated by a straight line of slope B_g. Furthermore, the generator is often controlled using a constant-flux control strategy. Under this assumption, changes in the control action (e.g., the stator frequency for the configuration of Figure 4.5b or the quadrature rotor voltage for the configuration of Figure 4.5c) bring about parallel displacements of this line. So, the generator torque characteristic is usually approximated by:

$$T_g = B_g(\Omega_g - \Omega_z) \tag{6.3}$$

where the zero-torque speed Ω_z can be regarded as the control input to the electromechanical system independently of the configuration of the power generator unit.

With regards to the aerodynamics, note that the torque coefficient C_Q of a fixed-pitch wind turbine is only function of the tip-speed-ratio λ. Thus, the linearization of the aerodynamic torque around its operating point (Ω,V) reads:

$$T_r = -B_r(\Omega,V)\Omega_r + k_{r,V}(\Omega,V)V \tag{6,4}$$

where:

$$B_r(\Omega,V) = -\left.\frac{\partial T_r}{\partial \Omega_r}\right|_{(\Omega,V)} = -\frac{-T_r(\lambda,V)}{\Omega}\left.\frac{\partial C_Q/\partial \lambda}{C_Q/\lambda}\right|_{(\lambda,V)} \tag{6.5}$$

$$k_{r,V}(\Omega,V) = -\left.\frac{\partial T_r}{\partial \Omega_r}\right|_{(\Omega,V)} = -\frac{-T_r(\lambda,V)}{V}\left(2-\left.\frac{\partial C_Q/\partial \lambda}{C_Q/\lambda}\right|_{(\lambda,V)}\right) \tag{6.6}$$

with λ being the tip-speed-ratio at the operating point, $\lambda = R\Omega/V$.

On the one hand, B_r shows up the intrinsic speed feedback of the turbine and plays an important role in the stabilization problem. Note that this coefficient can be viewed as damping taking positive values above λ_{Qmax} (where C_Q is a decreasing function of λ) and negative values below λ_{Qmax} (where C_Q increases with λ). On the other hand, $k_{r,V}$ denotes the gain between the wind speed and the aerodynamic torque. In normal

operation this gain is positive, whereas it becomes negative at low values of λ when the turbine stalls [1].

The linearization of the dynamic system (6.1) can be expressed as state space model:

$$G : \begin{cases} \dot{x} = A(\Omega,V)x + B(\Omega,V)u \\ T_r = C_t x \\ y = Cx + Du \end{cases} \tag{6.7}$$

where the state, output and parameter vectors are:

$$x = \begin{bmatrix} q_s & \Omega_r & \Omega_g \end{bmatrix}^T$$

$$y = \begin{bmatrix} \Omega_g & T_g \end{bmatrix}^T$$

$$u = \begin{bmatrix} V & \Omega \end{bmatrix}^T$$

The model (6.7) has two inputs and three outputs. The inputs are the wind speed and the control action Ω_z. The outputs are the effective aerodynamic torque T_r transferred to the shaft, the generator speed and the generator torque gathered in y matrix.

The matrices of the model are:

$$A(\Omega,V) = \begin{bmatrix} 0 & 1 & -1 \\ -\dfrac{K_s}{J_r} & -\dfrac{B_r(\Omega,V) + B_s}{Jr} & \dfrac{B_s}{Jr} \\ \dfrac{K_s}{J_g} & \dfrac{B_s}{J_g} & -\dfrac{B_s + B_g}{J_g} \end{bmatrix}$$

$$B(\Omega,V) = \begin{bmatrix} 0 & 0 \\ \dfrac{k_{r,V}(\Omega,V)}{J_r} & 0 \\ 0 & \dfrac{B_g}{J_g} \end{bmatrix}$$

$$C_t = \begin{bmatrix} K_s & B_s & -B_s \end{bmatrix}$$

$$C = \begin{bmatrix} 0 & 0 & 1 \\ 0 & 0 & B_g \end{bmatrix}$$

$$D = \begin{bmatrix} 0 & 0 \\ 0 & -B_g \end{bmatrix}$$

To completely characterize (6.7), some mathematical description of C_Q is required. A good approximation of $C_Q(\lambda)$ is a second-order polynomial of the form:

$$C_Q(\lambda) = C_{Q\max} - k_Q(\lambda - \lambda \max)^2 \tag{6.8}$$

For this quadratic approximation of C_Q, the coefficients B_r and $k_{r,V}$ are:

$$B_r(\Omega,V) = r\rho R^4 k_Q (R\Omega - \lambda_{Q\max} V) \tag{6.9}$$

$$k_{r,V}(\Omega,V) = r\rho R^4 k_Q \left(R\Omega - \left(1 - \frac{C_{Q\max}}{k_Q \lambda^2_{Q\max}}\right) \lambda_{Q\max} V \right) \tag{6.10}$$

6.2   Numerical Values of the State Space Model Parameters

Shaft Stiffness: $K_s = 83000000 Nm/rad$ [6]

Shaft Damping: $B_s = 1400000 Nms/rad$ [6]

Inertia of the rotor: $J_r = m_{shaft} \times \dfrac{D_{shaft}^2}{8} + (J_{blade} + m_{blade} \times d_{cog\_blade}^2) \times N_{blade}$

$$m_{shaft} = Pi \times \frac{D_{shaft}^2}{4} \times L_{shaft} \times r_{shaft}$$

$$m_{shaft} = Pi \times \frac{0,56^2}{4} \times 2,185 \times 7850 = 4224,6kg$$

$$J_r = 4224,6 \times \frac{0,56^2}{8} + (6,2 \times 10^5 + 6101 \times 8,775^2) \times 3 = 3269500 kgm^2 \ [7],[8]$$

Inertia of the generator: $J_g = 35000 kgm^2$ [9]

Slope of the generator torque-rotational speed graph:

$B_g = -1989,4 Nms/rad$ [10]

6.3 PI Controller Design

In order to obtain a simple controller, the low speed shaft of the mechanical system shown in Figure 4.4 is assumed to be perfectly rigid [11]. Then the mechanical system can be described by the following equation:

$$J_t \dot{w}_r = T_r - B_t w_r - T_g \tag{6.11}$$

where:

$$J_t = J_r + J_g \tag{6.12}$$

$$B_t = B_s + B_g \tag{6.13}$$

Then taking the Laplace of (6.11) and moving the ω_r terms to one side it is found that:

$$T_r(s) - T_g(s) = w_r(s)\left[J_t s + B_t\right] \tag{6.14}$$

$$w_r(s) = \frac{T_r(s) - T_g(s)}{J_t s + B_t} \tag{6.15}$$

Using (6.15) the controller will be designed depending on the following block diagram:
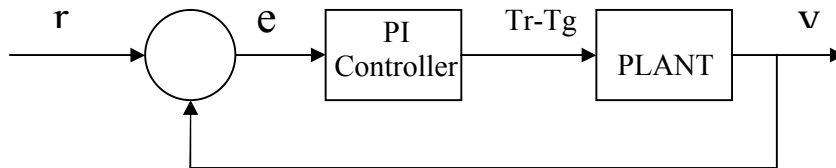
Figure 6.1 : The system block diagram used to design the controller

In this diagram r stands for the reference wind speed $\omega_{r\text{-ref}}$, y stands for the output wind speed ω_r and e is the error that is equal to the difference of the reference wind speed and the output wind speed. Sending the error to the controller, which is designed to control the plant, the signal giving the difference of the torques T_r-T_g is calculated. Then using this signal as a plant transfer function input, the output speed value is calculated.

Here the PI controller is defined by the transfer function below:

$$G_C = P + \frac{1}{I\,s} \qquad\qquad (6.16)$$

and the plant transfer function has the form:

$$G_P = \frac{k}{t\,s+1} = \frac{1/B_t}{J_t/B_t\,s+1} \qquad\qquad (6.17)$$

The next step done is to find the system transfer function and the characteristic equation.

$$(r-y)\left(P+\frac{1}{I\,s}\right)\left(\frac{k}{t\,s+1}\right) = y \qquad\qquad (6.18)$$

$$(r-y)\left(\frac{(PI\,s+1)k}{t\,I\,s^2 + I\,s}\right) = y \qquad\qquad (6.19)$$

$$(r-y)(PI\,s+1)k = y(t\,I\,s^2 + I\,s) \qquad\qquad (6.20)$$

$$k\,r\,(PI\,s+1) - k\,y\,(PI\,s+1) = y(t\,I\,s^2 + I\,s) \qquad\qquad (6.21)$$

$$k\,r\,(PI\,s+1) = y(t\,I\,s^2 + I\,s + PI\,k\,s + k) \qquad\qquad (6.22)$$

After these operations the system transfer function is found as follows:

$$\frac{y}{r} = \frac{k(PI\,s+1)}{t\,I\,s^2 + (I + PI\,k)s + k} \qquad\qquad (6.23)$$

The characteristic equation (polynomial) of the system can be written as:

$$P_C = s^2 + \left(\frac{I + PIk}{tI} \right) s + \frac{k}{tI} \tag{6.24}$$

Now the desired polynomial should be found to decide P and I controller coefficients. At first, percent overshoot equation is used to find the damping ratio. Determining an overshoot of 5% the damping ratio is calculated below:

$$P.O. = 100e^{-zp/\sqrt{1-z^2}} = 5 \tag{6.25}$$

$$z = 0.69$$

Second, settling time equation derived for a 2% steady state error is used to find the natural frequency. Desiring a settling time of 30 seconds, the natural frequency is calculated:

$$T_s = \frac{4}{zw_n} = 30 \tag{6.26}$$

$$w_n = 0{,}1931$$

Third, the roots of the characteristic polynomial are defined as follows:

$$s_{1,2} = -w_n z \pm w_n \sqrt{1-z^2}\, j \tag{6.27}$$

$$s_{1,2} = -0{,}1333 \pm 0{,}14 j$$

The desired polynomial is found by multiplying the roots:

$$P_d = s^2 + 0{,}2666s + 0{,}03737 \tag{6.28}$$

At last, the characteristic polynomial and the desired polynomial are equaled to define the controller coefficients:

$$s^2 + \left(\frac{I + PIk}{tI} \right) s + \frac{k}{tI} = s^2 + 0{,}2666s + 0{,}03737 \tag{6.29}$$

The equations of the coefficients are:

$$P = \frac{1}{k}(0{,}2666t - 1) \tag{6.30}$$

$$I = \frac{26{,}76\,k}{t} \tag{6.31}$$

A Matlab model shown below is used to check the controller performance.
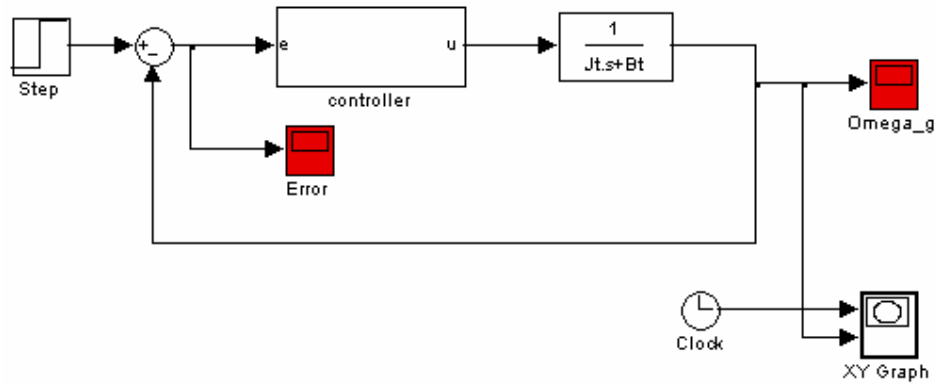
Figure 6.2 : The system used to check the controller performance

Looking at the step response graph of the system (Figure 6.4), it can be said that the system makes an overshoot $\cong 5\%$ and then reaches a value which remains within 2% of the final value in desired settling time 30 seconds. Finally the system settles to the step value.

6.4   Wind Turbine Model

In this subsection the formulas used in wind turbine model to calculate the numerical values of C_p and C_Q coefficients are represented. The specifications of the designed wind turbine are expressed next. Finally the block diagrams of the designed wind turbine model are explained.

6.4.1   Numerical calculations of C_P and C_Q

In order to calculate numerical values of C_P the equations below are used:

$$C_P(\mathsf{l},\mathsf{b}) = 0{,}22\left(\frac{116}{\mathsf{l}_i} - 0{,}4\mathsf{b} - 5\right) e^{-\frac{12.5}{\mathsf{l}_i}} \tag{6.32}$$

$$\frac{1}{l_i} = \frac{1}{l + 0.08b} - \frac{0.035}{b^3 + 1}$$

Figure 6.3 : Inside the controller block
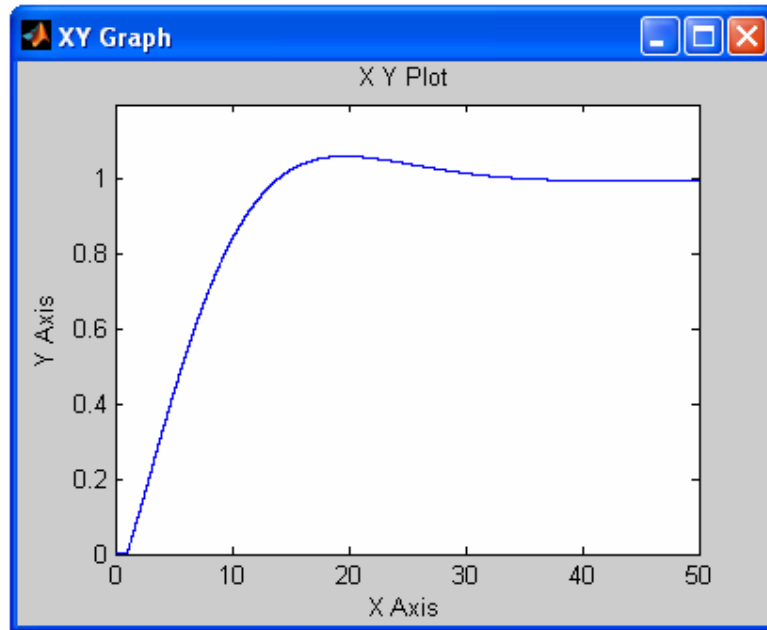
Figure 6.4 : Step response of the system

The maximum value of C_P can be found using a graphical method, which is 0.4381 in this case. This value corresponds to $\beta = 0$ and $\lambda = 6.4$. This tip speed value is assigned as the optimum tip speed. Based on this value, the optimum turbine speed curve at any given wind speed can be obtained. This curve is then used as a reference in the active power control [12].

Also the maximum values of C_Q can be calculated by using (6.32), (6.33) and (3.26). Maximum C_Q equals 0.0798 when $\beta = 0$ and $\lambda = 4.8$. C_Q can be calculated by using (6.8), too. In this equation k_Q is unknown. It is found by substituting the C_{Qmax}, λ_{Qmax}, C_Q and λ values in (6.8).

$$k_Q = 0{,}0073$$

6.4.2 Modelled wind turbine specifications

Rated power: 1,5 MW

Cut-in wind speed: 4 m/s   [13]

Cut-out wind speed: 25 m/s   [13]

Rated wind speed: 13 m/s   [13]

Number of blades: 3   [14]

Rotor diameter: 66 m   [14]

Swept Area: 3421 m^2 [14]

Hub Height: 86 m   [14]
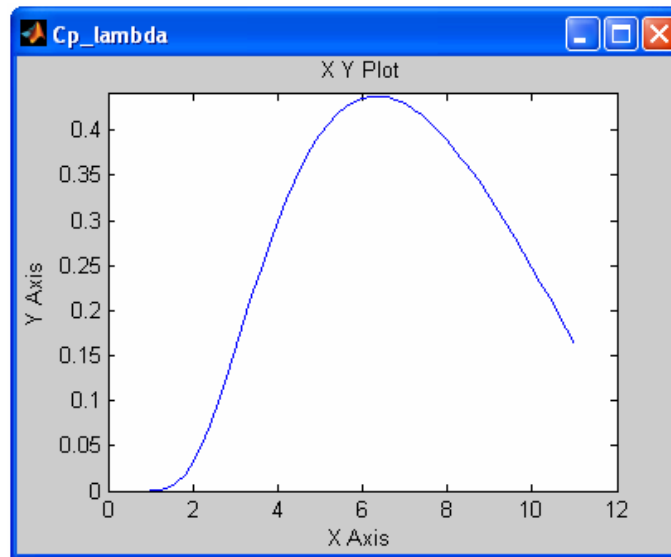
Figure 6.5 : C_p-λ graph
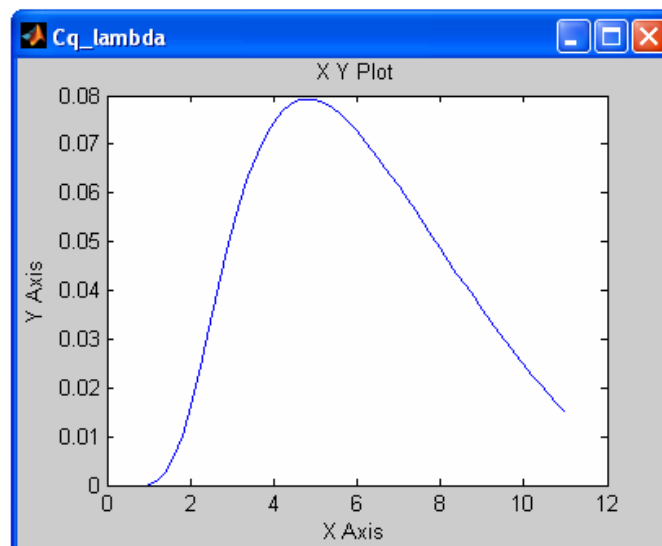
Figure 6.6 : C_Q-λ graph

6.4.3   Block diagrams of the wind turbine model
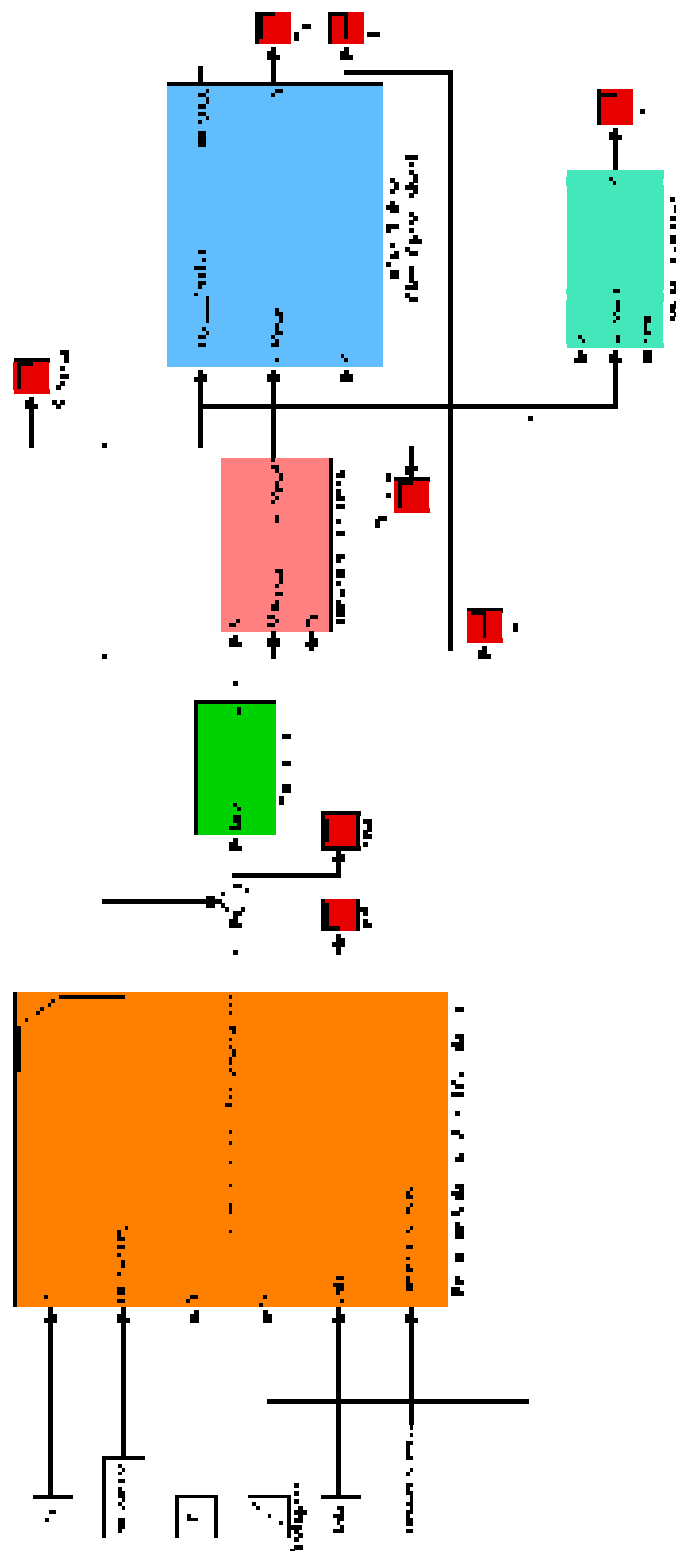
Figure 6.7 : Wind Turbine Block Diagram Model Designed in Matlab

99

6.4.3.1 Reference speed calculation block
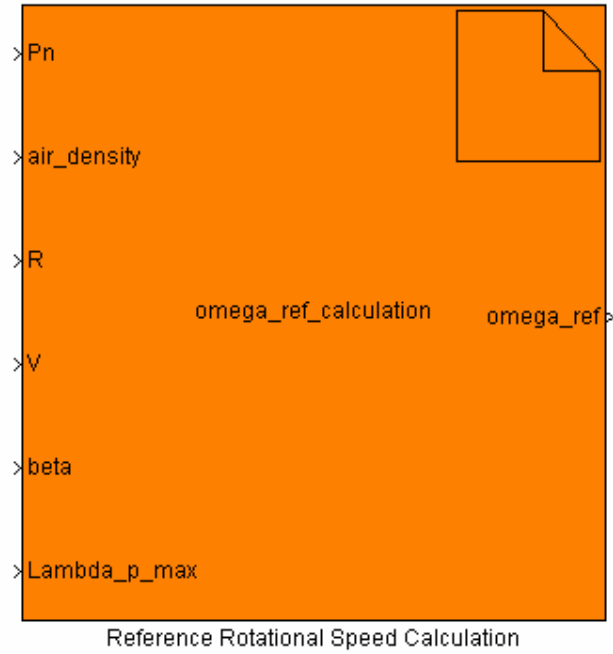
Figure 6.8 : Matlab S-Function Block designed to calculate the reference speed

An S-Function in Matlab is designed to calculate the reference speed. In accordance with the basic VS-FP control strategy, the speed reference is defined as:

$$
\Omega_{ref} = \begin{cases}
\lambda_o V / R & \text{if } V < V_{\Omega_N} \\
\Omega_N & \text{if } V_{\Omega_N} \leq V < V_N \\
\Omega_g : \dfrac{1}{2} r p R^2 C_P\left(\dfrac{R\Omega_g}{V}, b\right) V^3 = P_N, & \text{if } V > V_N
\end{cases}
\tag{6.34}
$$

This function is written as a C code in S-Function given below:

double Cp;

double lambda_i=1.0;

double lambda;

double pi=3.1415;

double V_omega_n=8.5903125;

100

```
double V_rated=13;

if(V[0]<V_omega_n) {

        omega_ref[0]=Lambda_p_max[0]*V[0]/R[0];

}

else if(V[0]>=V_omega_n && V[0]<V_rated){

        omega_ref[0]=1.666;

}

else if(V[0]>V_rated){

        Cp=Pn[0]/(0.5*air_density[0]*pi*pow(R[0],2)*pow(V[0],3));

        do {

                lambda_i=lambda_i+0.0001;

        } while((0.22*(116/lambda_i-0.4*beta[0]-5)*exp(-12.5/lambda_i)-Cp)<=-

                0.0001 || (0.22*(116/lambda_i-0.4*beta[0]-5)*exp(-12.5/lambda_i)-

                Cp)>=0.0001);

                lambda=(lambda_i*(pow(beta[0],3)+1)/(pow(beta[0],3)+1+0.035*

                lambda_i))-0.08*beta[0];

                omega_ref[0]=lambda*V[0]/R[0];

}
```

6.4.3.2 Controller block

The PI controller designed section 6.2 is used to control the speed. The block receives the speed error and generates a signal giving the torque difference $U=T_r-T_g$.
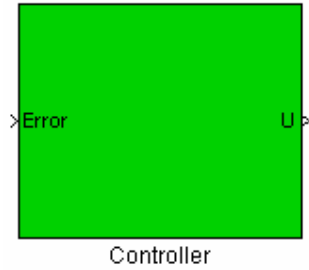
Figure 6.9 : Controller Block

6.4.3.3 Ω_Z calculation block

This block receives the torque differences $U=T_r$-T_g signal. Then using the equations below, the system control input Ω_z is calculated:

$$T_r - T_g = u \tag{6.35}$$

As T_g is defined as $T_g = B_g(\Omega_g - \Omega_z)$, substituting this into (6.35) Ω_z is found:

$$\Omega_z = \frac{B_g\,\Omega_g + u - T_r}{B_g} \tag{6.36}$$
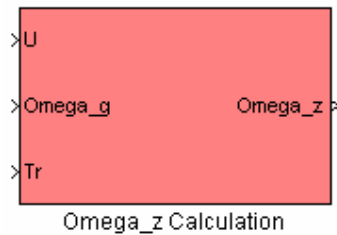
Figure 6.10 : Ω_Z Calculation block

6.4.3.4 Power calculation block

Receiving the signals wind speed V, generator speed Ω_g and pitch angle β, the power produced is calculated as shown in Figure 6.12:
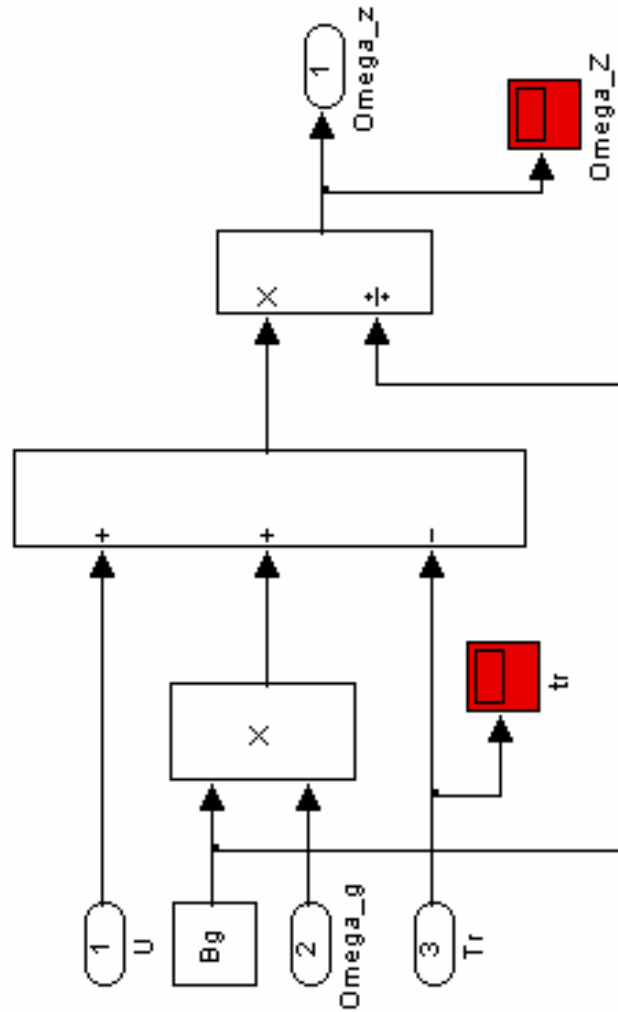
Figure 6.11 : Inside the Ω_Z Calculation block
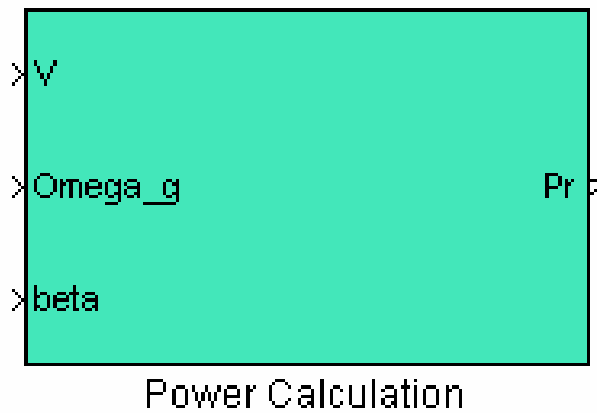
Figure 6.12 : Power calculation block
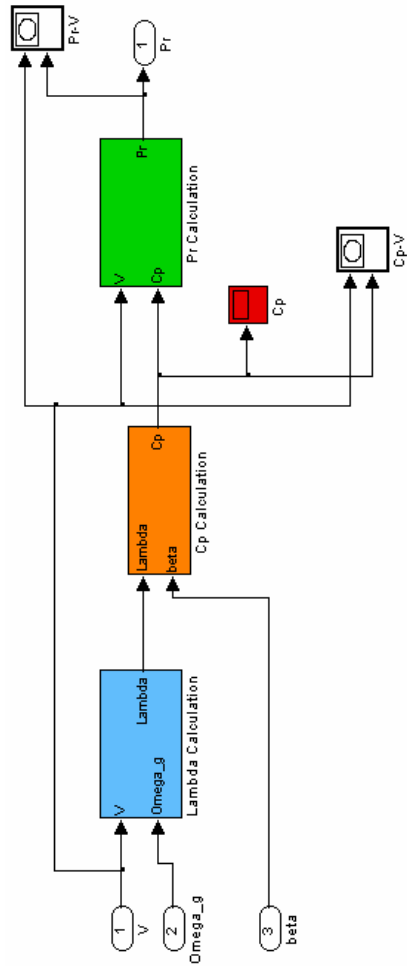
Figure 6.13 : Inside the power calculation block

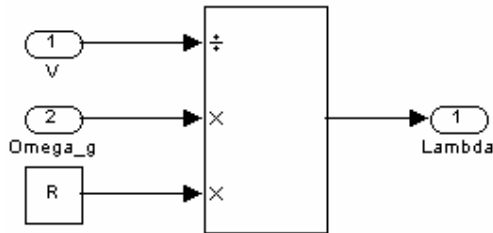λ value depending on the wind speed and generator speed at a sampling time is calculated using (3.27).

Figure 6.14 : Inside the λ calculation block

C_P which is a function of λ and β is found using (6.32), (6.33). The block diagram form of these equations is:
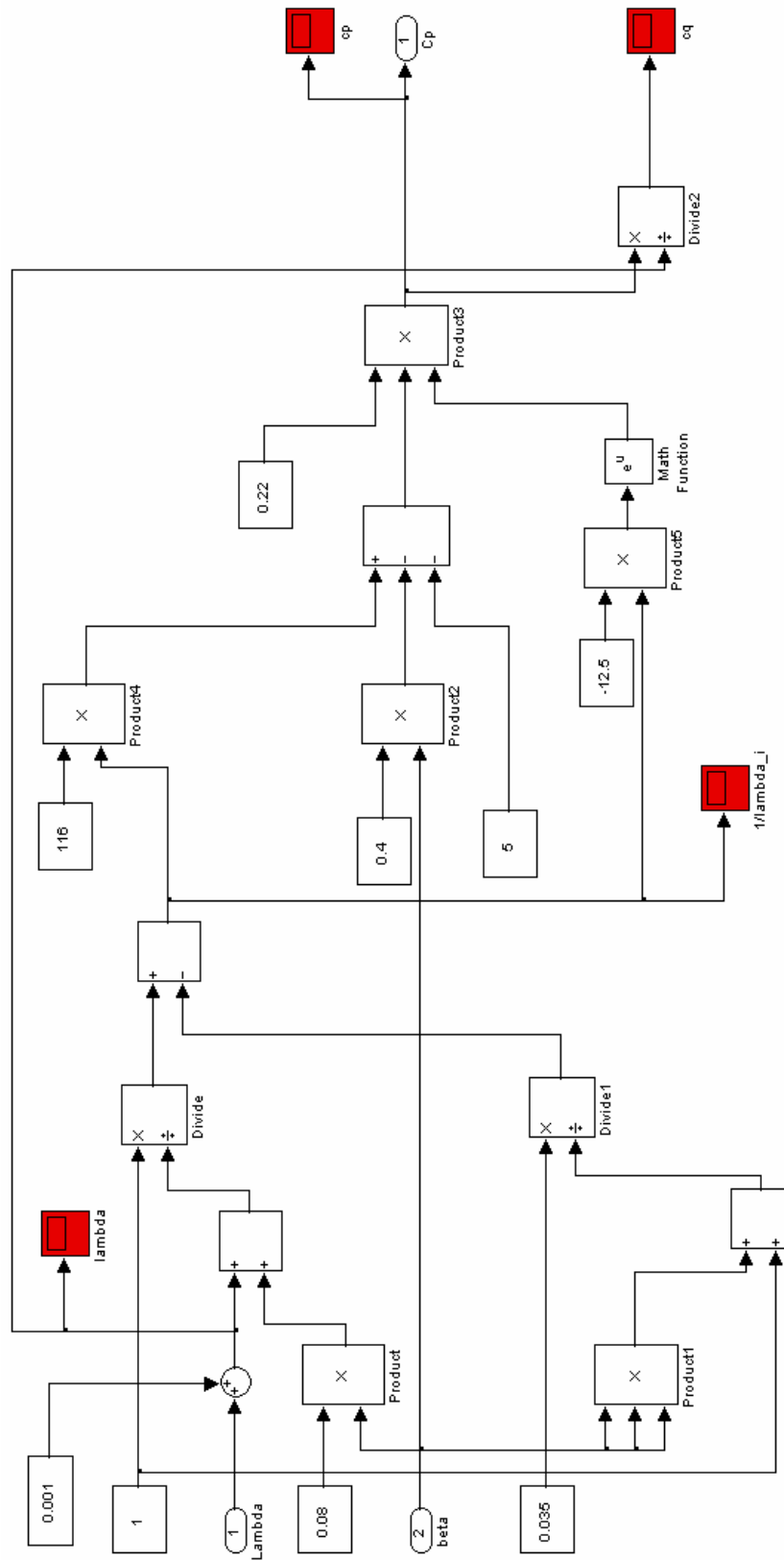
Figure 6.15 : Inside the C$_P$ calculation block

Then power as described in (3.25) is calculated:
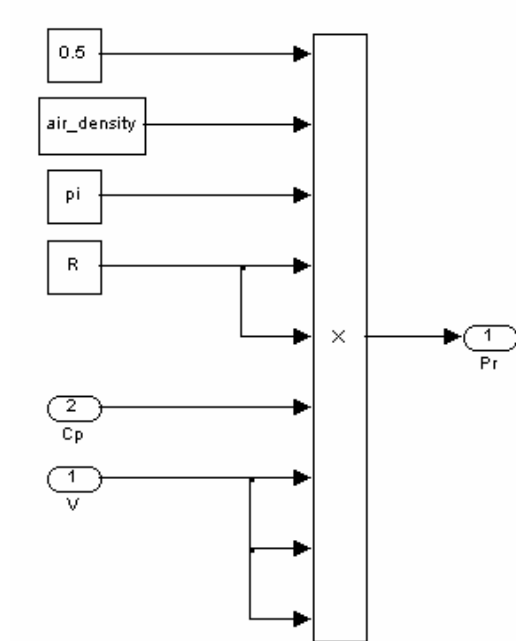
Figure 6.16: Block diagram of power calculation equation (3.25)

6.4.3.5 Wind turbine state space model block

Wind turbine state space model block receives the wind speed V and the control input Ω_z and calculates the outputs aerodynamic torque T_r, generator torque T_g and generator speed Ω_g.
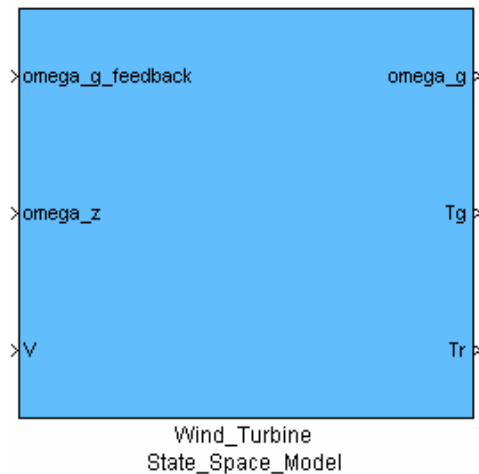

Figure 6.17 : Wind turbine state space model block

Inside the wind turbine state space model block the state space model described in (6.7) is formed as a block diagram and using this, model calculations are made:
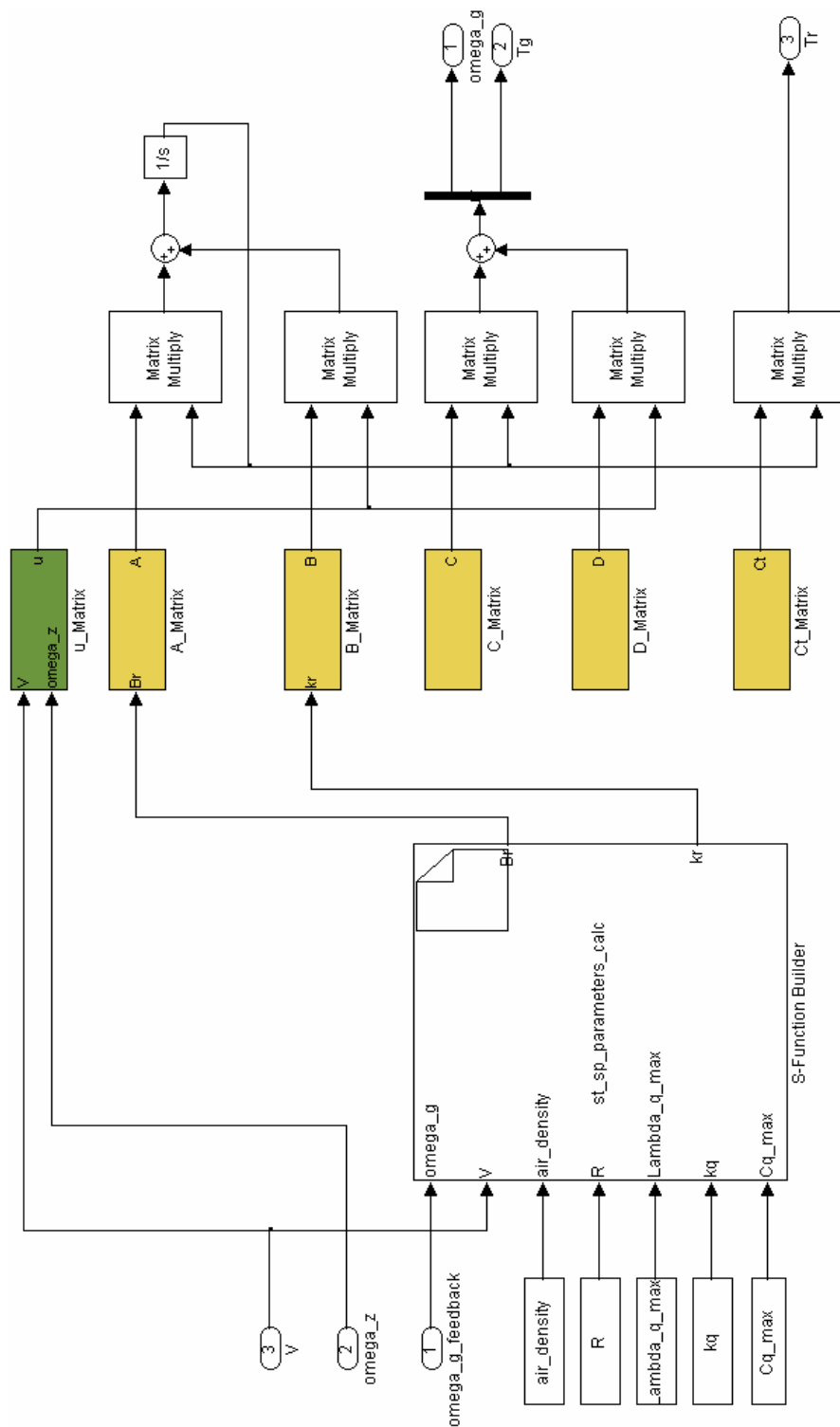

Figure 6.18 : Inside the wind turbine state space model block

7.   RESULTS AND COMMNETS

A ramp function representing the wind speed is used as an input. By this function the wind speed starting at 4 m/s speed and increasing to 18 m/s is applied to the system and the following results are obtained:
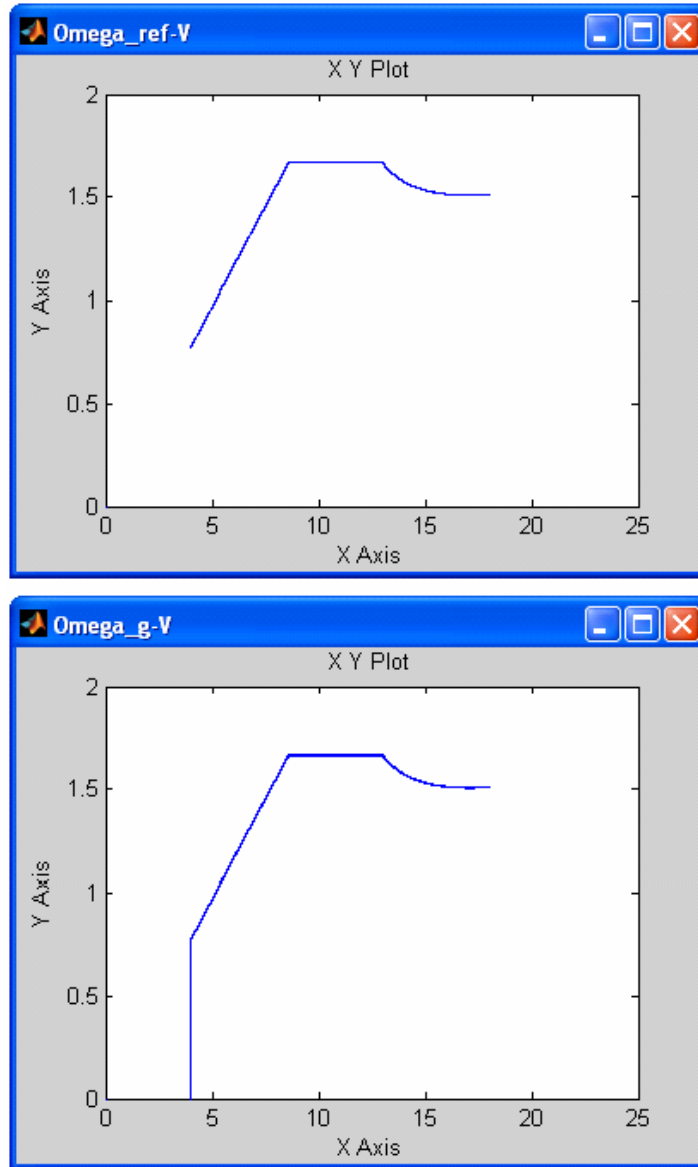

Figure 7.1 : Reference speed and the generator speed Ω_g graphs

Analyzing the speeds, it is seen that the turbine can follow the reference signal during changing wind speed by using PI controller designed.

During the simulation the difference between the reference speed Ω_{ref} and the generator speed Ω_g which is named as the error is as follows:
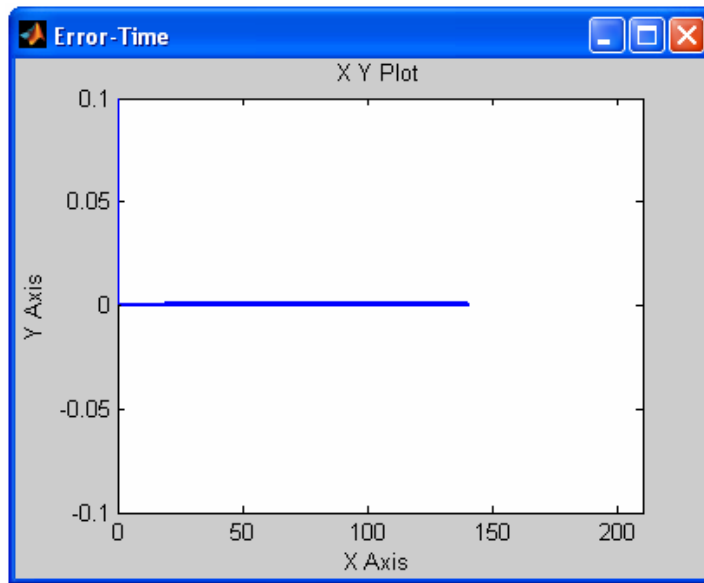

Figure 7.2 : The error of the system

Here the error has a degree of 10^{-3} which is a very good performance for a wind turbine.

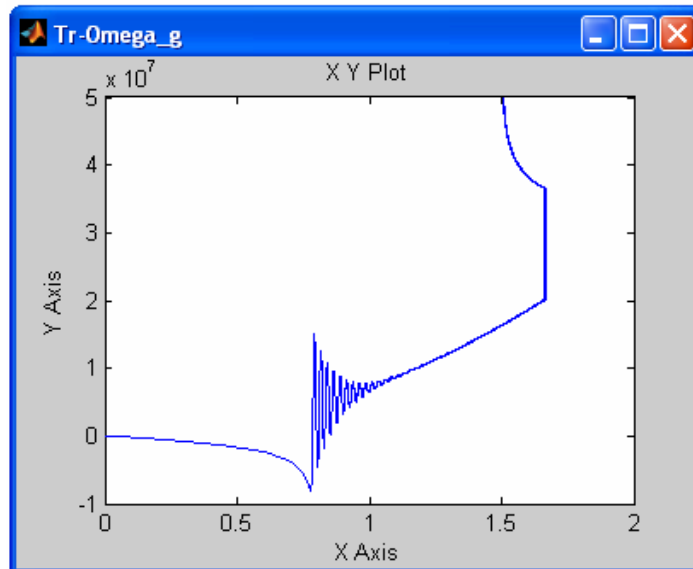The aerodynamic torque vs. generator speed graph is given below:

Figure 7.3 : Aerodynamic torque vs. generator speed graph

Comparing Figure 7.3 with Figure 5.11 it can be said that the system makes oscillations but shows the same characteristic given in Figure 5.11.

Power P_r vs. wind speed V graph is as follows:
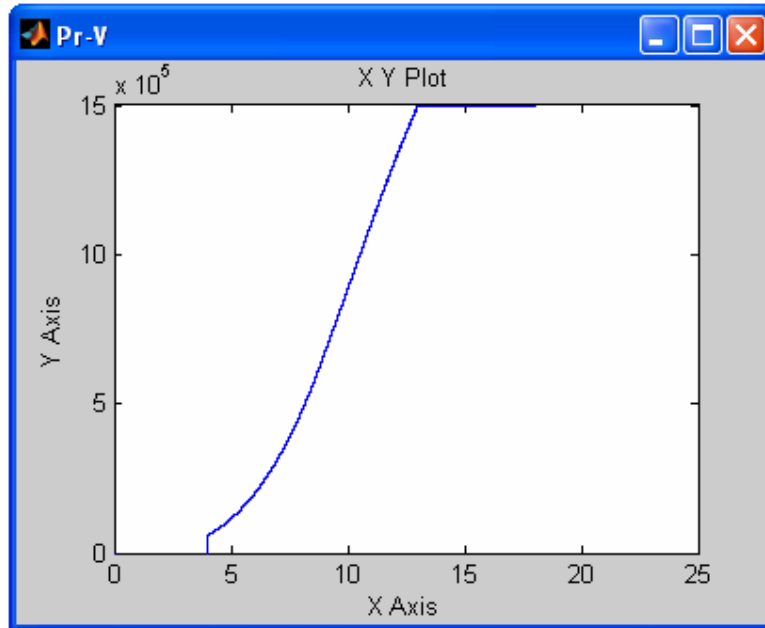

Figure 7.4 : Power vs. wind speed graph

It is observed that the system reaches the rated power 1,5 MW at the rated speed 13 m/s. Moreover, above rated speed the system has a good control performance keeping the generated power constant at the rated (following the rated power locus).

Power coefficient C_P vs. wind speed V graph is shaped as shown in Figure 7.5.

Analyzing the graph, it is observed that the system follows the C_{Pmax} locus which 0.4381. In the region between wind speed for rated rotational speed and rated wind speed C_P decreases with an decreasing acceleration but in above rated wind speeds C_P decreases with an increasing acceleration.

Commenting on the results it can be said that a simple wind turbine model controlled by a simple PI controller can show the desired wind turbine effort. Of course a complicated wind turbine and controller models can be developed, however if the simple one shows the desired performance there is no need to develop a complicated
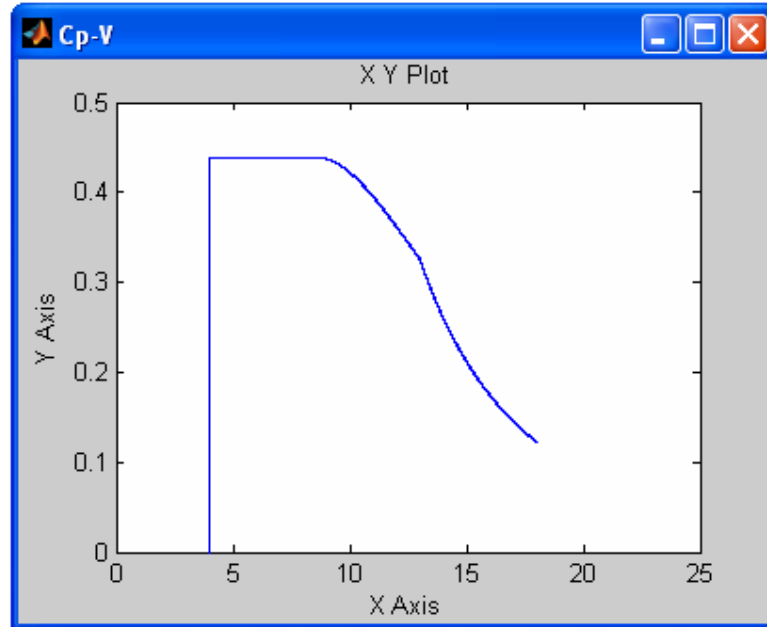
Figure 7.5 : Power coefficient vs. wind speed graph

one. Because it increases the design process time and the calculation time while the system is working. Also the devices to make the complicated control effort would be more expensive. As a result, a complicated model describing the non-linearities of the system and a high order controller for the complicated system can be designed and may show a better performance, but if a simple wind turbine model controlled by a first order controller satisfies the desired performance it is better to use this simple model.

REFERENCES

[1] **Bianchi, F.D. ; Battista, H.D. and Mantz R.J.,** 2007. Wind Turbine Control Systems, Springer Verlag London Limited, Germany.

[2] **Mathew, S.,** 2006. Wind Energy, Springer Verlag-Berlin Heidelberg, Netherlands.

[3] **Manwell, J.F. ; McGowan, J.G. and Rogers, A.L.**, 2002. Wind Energy Explained, John Wiley & Sons, West Sussex.

[4] **Det Norske Veritas and Wind Energy Department of Riso National Laboratory,** 2002. Guidelines for Design of Wind Turbines, Jydsk Centraltrykkeri, Denmark

[5] **Bindner H.,** 1999. Active Control: Wind Turbine Model, Technical Report RISO-R-920(EN), Roskilde, Denmark

[6] 2004. Study on the transient phenomena of wind generation, NTUST, Kyoto.

[7] **Malcolm, D.J. and Hansen, A.C.**, 2002. WindPACT Turbine Rotor Study, Subcontractor Report, NREL Colorado.

[8] **Stol, K.A.**, 2003. Geometry and Structural Properties for the Controls Advanced Research Turbine (CART) from Model Tuning , Subcontractor Report, NREL Colorado.

[9] **Versteegh, C.J.A.**, 2004. Design of the Zephyros Z72 wind turbine With emphasis on the direct drive PM generator, Technical Report, NTNU Trondheim.

[10] **Caldwell, J.,** 2005. Electrical Guide to Utility Scale Wind Turbines, Interim Report, AWEA Washington.

[11] **Boukhezzar, B. and Siguerdidjane, H**., 2005. Non-linear control of variable speed wind turbines without wind speed measurement, *The 44th IEEE*

Conference on Decision and Control, and the European Control Conference, Seville, Spain, December 12-15.

[12] **Perdana, A. ; Carlson, O. and Persson, J**., 2004. Dynamic response of grid connected wind turbine with doubly fed induction generator during disturbances, *The Nordic Workshop on Power and Industrial Electronics,* Trondheim

[13] General Electrics 1,5 MW wind turbine brochure

[14] **Smith, K.**, 2000. WindPACT Turbine Design Scaling Studies Technical Area 2: Turbine, Rotor and Blade Logistics, Subcontractor Report, NREL Colorado.

Curriculum Vitae

Gürol Çokünlü was born in Bursa in 1982. He started his education in Hamzabey Primary School and continued in Bursa Anatolian High School. In 2000 he entered the Mechanical Engineering Department of Istanbul Technical University and graduated from the department in 2004. After his graduation, he started working in Kale Altınay Robotics and Automation as a Robotic Welding Systems Engineer and he is still working there. At the same time he continued his education in the Mechatronics Engineering Master Programme of İstanbul Technical University and he still continues his education there.